Human Performance in Perceptual Tasks Involving Estimation and Navigation

John G. Raiti

School of Engineering

Brown University

Copyright Page

May 2012

This dissertation by John G. Raiti is accepted in its present form
by the Department of Biomedical Engineering as satisfying the
dissertation requirement for the degree of Doctor of Philosophy.

Date_______________ ___________________________________

Jerry Daniels, Advisor

Recommended to the Graduate Council

Date_______________ ___________________________________

James Anderson, Reader

Date_______________ ___________________________________

Gustav Engbretson, Reader

Date_______________ ___________________________________

John Stein, Reader

Date_______________ ___________________________________

Rashid Zia, Reader

Approved by the Graduate Council

Date_______________ ___________________________________

Peter Weber, Dean of the Graduate School

Curriculum Vitae

John Giulian Raiti

Born on August 12, 1978 in Baltimore, MD

Education

Sc.M. in Engineering, Brown University (2004)

M.S. in Neuroscience, Syracuse University (2002)

B.A. in Neuroscience, The Johns Hopkins University (2000)

Publications

Raiti, J. and Daniels, JD. Direct and Pairwise Area Estimation of Physical Shapes through Vision and Touch. *Perceptual and Motor Skills*, (Accepted with revisions), 2011.

Raiti, J. and Daniels, JD. Numerosity Estimation of Physical Objects By Vision and Touch. *Perception*, (Submitted for publication), 2011.

Acknowledgments

I would like to thank:

(1) my advisor JD Daniels for his guidance

(2) my dissertation committee

(3) my parents and my brother for their constant love and support

(4) Vishal Jain, Dan Crispell, and Harry Johnson for their friendship

Contents

1 Introduction **1**

2 Control Experiments Regarding Visualization of Navigation Field **5**

2.1 Background: Visual Psychophysics Experiments 5

2.2 Introduction 6

2.2.1 Degrading Stimuli by Blurring 6

2.2.2 Degrading Stimuli by Lowering Contrast 7

2.2.3 Degrading Stimuli by Block Averaging 8

2.2.4 Visual Search 8

2.2.5 Priming 9

2.2.6 Masking 12

2.3 General Methods 14

2.3.1 Monitor and Graphics Card 14

2.3.2 Participants and IRB approval 14

2.3.3 Navigation Field 15

2.3.4 Converging Stimuli 17

2.3.5 Single-resolution Stimuli 17

2.4 Experiment: Just Noticeable Difference of Hue 17

2.4.1 Introduction 17

2.4.2 Methods 18

2.4.3 Results 19

2.4.4 Discussion 20

2.5 Experiment: Converging *vs* Single Resolution Stimuli 24

2.5.1 Results 26

2.5.2 Discussion 27

2.6 Experiment: Low Resolution (Level 4) Priming 27

2.6.1 Methods 27

2.6.2 Results 28

2.6.3 Discussion 28

2.7 Experiment: Priming and Masking 29

2.7.1 Methods 29

2.7.2 Results 30

2.7.3 Discussion 31

2.8 Experiment: Visual Discrimination 31

2.8.1 Methods 32

2.8.2 Results 32

2.8.3 Discussion 34

2.9 Experiment: Gray Screen Test 34

2.9.1 Results 35

2.9.2 Discussion 35

2.10 Saccades made while inspecting regions 35

2.11 Summary 36

3 Navigating with Uncertainty **38**

3.0.1 Definitions 38
3.1 Introduction 38
3.2 Previous Work 39
3.2.1 Version of Navigation 40
3.2.2 Details of Orienteering 40
3.3 Methods 42
3.3.1 Virtual Terrain 42
3.3.2 Stimuli 42
3.3.3 Drone 42
3.3.4 Task 43
3.3.5 Protocol 43
3.3.6 Scoring Parameters 44
3.3.7 Scoring Equations 45
3.3.8 Subject Score 45
3.3.9 Time Penalty (Subject Score) 46
3.3.10 Experimenter (Observer) Score 46
3.3.11 Distance Cost 47
3.3.12 Time (Step) Cost (Experimenter Score) 47
3.3.13 Collision 48
3.4 Results 51
3.4.1 Collision Results 51
3.4.2 Level of Resolution Used at Each Step by a Subject 51
3.4.3 Elevation used by Subjects 55

3.4.4 Angle-to-Goal used by Participants 56

3.4.5 As-the-Crow-Flies (ACF) Paths to Goal 58

3.4.6 Drone to goal using Best First Search (BFS) Algorithm 60

3.4.7 Learning Curves 62

3.4.8 Converging Stimuli *vs* Single Resolution Navigation Results . . 62

3.5 Discussion 62

4 Path Optimization Methods and Results 66

4.1 Introduction 66

4.2 Examples of Terrains 66

4.3 Methods of Optimization 80

4.4 Best First Search (BFS) 81

4.5 A* Algorithm Grid-based 81

4.6 Dijkstra's Algorithm Grid-based 82

4.7 Breeding Algorithm 91

4.7.1 Mutations 92

4.7.2 Addition 93

4.7.3 Deletion 94

4.7.4 Slider 94

4.7.5 Breeding Algorithm Results and Discussion 95

4.8 Neural Network for Learning Local Terrain 100

4.9 Summary 106

5 Numerosity Estimation of Physical Objects By Vision and Touch 107

5.1 Introduction 107

5.2 Previous work on estimating quantities 107

5.3 Arrangement 113

5.4 Methods 113

5.5 Results 116

5.6 Discussion 118

6 Direct and Pairwise Area Estimation of Rigid Physical Shapes 121

6.1 Introduction 121

6.2 Methods 125

6.3 Results 127

6.4 Discussion 129

7 Conclusions and Future Directions 132

8 Appendix A: Definitions and Discussion 134

8.1 Definition of Performance 134

8.2 Definition of Quality 134

8.3 Definition of Numerosity 135

9 Appendix B: IRB Approved Protocols and Consent Forms 136

9.1 IRB Approved Protocol and Consent Form for Navigation Experiment 136

9.2 IRB Approved Protocol and Consent Form for Estimation Experiments 141

List of Figures

1 Different levels of blurred image. (Adapted from Loftus & Harley [51]) 7

2 Degraded image of President Lincoln: *(a)* blurred, *(b)* block averaged. (Adapted from Harmon & Julesz [31]). 8

3 Example of visual search. Task to find letter "J" 9

4 Example of conjunctive search. Task to find red vertical bar. Adapted from Kristjánsson, Wang & Nakajama [49] 9

5 Effect of number of display elements on response time (RT) search [67] 10

6 Stroop test. Subjects instructed to name the ink color. *(a)* blue ink and word spelled blue (no interference), *(b)* took longer to say "green" when word spelled "blue" (interference). 11

7 Response Time effect of interference on naming ink colors: *(1)* no interference, *(2)* interference. [80] 11

8 Example of Negative Priming. Task: name the red colored letter and ignore green letter in Probe condition, measured subjects' response times. *(a)* Prime displayed for 1 sec (attended condition) *(b)* Probe (ignored condition). If ignored letter in prime is the attended to target in the probe, then subjects' naming latency was impaired, *(c)* Control condition 12

9 *(a)* Subject stared at red X for 20 sec, *(b)* subject saw green X afterimage. . . 13

10 Cyan to Magenta field generated by $z = \cos\frac{2\pi}{3}x + \sin\frac{2\pi}{3}y$ with a period of 3 units and amplitude ranging from 2 to -2 (magenta = 2, cyan = -2). Color varies from cyan to magenta. 15

11 Symmetric field divided into 4 quadrants and each quadrant rotated by $\frac{\pi}{8}$ . . . 16

12 Tilted view of rotated field with cyan to magenta colormap elevation scale. . . . 16

13 Catalog of levels of resolution (1, 2, 3, 4, 6, 8, 10). *(a)* Level 1 (one region), *(b)* Level 2 (4 subregions), *(c)* Level 3 (9 subregions), *(d)* Level 4 (16 subregions), *(e)* Level 6 (36 subregions), *(f)* Level 8 (64 subregions), *(g)* Level 10 (100 subregions) 17

14 Colormap scale ranging from cyan (index = 1) to magenta (index = 64). 18

15 Schematic of just noticeable difference protocol. Participants viewed 2 stimuli for 1 sec, followed by a mask for 200 msec. A black screen then appeared indicating that the subject should enter their response by pressing "1" for same or "3" for different. They had unlimited time to enter their response. 19

16 *(a) left* pure cyan, *right* cyan index 6 away, *(b) left* pure magenta, *right* magenta index 6 away. 20

17 Participants' performance (measured by percent correct) increased as the number of indices separating each stimulus increased. Best fit line (black). 22

18 Indices apart: *(a)* 1, *(b)* 2, *(c)* 3, *(d)* 4, *(e)* 5, *(f)* 6. 23

19 Schematic of visual protocol. *Top Left*: Example of a single-resolution stimulus (level 10 only) displayed for 650 msec. *Top Right*: Response screen with mouse cursor in the form of crosshairs which participants used to enter their selection for the place where they best remembered the most saturated pure shade of magenta. *Bottom*: Participants viewed a level 1 resolution stimulus for 650 msec, followed by levels 2, 3, 4, 6, 8, 10 (each for 650 msec). After the level 10 resolution stimulus, a response screen appeared indicating that the subject should enter their response; they had unlimited time to enter their response by clicking the location on the screen where they best remembered the most pure shade of magenta to have been situated. 26

20 Fields: *(a)* normal used for valid priming, *(b)* rotated by -$\frac{\pi}{9}$. 28

21 Schematic of priming protocol. Participants viewed a level 4 resolution stimulus for 600 msec, followed by level 10 for 200 msec. After the level 10 resolution stimulus, a gray response screen appeared indicating that the subject should enter their response; they had unlimited time to enter their response by clicking the location on the screen where they best remembered the purest hue of magenta to have been situated. 29

22 Schematic of masking protocol. Participants viewed a level 4 resolution stimulus for 600 msec, followed by level 10 for 200 msec. After the level 10 resolution stimulus, the mask occured for 500 msec. A gray patch then appeared indicating that the subject should enter their response; they had unlimited time to enter their response by clicking the location on the screen where they best remembered the purest hue of magenta to have been situated. 30

23 Schematic of visual acuity protocol. Participants viewed 4 magenta circular regions in random positions on a cyan background for 2 sec, followed by the mask for 500 msec. After which a black response screen appeared. Subjects had unlimited time to enter their response by clicking the location on the screen where they best remembered the purest shade of magenta to have been situated. 32

24 Subjects picked the purest shade of magenta region in 84 out of the 120 trials. X axis = Trial. Y axis = magenta hue and width of peak (yellow curves = region width; magenta curves = magenta hue selected by subjects). 33

25 A gray patch appeared in 20 random positions. Subjects had as much time per presentation as they desired before clicking. 34

26 Saccadic movements while viewing a series of horizontally arranged magenta peaks. Subject looked to the far right then in steps to the left then directly to center. Scales = 100 mV/division and 200 msec/division. (a) Linear arrangement of magenta regions, (b) upwards excursions indicate rightward saccade, downwards indicates leftwards. 36

27 Saccadic movements while viewing a series of randomly arranged magenta peaks. *(a)* Stimuli in random arrangement. *(b)* Scales = 200 mV/division and 200 msec/division. Upwards excursions indicate rightward saccade, downwards indicates leftwards. . 37

28 Example of Orienteering Map [40]. Players need to find and go to the control points (check-posts) in numerical order. 41

29 Navigation experiment task start screen. Player's start position (black solid circle) in square patch. Drone mirror image start position (green circle). Subject's goal (solid blue circle). Drone mirror image goal (yellow circle). 44

30 Protocol. (a) Trials 1-12, (b) Trials 13-24. C = converging stimuli. S = single level 10 resolution. Step size of the drone. Step size of human player always 1.8. . . . 45
31 Distance Cost Function 48
32 Time (step) Cost Function (Experimenter Score) 49
33 Example of Collision. *(a)* Collision, *(b)* Collision color conventions. 50
34 Example of Levels of Resolution used by a subject. *(a)* Path and levels of resolution taken by a subject superimposed on the terrain, *(b)* levels of resolution used by a subject on black background (for clarity), *(c)* color conventions for levels of resolution representation. 53
35 Sequence of levels of resolution used by a subject from Trial 1 to Trial 12 54
36 Mean levels of resolution (blue) of all subjects across all trials (1-24). Time series averaged (red) showing that as subjects continued playing the game, they waited for higher levels of resolution. 55
37 Time Series Averaged (hist = 10) elevation scores over all converging stimuli trials 56
38 Time Series Averaged (hist = 10) elevation scores over all single resolution trials 57
39 Time Series Average for Angle-to-Goal Single Resolution. *(a)* Path and levels of resolution taken by a subject superimposed on the terrain, *(b)* Time Series Averaged (hist = 5) angle-to-goal scores over all single resolution trials 57
40 As-the-crow-flies (ACF) paths to the goal located at (6,4) from 5 different start positions. 58
41 Elevation scores for 5 ACF paths 59
42 5 BFS paths of drone to goal (6,46) from different start positions. 60
43 Elevation scores for drone to goal using best-first-search (BFS) algorithm. . . . 61

44 Learning curves for converging and single resolution stimuli. *(a)* Converging results, *(b)* Single resolution. Colors indicate participants competing against drone step-sizes of 1.6 (blue), 1.7 (pink), and 1.8 (yellow). Participants had a constant step-size of 1.8. 63

45 Subjects score more points when viewing single than converging stimuli resolution stimuli. Range of scores (68-77) was a reasonable order of magnitude for subjects to comprehend. 64

46 Examples of the terrains: *(a)* sinusoidal, *(b)* plasma fractal, *(c)* Complex Ginzburg-Landau, *(d)* rotated sinusoidal, *(e)* rotated plasma fractal, *(f)* rotated Complex Ginzburg-Landau. 67

47 Rotated sinusoidal terrains: *(a)* view(45,45), *(b)* view(20,40), *(c)* view(20,60), *(d)* view(30,60). 68

48 Terrain generated by plasma fractal code with no randomness. 70

49 Terrain generated by plasma fractal code with randomness. 70

50 Terrain generated by plasma fractal code with randomness and 4 random elements in the input array. 71

51 Terrain generated by plasma fractal code with randomness and 4 random elements in the input array plus randomness added through the algorithm. 72

52 Terrain generated by plasma fractal code with a random input array. 73

53 Terrain generated by plasma fractal code with a random input array and randomness from algorithm. 74

54 FFT of the sinusoidal terrain. 75

55 FFT of the plasma fractal terrain. 76

56 FFT of the CGLE terrain. 77
57 CGLE irregular terrain with $\alpha = 0$ and $\beta = 3$. 78
58 CGLE irregular terrain with $\alpha = -0.5$ and $\beta = 2.999$. 79
59 Best first search schematic. Start location indicated by black circle "1". Point with highest score and which the algorithm selects as the winner at each iteration is shown in green. ("G" = goal). 82
60 (a) Node tree diagram using A* , (b) Example of A* finding the lowest cost path (2+3+1) 82
61 Number of unique paths in grid sizes 2x2 to 14x14. 85
62 The number of unique paths (*y-axis*) increases exponentially with increasing square grid size (*x-axis*). 85
63 Dijkstra's algorithm using an 8x8 grid on the sinusoidal terrain scoring 36 points. 86
64 Dijkstra's algorithm using an 8x8 grid on the plasma fractal terrain scoring 23.523 points. 87
65 Dijkstra's algorithm using an 8x8 grid on the CGLE terrain scoring 30.528 points. 88
66 Dijkstra's grid (21x21) algorithm across 3 terrains: (a) sinusoidal, (b) plasma fractal, and (c) CGLE, compared to BFS across 3 terrains: (d) sinusoidal, (e) plasma fractal, and (f) CGLE. BFS scored more points than Dijkstra's grid based algorithm in each of the 3 terrains. 90
67 Addition Mutation 93
68 Addition Mutation. *Left:* Example of a section of original path. *Right:* Addition mutated path (red). 93

69 Deletion Mutation. *Left:* Example of a section of original path. *Right:* Deletion mutated path (red); point 2 of the original path was deleted and the new mutated path was formed (red). 94
70 Slider Mutation. *Left:* Example of a section of original path. *Right:* Slider mutated path (red). 95
71 Slider Mutation. *Left:* Example of a section of original path. *Right:* Slider mutated path (red). 95
72 Slider Mutation. *Left:* Example of a section of original path. *Right:* Slider mutated path (red). 96
73 Slider Mutation outperforms BFS 96
74 Top 16 (of 1000) Random 1st generation (parents) paths on sinusoidal terrain. . 97
75 Best First Search (black) scores 194.38 points and best mutated path (red) scores 206.02 points. 98
76 Breeding algorithm performance over 55 generations. Score (y-axis) vs Generation (x-axis) 98
77 (a) Top 16 (of 1000) Random 1st generation (parents) paths in Plasma Fractal terrain , (b) Score (y-axis) vs Generation (x-axis) 99
78 (a) Top 16 (of 1000) Random 1st generation (parents) paths in CGLE terrain , (b) Score vs Generation 99
79 Example of a neural network. Inputs $(x_1...x_n)$ are multiplied by weights $(w_1...w_n)$ 101
80 3 layers used in neural networks: input, hidden, and output 102
81 Neural network used in learning the local terrain, where μ is the learning rate and ϵ is the feedback error. 103

82 Neural network training (*red* = validation set, *blue* = training set). 104

83 Median estimates of number of dots shown on a screen. Kaufman *et al* [46] . . . 108

84 *Left*: Regular arrangement of 60 M&M's. *Right*: Irregular arrangement of 100 M&M's. 113

85 Example of quart size candy bag containing 305 candies (138 peanut M&Ms, 152 jelly beans, 15 gummy worms) used in all conditions 115

86 *(a)* equal spacing and number of M&M's; *(b)* top row longer line, fewer M&M's than bottom row; *(c)* top row shorter line and fewer M&M's than bottom row. (From Mehler & Bever [58]) 122

87 Evenly spaced dots with top row forming a longer line than the bottom row. Both rows have the same number of dots. 123

88 Catalog of six classes of shapes from top to bottom: triangles, quadrilaterals, polygons, ellipses, stars, and irregular. Adapted from Martinez and Dawson [55] . . 125

89 *(a)*: Shapes 1 - 5 (left to right) and unit reference square. *(b)*: Hand holding one of the five shapes 126

90 Mean Percent Error for each trial using the direct area estimation method. Subjects were given shapes in a random order, so each trial contains estimates from different shapes. 128

91 Mean estimates for each trial using the direct area estimation method. Subjects were given shapes in a random order, so each trial contains estimates from different shapes. Each shape had an area of 10 units. 129

92 U-shaped curve showing number of tests for a rat to complete discrimination task vs stimulus strength (units). Minima of the plots represent the best (optimal) performance, from Yerkes & Dodson [97] 135

1 Introduction

This thesis is centered around a novel computer navigation experience. A computer game was developed to study how humans navigate from a start position to a goal over a simulated terrain resembling a mogul field with a limited view and limited spatial resolution of the terrain. Participants learned by playing that elevation and angle-to-goal affected scoring.

The virtual mogul field inspired a tangible representation of the field in the form of peanut M&M clusters. Participants' performance in the estimation of tangible versus simulated (video) items using vision and/or touch was investigated. The theme of comparing estimation performance using virtual versus tangible items was continued in another experiment where participants were asked to estimate the areas of irregular flat shapes.

Chapter 2 presents visual psychophysics experiments that were controls for the navigation game. A set of details were examined such as: (1) just-noticeable-difference of the color map for elevation (z-axis) representation of the field, (2) whether priming, interference or masking affected game performance, and (3) reduced correlation between peak height and peak width. Since the terrain in the navigation game used colors ranging from cyan to magenta, the just-noticeable-difference of hue task was designed to assess human performance in discriminating shades on the cyan-magenta spectrum. Furthermore, the navigation game had two modes: converging and single. Converging stimuli presented participants with an increasingly resolved view of a patch of the terrain. The single resolution condition displayed a fixed resolution (level

10) view of a patch of the terrain. Priming, interference, and masking experiments (Chapter 2) showed that participants were unaffected by pre-target and post-target stimuli in both converging and single resolution conditions. Therefore, the game as described in Chapter 3 needed no significant changes.

Chapter 3 pertains to the navigation game itself. Each participant competed against a computer-generated drone to reach the goal first. Participants were allowed to explore the terrain by clicking the location they wanted to advance to next in a constant step-size, akin to "hopping" towards the goal. Only a square local patch of the global terrain was revealed to the participant at each step. Two modes (converging and single view) of the game were employed to examine whether participants performed better (scored more points) with an increasingly resolved view of the patch (converging) or with a single view. Game score improvement was studied in subjects with no practice sessions. Participants learned that elevation and angle-to-goal affected scoring. Not only did participants learn the two scoring factors, but they also learned that clicking magenta colors resulted in scoring more points. A learning curve was found for this open-ended experience involving navigation to a goal with only a local patch of the terrain visible for the next jump. A traveling method that involved jumps of a fixed size has unique characteristics that cannot be studied or optimized directly by "grid" methods; certain advances in understanding "hop" navigation were achieved and discussed. A learning curve is shown, the first of its kind for free-range navigation.

Related to this game, path optimization is examined in Chapter 4. An unanswered question arose from the navigation game chapter: What would be the optimal path from start to goal with the fixed step means of traveling? Human practice and the best-first algorithm were unable to supply the answer. In chapter 4 a breeding algorithm for optimization, featuring specially designed mutations of good (but not best) paths, was shown to come arbitrarily close to optimal answers (with certain constraints on the features of the mogul field terrain). A variety of algorithms including: best-first-search, A*, and breeding algorithms were used to find optimal paths across different simulated terrains. Neural networks were implemented to learn the local terrain and extrapolate into terrain beyond the local patch of the terrain.

Chapter 5 was inspired by the color-coded appearance of the top-down view from the computer mogul field, and by curiosity about the difference between navigating in a virtual world versus the real world. A quantitative method for measuring differences in the perception of real and virtual objects was developed. In addition to studying how participants estimate path planning (consisting of a number of discrete steps), Chapter 5 examines human performance in estimating the number of items in a transparent sealed bag. Performance in estimating 305 candies was compared across five conditions: (1) vision-plus-touch, (2) binocular vision, (3) monocular vision, (4) video, and (5) touch (blindfolded). It was found that estimation after seeing plus feeling the bag was better than seeing (binocular) alone, and binocular was better than monocular viewing, and either way of viewing real objects was better than looking at a video of the objects, and all those involving vision were better than feeling the bag blindfolded.

In Chapter 6, the theme of comparing the estimation performance using virtual versus real world items was continued with the use of irregular shapes. Two estimation techniques were used: (1) direct and (2) pairwise. The direct method entailed participants being handed one shape at a time and a square unit reference shape and asked to estimate the area of the irregular shape based on the unit square. The pairwise method involved a participant being handed two irregular shapes at a time and asked to estimate if the shapes were equal in area or whether one shape was larger in area than the other, if so by how much. Adamic et al [1] found that participants, while viewing the shapes projected on a screen, made fewer errors in the pairwise method than in the direct method. The experiment in Chapter 6 extended the work of Adamic et al [1] by using real world tangible shapes instead of two-dimensional projected images of the irregular shapes. The author of this thesis is the first to show that the use of tangible shapes with the perceptual combination of vision plus touch decreases the error in area estimation versus two-dimensional projected images of irregular shapes.

To summarize: the study of participants in a computer navigation experiment led to: (1) control studies, (2) a search for optimal paths, and (3) the inspiration for comparing the perception of real objects to their images by estimation techniques. Participants discovered scoring parameters when presented with only a restricted view (patch) of the terrain coupled with low resolution images, demonstrating that perfect (highest) resolution is not required for learning to navigate through a novel environment. Given the performance of participants with limited resolution images of the terrain, performance using real objects was then examined in this thesis. Real objects improved performance over virtual images in both numerosity and area estimation tasks.

2 Control Experiments Regarding Visualization of Navigation Field

2.1 Background: Visual Psychophysics Experiments

Experiments described here were used to develop parameters for the navigation game (Chapter 3). The navigation game featured a colormap ranging from cyan to magenta. In this chapter, participants differentiated between shades of cyan and magenta to find the just-noticeable-difference between indices of the colormap. Also, the navigation game contained 2 types of stimuli (converging and single resolution); subjects viewed a progression of increasingly higher resolution images (converging stimuli) and results were compared to subjects who viewed single resolution stimuli. Priming and masking effects of the stimuli were also tested. The themes of visual search and stimulus resolution were explored in the following experiments, Table 1.

Experiment	Description
1: Just Noticeable Difference	2 colormap indices presented simultaneously; subject asked to decide if stimuli are same or different
2: Converging *vs* Single Resolution	how subjects responded to a progression of levels of resolution *vs* a single level of resolution
3: Priming	subjects inspected a level 4 resolution stimulus followed by a level 10 stimulus that was misaligned (deviated) in half of the trials
4: Masking	level 4 resolution stimulus then level 10 then mask then respond
5: Variable Peaks	irregular pattern background
6: Visual Acuity	4 magenta peaks with different widths on a cyan background
7: Visual Acuity with Deviated Prime	effect of a rotated stimulus on accuracy
8: Gray Screen Test	effect of clicking random locations in a gray patch

Table 1: Visual Psychophysics Experiments

2.2 Introduction

2.2.1 Degrading Stimuli by Blurring

Bruner and Potter [10] demonstrated that subjects took longer to recognize "very-blurred" (VB) objects than "lightly-blurred" (LB) ones. The experimenters asked subjects to identify the object shown on a projector screen. The authors varied the initial point of focus and the amount of time the stimulus remained on the screen. Bruner and Potter found that subjects most often recognized the object with longest viewing times and least amount of blur, and least often recognized an object when least amount of viewing time and highest amount of blur, Table 2.

Avg Viewing Time (sec)	VB	MB	LB
122	25	50.7	72.9
35	25.4	44.4	63.8
13	19.4	39.1	42.7

Table 2: Percentage of pictures recognized in various timing conditions and degrees of blur: very blurred (VB), medium blurred (MB), and lightly blurred (LB). (Adapted from Bruner & Potter [10])

In the last dozen years, there has been much interest in blurring stimuli [30, 25, 68, 43, 29, 75, 7, 21, 89, 51]. Loftus *et al* [51] blurred versions of commonly recognizable faces (Figure 1) by Fourier-transforming the display from pixel space into spatial-frequency space, multiplying the resulting frequency amplitude spectrum by a low-pass filter and inverse-Fourier transforming the result back into pixel space. Loftus *et al* found that participants remembered identifying the face in a blurrier state than their actual response; the result follows the hindsight bias effect [19] demonstrating that people report that an event was more likely to have occurred afterwards than at the actual time.

Figure 1: Different levels of blurred image. (Adapted from Loftus & Harley [51])

2.2.2 Degrading Stimuli by Lowering Contrast

Other researchers degraded stimuli by reducing contrast. Harley, Dillon, & Loftus [30] employed low and high contrast levels and found that performance improved with longer stimulus durations; performance increased from low contrast to high contrast conditions. The authors formulated a multiplicative model of stimulus contrast and stimulus duration; their model states that stimulus contrast and stimulus duration multiply together to yield information. They proposed that a stimulus can be represented by a rectangular function, *f(t)*, with a width of stimulus duration and an amplitude of stimulus contrast. The authors then explain that the sensory response function, $a_\theta(t)$, convolves *f(t)* with the impulse response function. In their model, information, *I(t)* is the integral over time of *r(t)*. Finally, the rate, *r(t)*, which information is extracted from the stimulus is proportional to the product of $a_\theta(t)$ and [1-*I(t)*], see Equation 1, where $A_\theta(t)$ is the integral under $a_\theta(t)$ from 0 to t.

$$I(t) = 1.0 - e^{-A_\theta(t)/c} \tag{1}$$

2.2.3 Degrading Stimuli by Block Averaging

In addition to blurring images, some researchers [31, 70] have degraded displays by block averaging the full resolution display, Figure 2. Block averaging divides the original image into an equal number of subregions and then computes the average intensity of each subdivision. Harmon and Julesz found that block averaged images are difficult to identify. The authors demonstrated that blurring a block averaged image improves recognition.

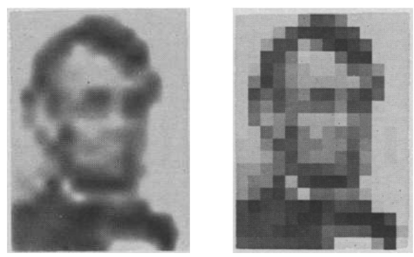

(a) (b)

Figure 2: Degraded image of President Lincoln: *(a)* blurred, *(b)* block averaged. (Adapted from Harmon & Julesz [31]).

2.2.4 Visual Search

In studying attention experimenters can instruct subjects to search by either: (1) feature, or (2) conjunction [83, 84, 85]. The two search models differ by the number of attributes: feature search involves one required essence, whereas conjunction search requires combining two features. An example of feature search is instructing participants to located the letter J in a display filled with different letters of the alphabet, Figure 3.

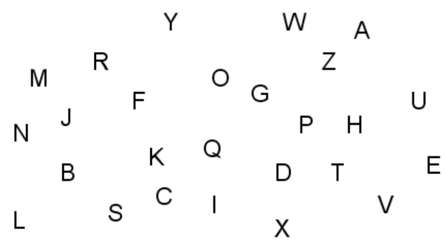

Figure 3: Example of visual search. Task to find letter "J"

In a conjunction search task, subjects could be asked to identify whether a *red vertical* bar is in a display of *green vertical* and *red horizontal* distractors, Figure 4.

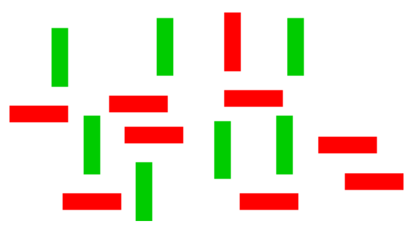

Figure 4: Example of conjunctive search. Task to find red vertical bar. Adapted from Kristjánsson, Wang & Nakajama [49]

Quinlan and Humphreys [67] demonstrated that the number of relevant shared features affected the *rate* of search. They found that the response times increased with larger numbers of display elements, Figure 5. The authors stated that the speed of search in the two-feature condition was slower than in the one-feature condition; they stated that subjects were three times slower in the conjunction condition than in the feature condition.

2.2.5 Priming

Researchers have studied the effect of perceptual priming [94, 61, 79] on pattern recognition. Perceptual priming is an unconscious form of short-term memory [94],

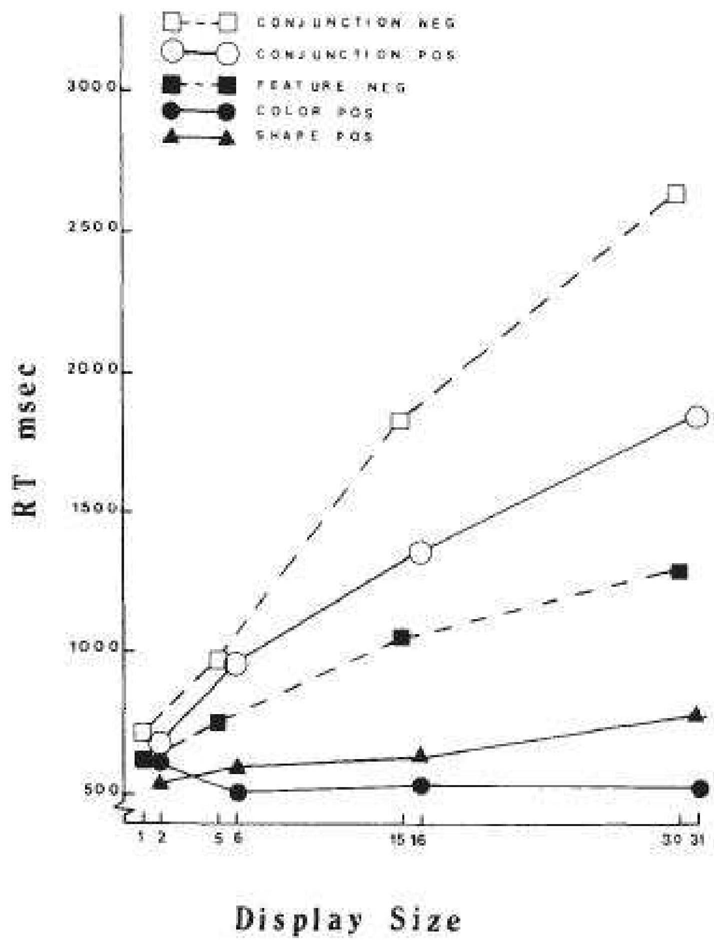

Figure 5: Effect of number of display elements on response time (RT) search [67]

and if properly timed enhances identification of perceptual objects [86]. Age does not seem to degrade priming ability; older adults do not differ from younger adults in perceptual priming tasks [74].

In 1935 J.R. Stroop [80] developed an experiment known as the Stroop test: a classic example of stimulus feature interference. Stroop asked subjects to say the ink color of a word. In half the trials the ink color matched the word; in the other half the ink color was different than the word. Subjects were instructed to correct themselves if they realized they made an error. If subjects failed to correct the error, then the experimenter added twice the average response time per word. For example, participants took longer to respond to the word *blue* written in *green* ink, than the word *blue* written in *blue* ink, Figure 6. Stroop found that subjects were significantly slower (average of 2.3 sec longer) in naming the ink color when it was incompatible with the word, Figure 7. The results suggest that semantic processing occurs first and then color of the word interferes with naming of conflicting ink color.

(a) (b)

Figure 6: Stroop test. Subjects instructed to name the ink color. *(a)* blue ink and word spelled blue (no interference), *(b)* took longer to say "green" when word spelled "blue" (interference).

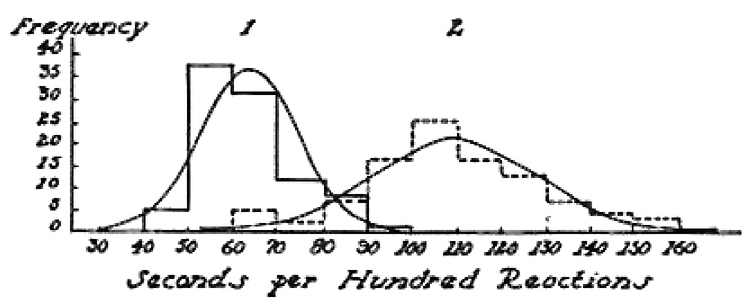

FIG. 1. Showing the effect of interference on naming colors. No interference (1); interference (2).

Figure 7: Response Time effect of interference on naming ink colors: *(1)* no interference, *(2)* interference. [80]

Tipper [82] extended Stroop's work to generalize stimulus feature interference. Tipper designed experiments in which subjects were instructed to identify the target (red letter) in each of two sequential displays: *prime* then *probe*. Tipper used 3 conditions: *(1)* attended, *(2)* control, and *(3)* ignored, Figure 8. In the attended prime condition, a red target letter was presented with a different color occluded letter. The control condition featured a red non-target letter with a non-target overlapping letter. During ignored prime conditions, the prime distractor was the same as the probe target. Tipper found that individuals' response times were fastest in the attended prime condition, slower in the control prime condition, and slowest in the ignored prime condition. Tipper named the effect *negative priming*.

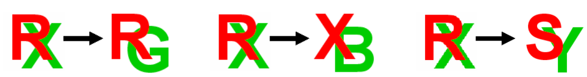

(a) (b) (c)

Figure 8: Example of Negative Priming. Task: name the red colored letter and ignore green letter in Probe condition, measured subjects' response times. *(a)* Prime displayed for 1 sec (attended condition) *(b)* Probe (ignored condition). If ignored letter in prime is the attended to target in the probe, then subjects' naming latency was impaired, *(c)* Control condition

2.2.6 Masking

In addition to priming, the psychophysics paradigm of pattern masking was used in the experiments below. There are two types of masking: *(1)* pattern masking, and *(2)* metacontrast masking [18]. Pattern masking has the spatial characteristic of the mask obscuring the target. Metacontrast masking involves a mask closely resembling the contours of the target. The temporal characteristics come in two types: *(1)* integration or *(2)* interruption. Integration masking occurs when the target and mask appear at a stimulus onset asynchrony (SOA) of zero and functions to add noise (mask) to the signal (target) during early stages of visual processing [18].

Interruption temporal masking happens when the mask appears before the target has been fully processed and creates competition for higher-level cortical resources [87].

Masking was used in the following experiments to minimize afterimages [77], Figure 9. Afterimages are produced by extended viewing of a stimulus leading to adaption in retinal cones. For example, if a subject stares at a red X on a black background for about 20 sec and then looks at a black background, he will see an afterimage of a green X. The opponent color theory [41] helps to explain why we see a green X afterimage; the theory postulates two antagonistic color channels: *(1)* red-green and *(2)* blue-yellow. The red-green opponent system receives input from only the L (long wavelength) and M (middle wavelength) cones. The green X illusion is due to adaption of the red-selective cones causing them to reduce firing on account of hyperpolarizing response to the red X stimulus.

(a) (b)

Figure 9: *(a)* Subject stared at red X for 20 sec, *(b)* subject saw green X afterimage.

McCollough [57] found that alternating between staring at a red horizontal grating and a green vertical grating, caused a black and white horizontal grating to appear green and a black and white vertical grating to appear red. The McCollough effect can last hours.

2.3 General Methods

2.3.1 Monitor and Graphics Card

Stimuli were displayed on a ViewSonic VA1912wb LCD monitor with a resolution of 1440x900 and contrast of 70%. The monitor was set by an "Nforce" Nvidia graphics card. Matlab graphics commands formatted the display. The same monitor was used in all experiments.

2.3.2 Participants and IRB approval

Table 3 shows the number of participants in each experiment. 15 out of the 34 subjects participated in only one experiment. Participants were Brown University undergraduates, graduate students, and one professor.

Experiment	# Subjects	Gender	Age
1. Converging *vs* Single Resolution Stimuli	3	all male	19 - 22
2. Priming	5	all male	19 - 62
3. Masking	4	3 male 1 female	19 - 30
4. Variable Peaks	5	3 male 2 female	19 - 30
5. Just Noticeable Difference	3	all male	19 - 30
6. Visual Acuity	6	all male	19 - 62
7. Visual Acuity with Deviated Prime	5	all male	19 - 62
8. Gray Screen Test	3	all male	19 - 62

Table 3: Number, gender, and age range of participants in each experiment. Total of 34 subjects.

The experiments were approved by Brown University's Institutional Review Board (IRB), see Appendix B for IRB-approved protocol, script, and consent forms.

2.3.3 Navigation Field

The author wrote code in Matlab to generate a horizontally and vertically symmetric (4-fold) field, resembling moguls, defined by Equation 2 with a period of 3 units and amplitude from -2 to 2, Figure 10. The mogul field appeared continuous to a subject. The field measured 19° x 19°, with the subject viewing the screen from 57 cm.

$$z = \cos\frac{2\pi}{3}x + \sin\frac{2\pi}{3}y \tag{2}$$

50 units of the field measured 19cm for a spatial frequency of 0.9 cycles/deg formed a reasonable density of peaks and troughs for a subject to explore. The field was divided into 4 quadrants and each quadrant was rotated by $\frac{\pi}{8}$ to minimize subjects extrapolating the field beyond the locally exposed patch, Figure 11. Figure 12 shows a tilted view of rotated field with cyan to magenta colormap elevation scale.

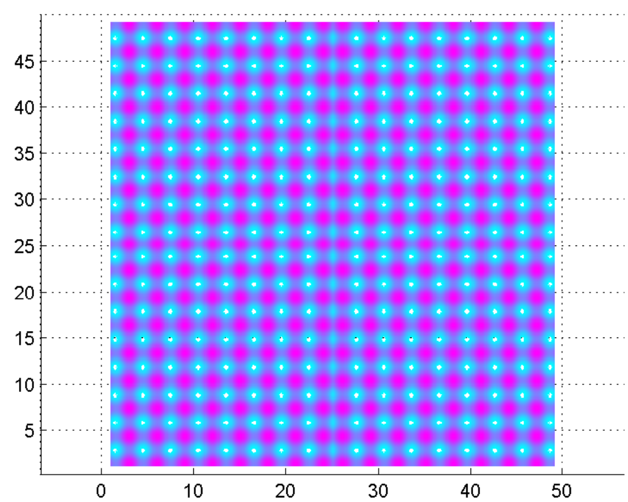

Figure 10: Cyan to Magenta field generated by $z = \cos\frac{2\pi}{3}x + \sin\frac{2\pi}{3}y$ with a period of 3 units and amplitude ranging from 2 to -2 (magenta = 2, cyan = -2). Color varies from cyan to magenta.

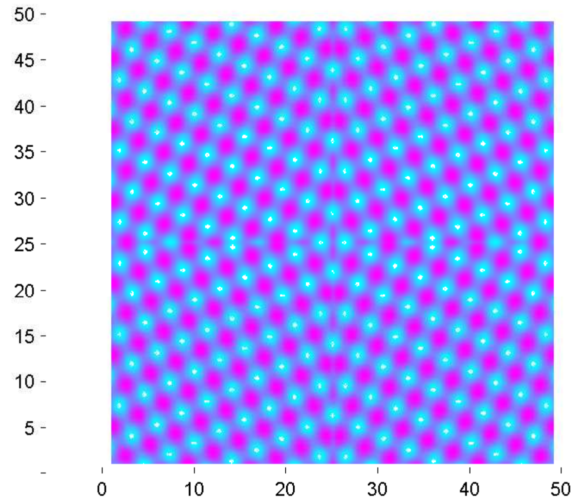

Figure 11: Symmetric field divided into 4 quadrants and each quadrant rotated by $\frac{\pi}{8}$

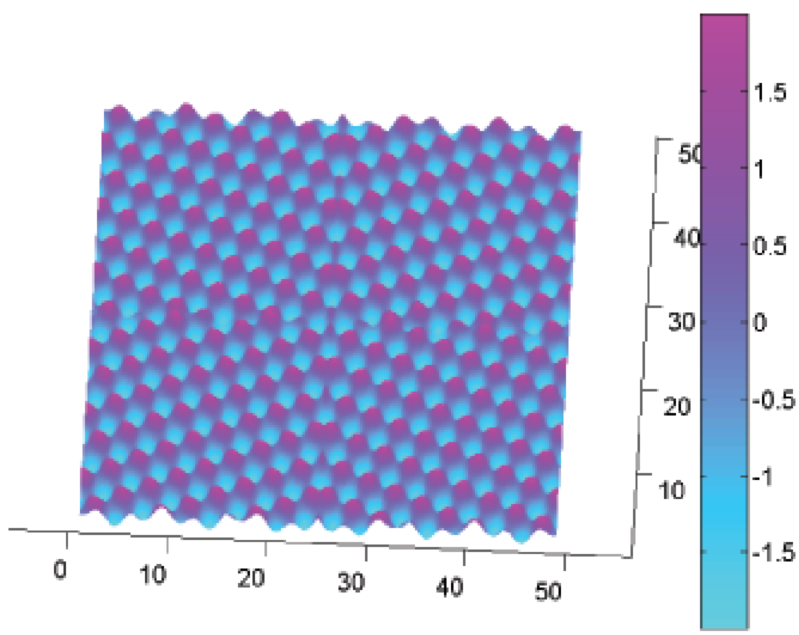

Figure 12: Tilted view of rotated field with cyan to magenta colormap elevation scale.

2.3.4 Converging Stimuli

Converging stimuli consisted of time series squares of block-averaged colors, Figure 13.

Levels of color resolution were computed by averaging the elevations in each subregion and using the Matlab colormap: cool (ranging from cyan to magenta). The RGB color values for pure cyan were [0 255 255] and RGB color values for magenta equal [255 0 255]. In level 1 the colors of all the pixels in the whole patch were averaged together to yield one solid color region (Figure 13a), level 2 is 4 (2^2) subregions (Figure 13b), and so on up to level 10 (100 subregions), (Figure 13g).

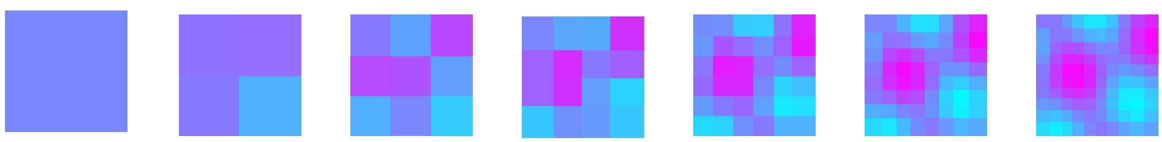

(a) (b) (c) (d) (e) (f) (g)

Figure 13: Catalog of levels of resolution (1, 2, 3, 4, 6, 8, 10). *(a)* Level 1 (one region), *(b)* Level 2 (4 subregions), *(c)* Level 3 (9 subregions), *(d)* Level 4 (16 subregions), *(e)* Level 6 (36 subregions), *(f)* Level 8 (64 subregions), *(g)* Level 10 (100 subregions)

2.3.5 Single-resolution Stimuli

Single-resolution stimuli were level 10 block-averaged patches, Figure 13g.

2.4 Experiment: Just Noticeable Difference of Hue

2.4.1 Introduction

The accuracy with which subjects could differentiate nearby instances of the cyan to magenta colormap was examined, Figure 14.

There are two models used to describe colors: *(1)* additive, and *(2)* subtractive [39]. In the additive model there are three primary colors (red, blue, and green) that can mix in equal amounts to produce secondary colors: magenta (red and blue), cyan (blue and green), yellow (red and green), and white (red and blue and green). The subtractive model describes how the secondary can be mixed in equal amounts to yield: red (magenta and yellow), green (cyan and yellow), blue (cyan and magenta), and black (cyan and yellow and magenta).

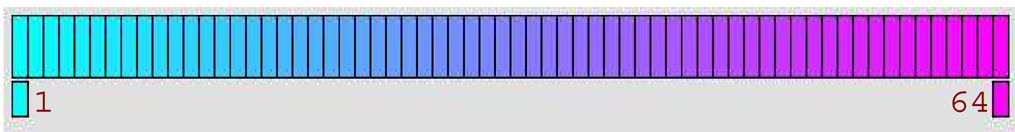

Figure 14: Colormap scale ranging from cyan (index = 1) to magenta (index = 64).

Investigators have shown in the visible spectrum (red to violet), humans can differentiate small changes in wavelength ($\lambda + \delta\lambda$), measured by just-noticeable-difference (JND) [60, 52, 96, 90, 26, 9]. Bedford and Wyszecki [9] found three local minima at 440, 480, and 575 nm with wavelength differences of about 3, 1.5, and 1.5 nm respectively. However, the author is the first to test human hue discrimination using equiluminant [15, 50] stimuli ranging from cyan to magenta (not part of the red to violet spectrum).

2.4.2 Methods

Two-alternative force-choice (2AFC) [45] was used in this experiment. Participants viewed 2 stimuli of patches of the colormap for 1 sec, followed by a mask for 200 msec. A black screen then appeared indicating that the subject should enter their response by pressing "1" for same or "3" for different on the number pad of the keyboard. They had unlimited time to enter their response, Figure 15. Each trial consisted of 64 random presentations. 32 presentations were of equal-hue stimuli, the other 32 were all the same colormap separation, 1 to 6 of the 64 steps (Figure 14), thus each subject went through 6 trials. Half the stimuli of each trial were the same and the other half were different. Each stimulus measured 4° x 4°. The distance between each stimulus was 1° to minimize edge effects.

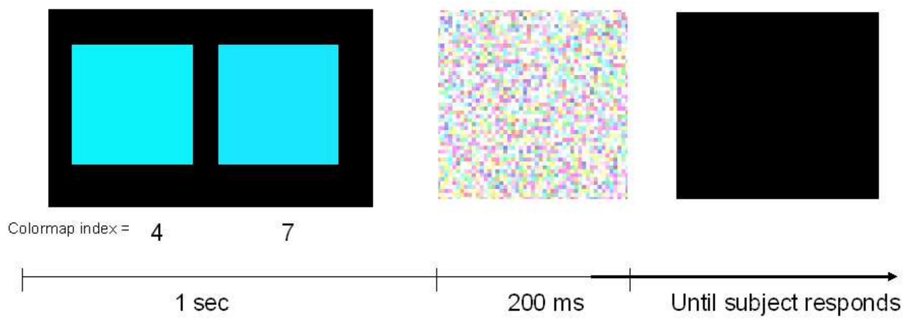

Figure 15: Schematic of just noticeable difference protocol. Participants viewed 2 stimuli for 1 sec, followed by a mask for 200 msec. A black screen then appeared indicating that the subject should enter their response by pressing "1" for same or "3" for different. They had unlimited time to enter their response.

2.4.3 Results

Discriminability of pure cyan and 6 indices from pure cyan is no harder to detect than pure magenta and 6 indices from pure magenta, Figure 16.

The number of incorrect responses when the same stimuli were presented are shown in Table 4.

The number of correct responses when different stimuli were presented for each

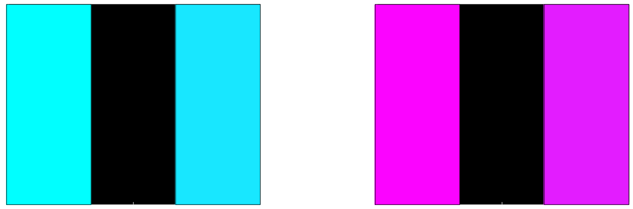

(a) (b)

Figure 16: *(a) left* pure cyan, *right* cyan index 6 away, *(b) left* pure magenta, *right* magenta index 6 away.

Index away	1	2	3	4	5	6
JT	14	10	6	2	3	2
JGR	16	12	5	1	4	4
HG	5	3	2	0	0	0
Totals	35	25	11	3	7	6

Table 4: Number of incorrect responses when the same stimuli were presented for each index away. 32 same stimuli were presented for each index separation.

trials of number of indices away is shown in Table 5.

Participants' performance (measured by percent correct) increased as the number of indices separating each stimulus increased, Table 6, Figure 17.

2.4.4 Discussion

Sensitivity and specificity of subjects' responses through signal detection analysis of hit rates and false alarms was examined, Figure 18. For index separation of 1 (Figure 18a) the *d'* value (difference between means of the Signal Absent and Signal Present curves) of 0.72 and criterion value (measure of eagerness of a participant to respond that the signal was present) of 0.37 indicated that participants were giving

Index away	1	2	3	4	5	6
JT	14	10	8	7	7	2
JGR	16	15	11	9	12	5
HG	24	17	11	7	7	0
Totals	34	32	30	21	25	7

Table 5: Number of correct responses when different stimuli were presented for each index away. 32 same stimuli were presented for each index separation.

Indices away	JGR	JT	HG	Mean
1	0.516	0.563	0.547	0.542
2	0.578	0.688	0.688	0.651
3	0.895	0.781	0.797	0.824
4	0.891	0.859	0.891	0.880
5	0.938	0.845	0.891	0.891
6	0.906	0.938	1.0	0.948

Table 6: Participants' performance (measured by percent correct) increased as the number of indices separating each stimulus increased.

the response "same" equally as often for when the stimuli were the same as when the stimuli were different. Whereas, index of separations greater or equal to 3, had criterions greater than 1.5 indicating that the subjects were discriminating between the indices and not simply responding "same" to everything.

When colors were separated by 3 or more indices, subjects average at least 82.4% correct. Participants' performance decreased to about chance (50%) when faced with deciding between two stimuli that were separated by one color map index (difference of ±4 red or green pigments).

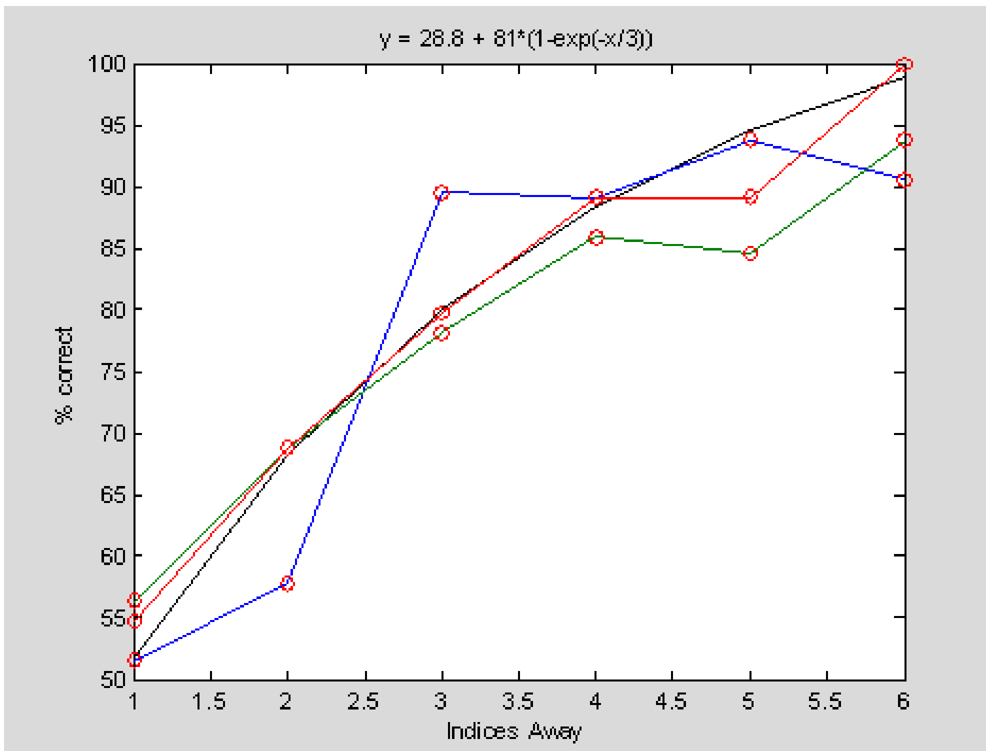

Figure 17: Participants' performance (measured by percent correct) increased as the number of indices separating each stimulus increased. Best fit line (black).

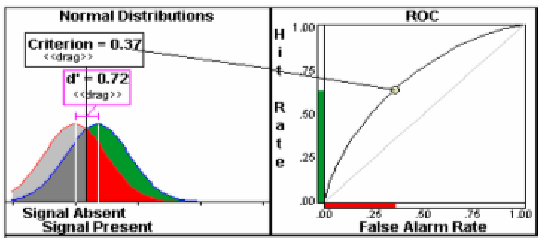

(a)

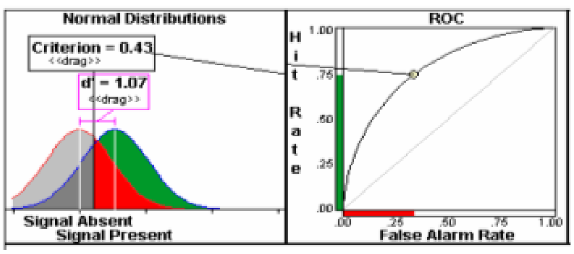

(b)

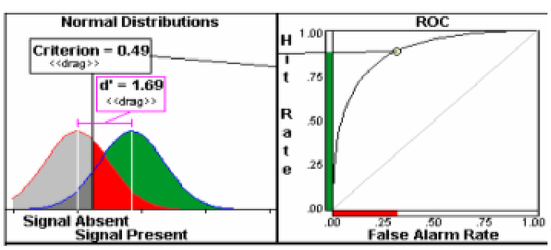

(c)

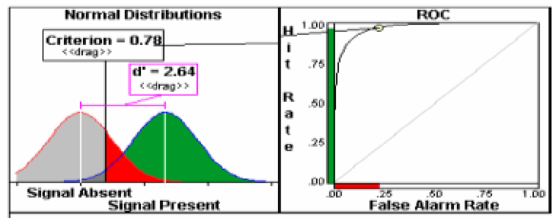

(d)

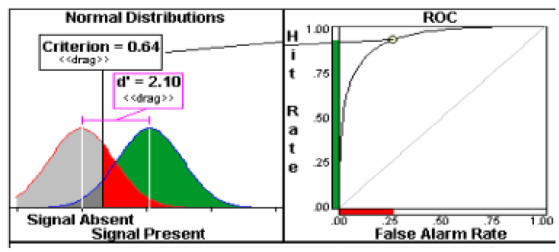

(e)

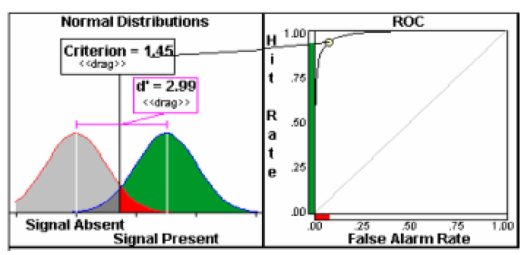

(f)

Figure 18: Indices apart: *(a)* 1, *(b)* 2, *(c)* 3, *(d)* 4, *(e)* 5, *(f)* 6.

2.5 Experiment: Converging *vs* Single Resolution Stimuli

3 subjects each viewed a random mix of 10 converging and 10 single resolution stimuli. Participants were instructed to identify, locate, and click the brightest shade of magenta in the target patch, Figure 19.

A schematic of a converging stimulus is shown in Figure 19 and a single-resolution stimulus in Figure 19. A converging stimulus changed levels of resolution every 650 msec, after which the stimulus changed to a gray patch indicating the response screen. The gray patch remained on the screen until the participant entered their response by clicking the location where they best remembered the location with the purest shade of magenta.

For single resolution stimuli, a "+" symbol appeared for 500 msec prior to onset of the stimulus. Subjects were asked to fixate on the "+" sign, participants were told that a single-resolution image would follow. The fixation point helped to prevent subjects from making a saccade when a single-stimulus was displayed. A single-resolution stimulus remained on the screen for 650 msec, followed by a gray patch indicating the response screen.

The mouse cursor was hidden during the stimulus presentation, but appeared in the form of crosshairs during the response period. The location of the mouse was randomly reset after a click to prevent a subject from remembering how far from their last click to move the mouse to their new selection point. Participants had unlimited time to click a spot in the response patch where they best remembered the most saturated hue of magenta was located.

At the end of the experiment, the subject's average score (maximum of 2: purest magenta, and minimum of -2: purest cyan) was displayed and the subject was told that if their score was greater than 1.75, they would receive a candy reward. The score was computed by taking the mean of the locations which they clicked during the trial. Mean converging and single resolution scores were also calculated.

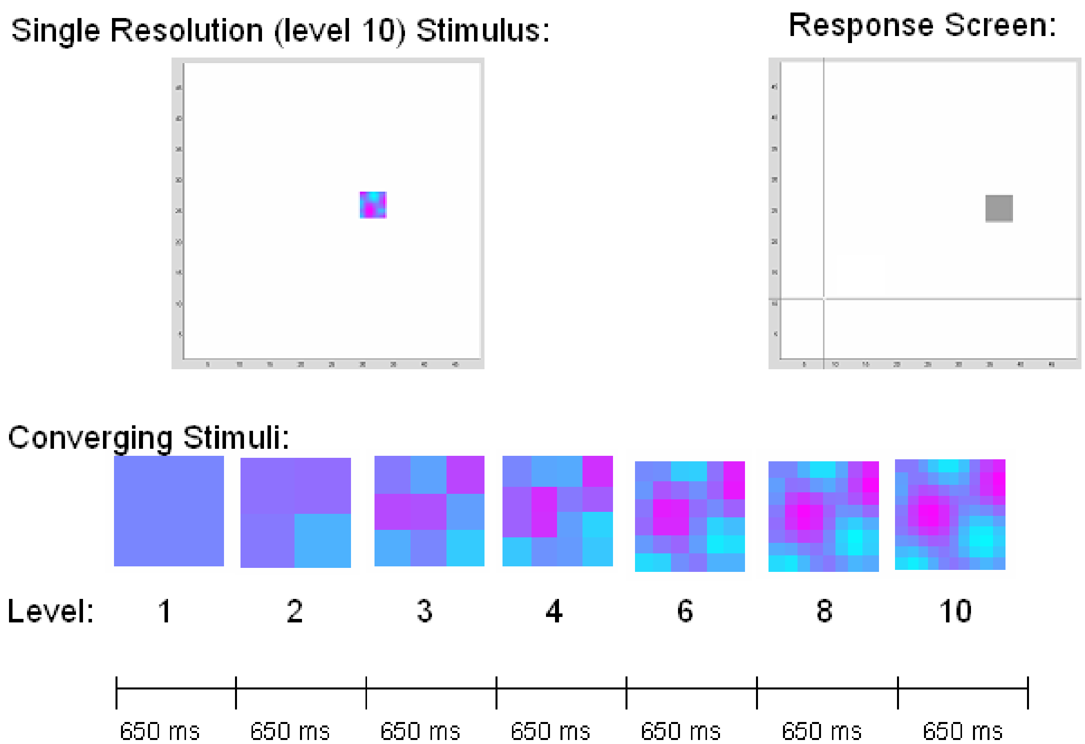

Figure 19: Schematic of visual protocol. *Top Left*: Example of a single-resolution stimulus (level 10 only) displayed for 650 msec. *Top Right*: Response screen with mouse cursor in the form of crosshairs which participants used to enter their selection for the place where they best remembered the most saturated pure shade of magenta. *Bottom*: Participants viewed a level 1 resolution stimulus for 650 msec, followed by levels 2, 3, 4, 6, 8, 10 (each for 650 msec). After the level 10 resolution stimulus, a response screen appeared indicating that the subject should enter their response; they had unlimited time to enter their response by clicking the location on the screen where they best remembered the most pure shade of magenta to have been situated.

2.5.1 Results

Subjects achieved a mean score of 1.894 (out of a maximum of 2) when viewing a converging stimulus and a mean score of 1.834 with a single-resolution stimulus, Table 7. Participants were not significantly better with converging stimuli than single resolution stimuli ($p = 0.208$).

t-Test	Conv	Single
Mean	1.894	1.834
Std Dev	0.1449	0.2145
# Subjects	3	3
p-value two-tail	0.208	

Table 7: Participants were not significantly better with converging stimuli than single resolution stimuli.

2.5.2 Discussion

The mean converging stimuli score (1.894) was not significantly different than the mean single-resolution score of 1.834. Bruner and Potter [10] found that converging information decreases performance because participants generate multiple hypotheses, many of which are incorrect. However, the results demonstrate that subjects do not seem to be distracted by multiple hypotheses even when that information is of low quality.

2.6 Experiment: Low Resolution (Level 4) Priming

2.6.1 Methods

Primes were either valid (same orientation as target) or invalid (rotated orientation to target), Figure 20. Subjects were told to identify the purest shade of magenta in the target patch (second stimulus), Figure 21. Participants viewed 10 valid primes and 10 invalid primes in a random order.

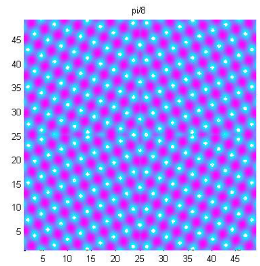

(a)

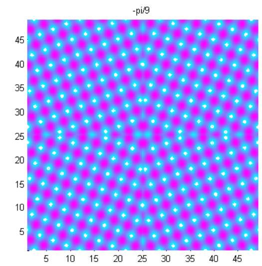

(b)

Figure 20: Fields: *(a)* normal used for valid priming, *(b)* rotated by -$\frac{\pi}{9}$.

2.6.2 Results

The mean score for subjects viewing a valid prime was 1.852 (out of 2), and participants scored 1.791 with an invalid prime, Table 8. Participants were not significantly better when viewing valid primes than invalid ones.

t-Test	Valid Prime	Invalid Prime
Mean	1.852	1.791
Std Dev	0.1342	0.2498
# Subjects	5	5
p-value two-tail	0.5089	

Table 8: Participants were not significantly better with valid primes than invalid primes.

2.6.3 Discussion

Mean valid prime (aligned with target) scores (1.852) were less than the mean converging score of 1.894 and the mean invalid prime score (1.791) was less than the mean single score of 1.834. Valid prime information did not significantly assist subjects in the task by guiding their hypotheses of the location of the purest hue of magenta.

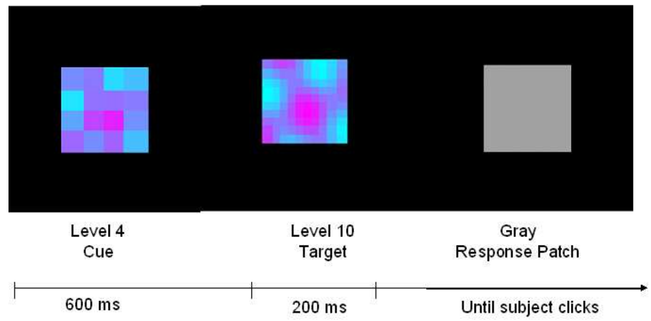

Figure 21: Schematic of priming protocol. Participants viewed a level 4 resolution stimulus for 600 msec, followed by level 10 for 200 msec. After the level 10 resolution stimulus, a gray response screen appeared indicating that the subject should enter their response; they had unlimited time to enter their response by clicking the location on the screen where they best remembered the purest hue of magenta to have been situated.

Since there was not signficant difference, priming was not needed in the navigation game (Chapter 3).

2.7 Experiment: Priming and Masking

2.7.1 Methods

The mask was generated using the Matlab Image Processing toolbox function "imnoise" from a random set of numbers. For example: rndimge = rand*ones(200,200); rndimge2 = imnoise(rndimge); imshow(rndimge2). The same mask was used in all trials.

Participants viewed a level 4 resolution stimulus (prime) for 600 msec, followed by level 10 for 200 msec. After the level 10 resolution stimulus, the mask was presented for 500 msec. A gray patch then appeared indicating that the subject should enter their response. The task was for subjects was to click the location on the screen where they best remembered the purest shade of magenta to have been situated with unlimited time to enter their response, Figure 22. Subjects ran 20 trials, 10 with valid primes (same orientation as target) and 10 with invalid (rotated orientation to target) in a random order.

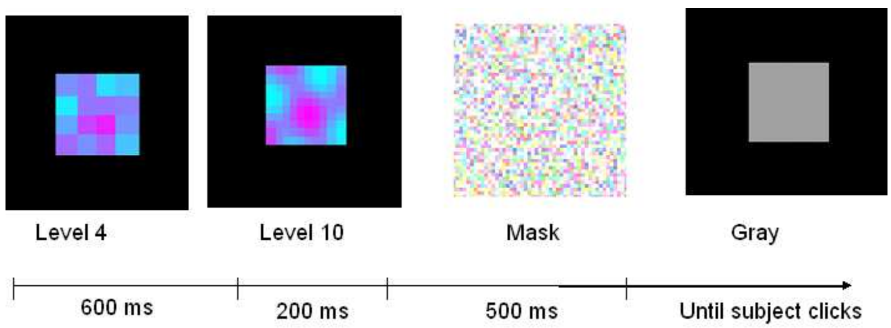

Figure 22: Schematic of masking protocol. Participants viewed a level 4 resolution stimulus for 600 msec, followed by level 10 for 200 msec. After the level 10 resolution stimulus, the mask occured for 500 msec. A gray patch then appeared indicating that the subject should enter their response; they had unlimited time to enter their response by clicking the location on the screen where they best remembered the purest hue of magenta to have been situated.

2.7.2 Results

Participants scored more points when the prime was aligned with the target than when misaligned, Table 9. The difference in score for valid primes (1.839) *vs* a negatively rotated prime (1.761) was not enough to be statistically significant due to variance in the estimates.

t-Test	Valid	Invalid
Mean	1.839	1.761
Variance	0.117	0.202
# Subjects	5	5
p-value two-tail	0.315	

Table 9: Participants were not significantly better with valid primes than invalid (negatively rotated) primes with mask following the target.

2.7.3 Discussion

The performance of participants with priming and masking demonstrated that even with the addition of a mask to help reduce afterimage effects, subjects did not achieve significantly higher scores when viewing valid primes than with invalid primes. Participants scored about the same in this experiment (mask present) as in the cue-only experiment suggesting that subjects were not affected by the mask and that afterimages did not seem to affect subjects. Therefore, masking was not necessary for the navigation game (Chapter 3).

2.8 Experiment: Visual Discrimination

Since the navigation experiment (Chapter 3) involved learning that magenta colored areas represented higher scores, subjects' performance in discriminating the purest hue of magenta was tested by varying width (area) of magenta regions.

2.8.1 Methods

Participants viewed 20 trials of 4 magenta circular regions on a cyan background for 2 sec, followed by the mask for 500 msec, after which a black response screen appeared. Subjects were instructed to locate the purest shade of magenta in the target screen and click the position in the black response screen where they best remembered the location, Figure 23. Peaks (magenta) of stimuli were constant 3 colormap indices different from each other.

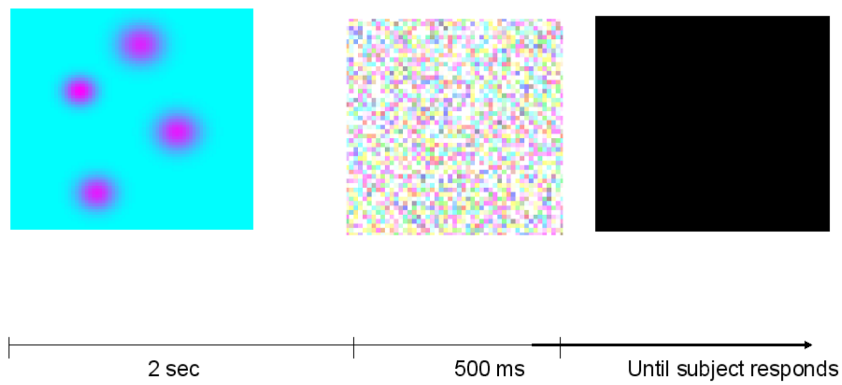

Figure 23: Schematic of visual acuity protocol. Participants viewed 4 magenta circular regions in random positions on a cyan background for 2 sec, followed by the mask for 500 msec. After which a black response screen appeared. Subjects had unlimited time to enter their response by clicking the location on the screen where they best remembered the purest shade of magenta to have been situated.

2.8.2 Results

Subjects picked the purest shade of magenta region in 84 out of the 120 trials, see Figure 24. Participants correctly identified the purest shade of magenta region in the widest regions in 32 out of the 84 trials.

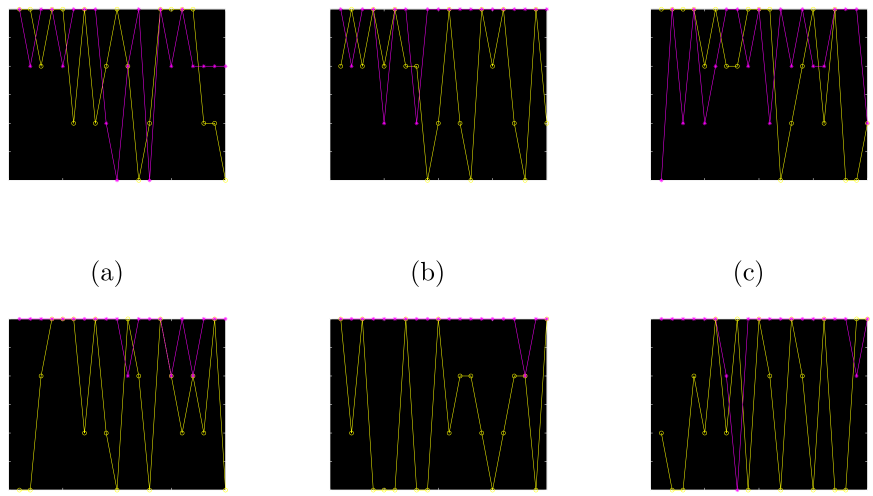

(a) (b) (c)

(d) (e) (f)

Figure 24: Subjects picked the purest shade of magenta region in 84 out of the 120 trials. X axis = Trial. Y axis = magenta hue and width of peak (yellow curves = region width; magenta curves = magenta hue selected by subjects).

The mean ranking of magenta was 3.62 (with 4.0 representing the region with the purest shade of magenta) and a standard deviation of 0.75, see Table 10. On average, subjects clicked 5.08° from the peak of the the region they selected.

	Region Selected	Distance to Peak (degree visual angle)
Mean	3.62	5.08
Std Dev	0.75	2.7

Table 10: Mean and standard deviations for region (4 = purest shade of magenta) and distance (degrees of visual angle) to peak magenta of region.

2.8.3 Discussion

The relationship between width of peak and purest hue of magenta of stimuli was examined. In the sinusoidal field there was a correlation of 0.980 between width-of-peak and hue. In the visual discrimination experiment with random isolated peak regions, there was a correlation of 0.62. Participants correctly identified the region with the purest shade of magenta in 70% of the trials. Subjects were 12.4% better in the just-noticeable-difference (JND) task than in the visual discrimination task. Since there were 4 stimuli simultaneously presented in the visual discrimination task, subjects made more saccades than in the JND; the additional items in the display led to more errors.

2.9 Experiment: Gray Screen Test

Subjects' performance was examined when presented with a stimulus patch void of any cyan or magenta colors. A gray patch appeared in 20 random positions, and each participant was instructed to click a point anywhere in the gray patch. Subjects had as much time per presentation as they desired before clicking, Figure 25.

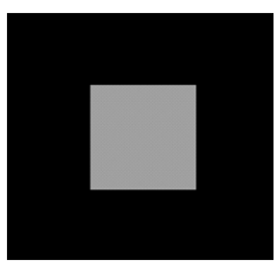

Figure 25: A gray patch appeared in 20 random positions. Subjects had as much time per presentation as they desired before clicking.

2.9.1 Results

Subjects scored approximately zero when clicking on a gray patch, Table 11.

Subject	Score	Stimulus
JGR	0.0102	Gray only
JDD	0.088	Gray only
JT	0.12	stared at field for 1 min then gray only

Table 11: Subjects scored approximately zero when clicking on a gray patch

2.9.2 Discussion

Subjects scored approximately zero when viewing a solid gray patch. The result suggests that when subjects are not given any color representations of the terrain, they randomly select locations that are neither peaks nor troughs. One subject was instructed to stare at the full resolution sinusoidal terrain for one minute prior to the gray patch stimuli and produced score slightly above zero.

2.10 Saccades made while inspecting regions

A subject's saccadic eye movements was tested while the subject looked at a horizontal arrangement of peaks. A participant took a total of 1200 msec to look to the far right then in steps to the left then directly to the center, Figure 26.

Saccades were investigated while looking at random positions of peaks, Figure 27. Random arrangement of peaks took a subject 1800 msec to survey the entire terrain compared to 1200 msec in the linear arrangement.

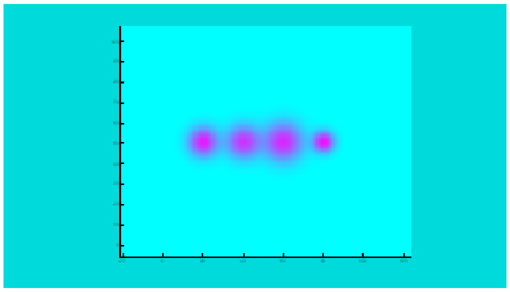

(a)

(b)

Figure 26: Saccadic movements while viewing a series of horizontally arranged magenta peaks. Subject looked to the far right then in steps to the left then directly to center. Scales = 100 mV/division and 200 msec/division. (a) Linear arrangement of magenta regions, (b) upwards excursions indicate rightward saccade, downwards indicates leftwards.

A subject took longer to view each of the stimuli in a nonlinear arrangement than when the stimuli were in a linear arrangement. Perhaps when confronted with novel, non-linear arrangements, the subject had to decide which order and locate where the peaks were situated before making saccades. The distance between regions was greater in the nonlinear arrangement which could have led to longer overall time to saccade to each region.

2.11 Summary

The just-noticeable-difference between indices of the cyan to magenta colormap was 3. The relevance for the navigation game was that as subjects learned that clicking magenta colors produced higher scores, they could discriminate at most between 3 hues of magenta.

There was no significant difference between converging and single resolution stim-

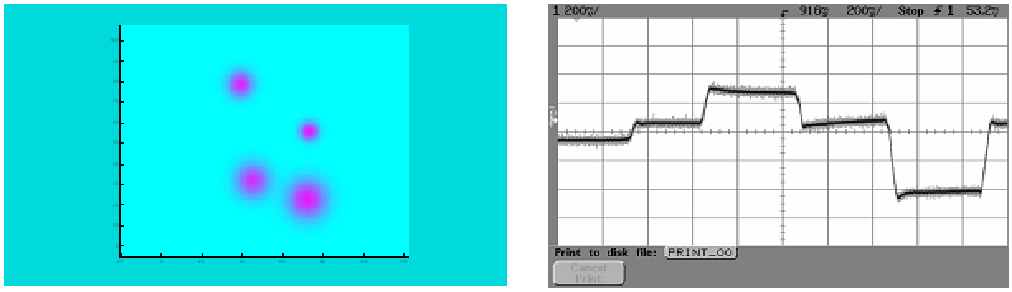

(a) (b)

Figure 27: Saccadic movements while viewing a series of randomly arranged magenta peaks. *(a)* Stimuli in random arrangement. *(b)* Scales = 200 mV/division and 200 msec/division. Upwards excursions indicate rightward saccade, downwards indicates leftwards.

uli. The implication for the navigation game (Chapter 3) was that prior to any possible learning effects developed through playing the game, there was no advantage of converging *vs* single resolution stimuli.

Since priming and/or masking had no significant effect on subjects' performance, then there was no need to prime or mask the stimuli in either the converging or single resolution conditions of the navigation game (Chapter 3).

3 Navigating with Uncertainty

3.0.1 Definitions

The Oxford English dictionary defines navigation as the following:

(1) The action or practice of directing the course of a motor vehicle; map-reading for, or the giving of directions to, the driver of a motor vehicle

(2) the science of getting ships, aircraft, or spacecraft from place to place; especially : the method of determining position, course, and distance traveled

3.1 Introduction

We sometimes need to drive in snowstorms with reduced visibility. When visibility is poor, viewing distance is decreased making it hard to see far in front of the car. In such inclement conditions, one needs to avoid icy spots and estimate increased braking distance. Drivers must learn navigation strategies to cope with diminished quality of sensory information.

Humans encounter the tradeoff between information quality (see Appendix A for definition) and performance (Appendix A) in common experiences (Table 12). For example, a driver could decide to speed at 95 mph on a curvy highway, such as the Pacific Coast Highway, trying to get to his destination. However, he might miss the sign for his exit and cause him to take a longer route. Alternatively, he could drive cautiously at 40 mph and process all the scenery and road signs while taking much longer to reach his destination. In both cases, performance is less than optimal:

a moderate speed would allow for better processing of the surroundings and allow him to arrive at his destination without detours. In the following navigation game, subjects were instructed to navigate from a start position to a goal while viewing a small patch (degraded in resolution) of the terrain.

Activity	**Possible Risks**
driving	ice
biking	cars
hang gliding	wind and cliffs (other obstacles)
sailing	buoys, wind, waves and other boats
rock climbing	rock formations, equipment failure and other climbers
skiing	goggles mist difficult to view course

Table 12: Examples of activities

3.2 Previous Work

Rushworth and Behrens [73] state that exploratory behavior is modulated by at least 2 factors:

(1) expected immediate cost and return on that action

(2) expected degree to which the information obtained from making the action might influence future predictions.

Foo, Warren, Duchon, and Tarr [20] suggest 5 types of navigation (exploratory) strategies with increasing complexity:

(1) guidance: travel in relation to a beacon

(2) landmark: orient to a known object

(3) path integration: update distance and direction traveled from start position

(4) route-based: remembering sequences of positions

(5) map-based: knowledge of the environment

The navigation game developed and discussed below would be most similar to Foo *et al*'s map-based system of navigation.

3.2.1 Version of Navigation

Navigation in the context of the experiments below can be described as: virtual traveling to destination on a route that appears to be accumulating the best score based on local terrain feedback with uncertainty beyond the local view. Real world examples of similar navigation are shown in Table 13.

Orienteering
Racecar Driving
Sailing
Sky Diving
Technical Mountain Climbing
Skiing: Alpine, Cross-country

Table 13: Examples of navigation

3.2.2 Details of Orienteering

Orienteering in the real world is similar to the virtual, (computer screen) navigation experiments below. Both orienteering and navigating in the experiments here involve the use of visual information and path planning.

Orienteering originated in the late 19th century in Sweden and emerged from military training for overland navigation. Orienteering competitions involve navigation using a compass and map. The objective is to navigate the fastest routes between control points (marked by orange and white flags, numbered 1-4 in Figure 28) in a specific order while advancing to the finish point; the winner is the fastest to accomplish the task, Figure 28.

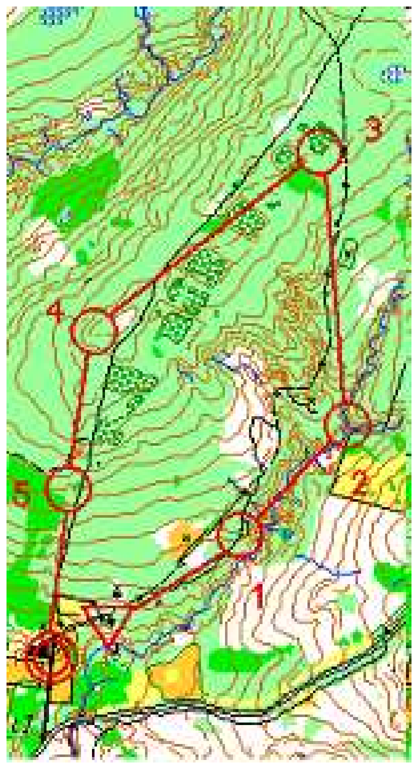

Figure 28: Example of Orienteering Map [40]. Players need to find and go to the control points (check-posts) in numerical order.

3.3 Methods

3.3.1 Virtual Terrain

An open terrain (unrestricted path) was allowed in the following navigation studies. Some features of the terrain include:

(1) peaks and valleys (elevation)

(2) constant step size of 1.8

(3) 2D spatial frequency of elevation changes (sinusoidal terrain)

3.3.2 Stimuli

2 types of visual stimuli were used:

(1) converging

(2) single resolution

Both converging and single resolution stimuli were the same as those introduced in the Visual Psychophysics experiments (Chapter 2). Converging stimuli ranged in levels of resolution from 1,2,3,4,6,8, through 10 and single resolution mode used only level 10.

3.3.3 Drone

A drone (computer algorithm) was created to compete and motivate the human player. The speed (step size) of the drone was either 1.6, 1.7, or 1.8. The drone used a Best-First-Search Algorithm.

3.3.4 Task

Subject shown:

(1) start position (solid black circle) in square patch

(2) goal position (solid blue circle)

(3) mirror image Drone start position (green circle)

(4) mirror image Drone goal position (yellow circle)

(5) subject score at top of display; drone score at bottom of display

Subject told:

(1) click any place on ring around solid black circle

(2) to step to goal while scoring as many points as possible

(3) to try to arrive at goal before Drone

(4) receive bonus points for arriving at goal before Drone

(5) if timeout, then auto-advance as-crow-flies to goal

(6) colliding with Drone may or may not assist in scoring points or getting to goal first

Subject were not told what parameters affected scoring, and there were no practice sessions, Figure 29.

3.3.5 Protocol

11 subjects (9 M, 2 F) were studied. The navigation experiments consisted of a series of 24 trials. The mode (converging or single) of the experiment repeated in

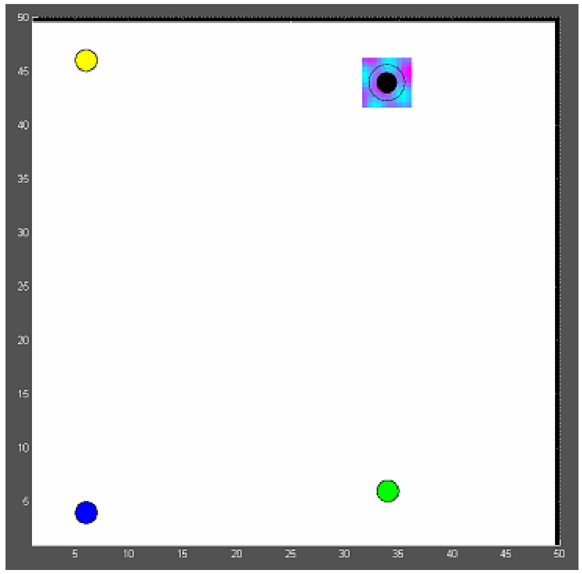

Figure 29: Navigation experiment task start screen. Player's start position (black solid circle) in square patch. Drone mirror image start position (green circle). Subject's goal (solid blue circle). Drone mirror image goal (yellow circle).

converging, single, single, converging patterns. The drone speed (step size) started at 1.6 and increased to 1.7 after 8 trials, and then to 1.8 for trials 17 - 24, Figure 30. The speed (step size) of the human player 1.8 in all trials.

3.3.6 Scoring Parameters

(1) Angle to goal: the angle between the line directly from the player to goal and the line representing the player's heading $\cos(\theta)$.

(2) Elevation (z) ranging from -2 to 2.

(3) Distance to goal from current position of player (d).

(4) Elapsed time since beginning of navigation (δt).

(5) Speed: represented by the length of step between equal time clicks or inverse length of time spent waiting for better resolution of elevation data

Trial	Stimuli	Step Size
1	C	1.6
2	S	1.6
3	S	1.6
4	C	1.6
5	C	1.6
6	S	1.6
7	S	1.6
8	C	1.6
9	C	1.7
10	S	1.7
11	S	1.7
12	C	1.7

(a)

Trial	Stimuli	Step Size
13	C	1.7
14	S	1.7
15	S	1.7
16	C	1.7
17	C	1.8
18	S	1.8
19	S	1.8
20	C	1.8
21	C	1.8
22	S	1.8
23	S	1.8
24	C	1.8

(b)

Figure 30: Protocol. (a) Trials 1-12, (b) Trials 13-24. C = converging stimuli. S = single level 10 resolution. Step size of the drone. Step size of human player always 1.8.

(6) bonus points for reaching the goal before the drone.

3.3.7 Scoring Equations

2 scoring systems were used in the experiments:

(1) Subject Score

(2) Experimenter Score

3.3.8 Subject Score

The subject score is displayed at the top of the screen. The score shows the subject's current score and adjacent the number of points lost/gained in moving to the subject's current location. The subject score, Equation 3 is computed using the parameters:

(1) elevation (elev)

(2) angle-to-goal (A2G)

(3) time (number of steps) penalty

The subject is not told of the scoring metric.

$$Subject\_score = (Elev + cos(A2G)) * TimePenalty \tag{3}$$

3.3.9 Time Penalty (Subject Score)

A time penalty function was devised to help motivate subjects to go towards the goal, Equation 4. Where the variables: *tim4res_diff* means the response time for the subject and *tim2wt4clk* means the maximum time before auto-advance as-the-crow-flies towards the goal, in this case 1.5 sec.

$$TimePenalty = 2 - \frac{tim4res\_diff}{tim2wt4clk} \tag{4}$$

3.3.10 Experimenter (Observer) Score

The experimenter score is hidden from the subject. Equation 5 computes the score based on the following 4 parameters:

(1) elevation (elev)

(2) angle to goal (A2G)

(3) distance cost

(4) time (step) cost

$$Experimenter\_score = step\_size * \Sigma(elev + cos(Ang2Goal) + dist\_cost + time\_cost) \quad (5)$$

3.3.11 Distance Cost

The Distance Cost function computes a value for each step that the subject takes based on how far the player's current position is from the goal. As shown in Figure 31, the closer the subject's position is to the goal the higher the computed value. For example, if a player were to stay around the start position and not advance towards the goal then negative costs would be computed and inserted into the Experimenter Score Equation (Eqn 5).

An inverse tanh function was used and adjusted it to have a zero cost at approximately half the distance from the start position to the goal, where the variable *dist2goal* means the distance from the subject's current position to the goal.

$$Distance\_cost = -\tanh(\frac{dist2goal - 25}{70}) * 2) \quad (6)$$

3.3.12 Time (Step) Cost (Experimenter Score)

The Time (Step) Cost function (Figure 32) computes a value based on the number of steps that the subject takes. For example if the subject wanders around in paths perhaps seeming to score points based on hitting favorable elevations, then the Time (Step) Function will take this into account and penalize the total score, Equation 8. Equation 7 computes the as-the-crow-flies distance factor, *crow_dist_fac*, used

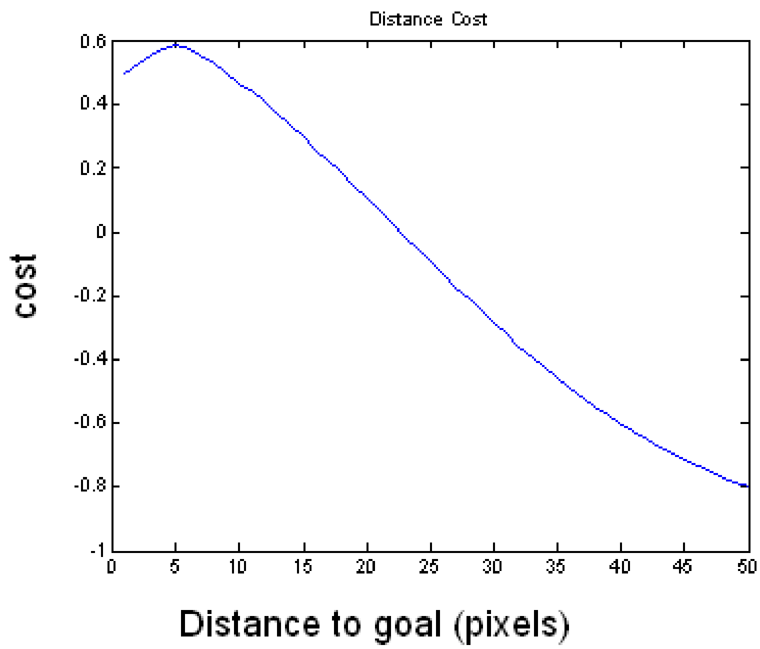

Figure 31: Distance Cost Function

in Equation 8. The variable *init_dist*, computes the distance between the subject's start position and the goal. The variable *stp_sze* means the step size for the subject equal to 1.8.

$$crow\_dist\_fac = \frac{init\_dist}{2 * stp\_sze} \tag{7}$$

$$Time\_cost = 2.5 - log_{10}(10^{\frac{ii}{crow\_dist\_fac}} + 3 * crow\_dist\_fac) \tag{8}$$

3.3.13 Collision

Collision between the human player and the drone may occur during a trial, Figure 33(a). If a collision occurs, then the trial is paused while the collision information is displayed. The cyan solid circle represents the subject's position before the collision. The royal blue circle shows the subject's position at the moment of collision and the

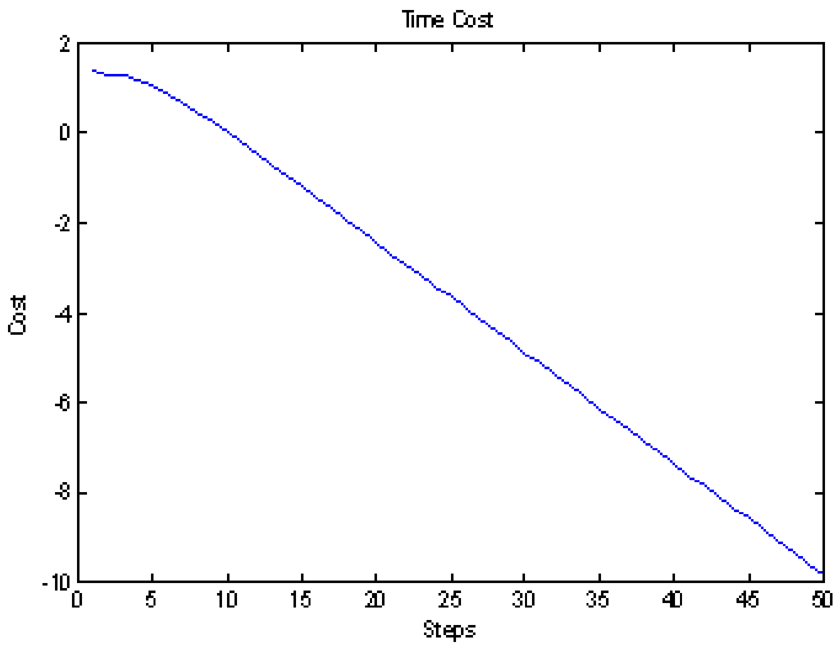

Figure 32: Time (step) Cost Function (Experimenter Score)

black circle shows the subject's position after the collision, Figure 33(b). Collisions are computed using momentum equations to simulate billiard ball collisions.

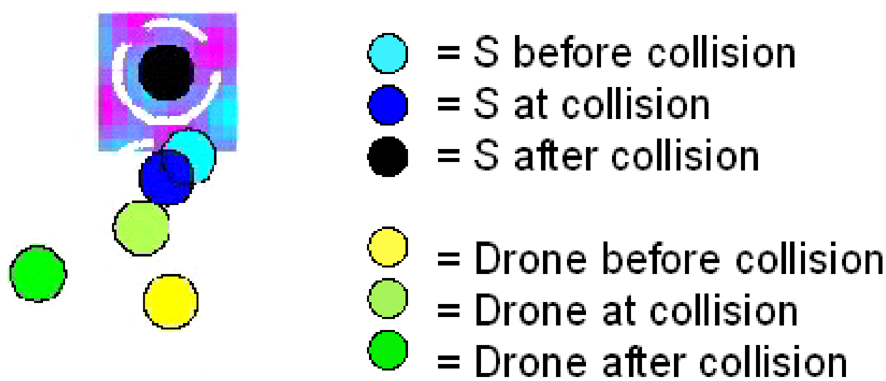

(a) (b)

Figure 33: Example of Collision. *(a)* Collision, *(b)* Collision color conventions.

3.4 Results

3.4.1 Collision Results

Collision data show that subjects did not have significantly more collisions in the converging mode than the single resolution mode of the experiment, Table 14. There were 208 collisions in 264 trials. The rate of collisions did not significantly change from the first four trials (57 collisions) compared to the last four trials (72). In the last four trials of converging stimuli there were 29 versus 43 collisions in the last four single resolution trials.

Stimuli	Mean # Collisions	Std Dev	Total # Collision
Converging	0.720	0.152	95
Single	0.856	0.234	113

Table 14: Collision Data

3.4.2 Level of Resolution Used at Each Step by a Subject

An examination of the levels of resolution that a subject used during Trial 9 show a mean level of resolution of 3, Figure 34. The subject was motivated to proceed to the goal to beat the drone.

A subject used different levels of resolution in different trials, Figure 35. Initially, a subject used a mean level of resolution of 2. Whereas, towards the middle of the converging trials the subject used a mean level of resolution of 4. The change in mean level of resolution is perhaps due to the subject exploring the terrain and being curious as to what happens with more time per step watching the different stimuli at a given step.

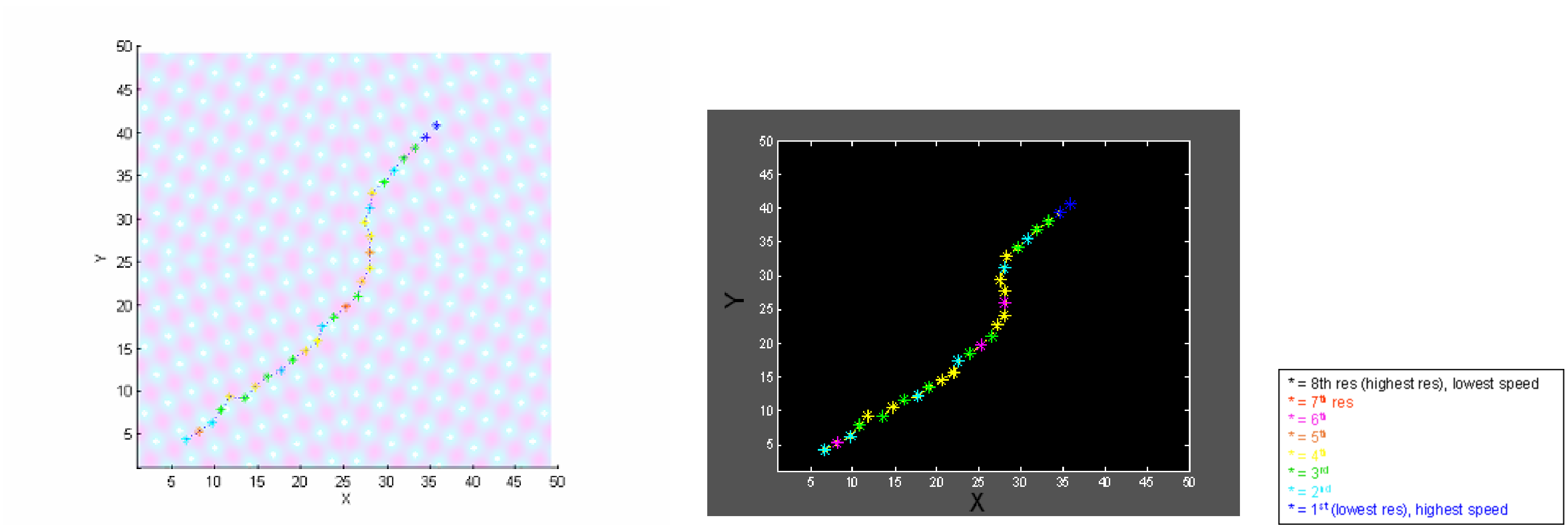

(a) (b) (c)

Figure 34: Example of Levels of Resolution used by a subject. *(a)* Path and levels of resolution taken by a subject superimposed on the terrain, *(b)* levels of resolution used by a subject on black background (for clarity), *(c)* color conventions for levels of resolution representation.

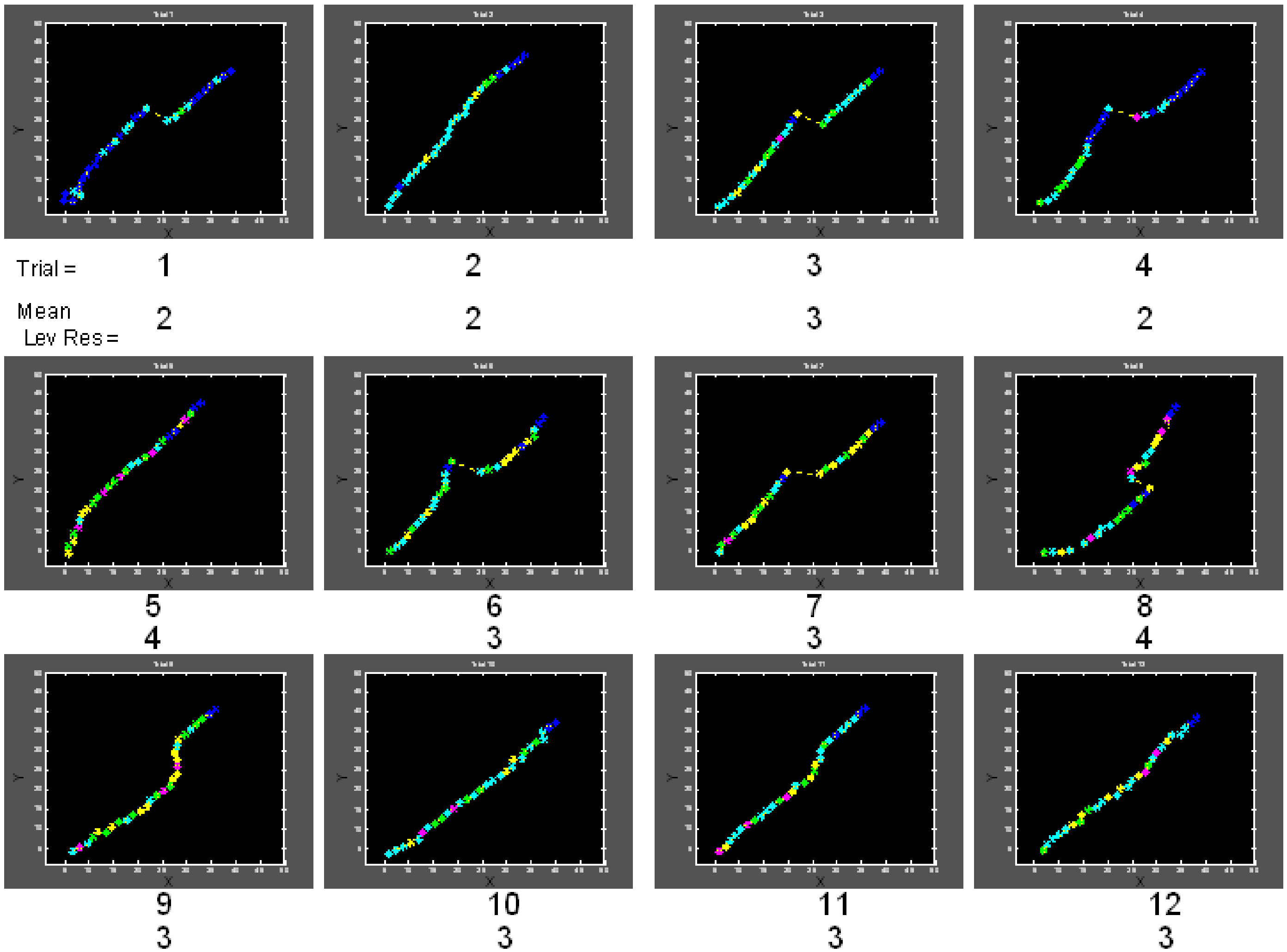

Figure 35: Sequence of levels of resolution used by a subject from Trial 1 to Trial 12

Mean levels of resolution (blue) of all subjects across all trials (1-24) are shown in Figure 36. Time series averaged (red) showing that as subjects continued playing the game, they waited for higher levels of resolution. Participants begin by selecting low resolutions. As subjects learned how to score points, the levels of resolution increased (Trials 5-13). Once subjects learned how to score points, the level of resolution selected by particapants settled around 3. The overall mean level resolution was 2.81 with a standard deviation of 0.679.

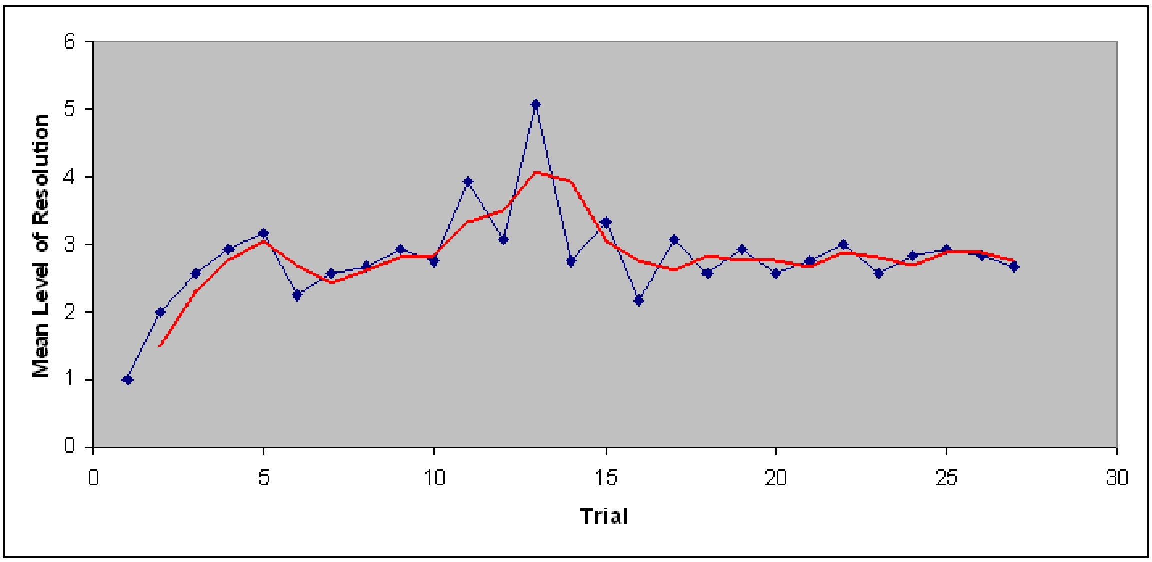

Figure 36: Mean levels of resolution (blue) of all subjects across all trials (1-24). Time series averaged (red) showing that as subjects continued playing the game, they waited for higher levels of resolution.

3.4.3 Elevation used by Subjects

During the first run of the game, subjects were presented with converging stimuli. Participants tended to click negative areas of the terrain during their initial steps. Subjects clicked increasingly positive elevations, see Figures 37, 38.

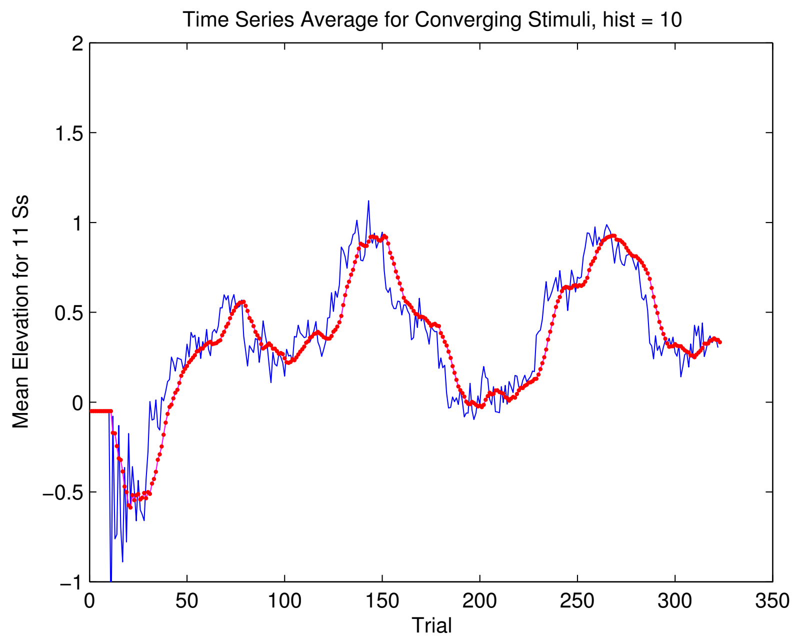

Figure 37: Time Series Averaged (hist = 10) elevation scores over all converging stimuli trials

3.4.4 Angle-to-Goal used by Participants

Time Series Average for Angle-to-Goal Single Resolution. Subjects headed on a direct path to the goal except for when they approached the center of the terrain. Participants changed direction and headed in a downward direction near the center of the terrain, Figure 39.

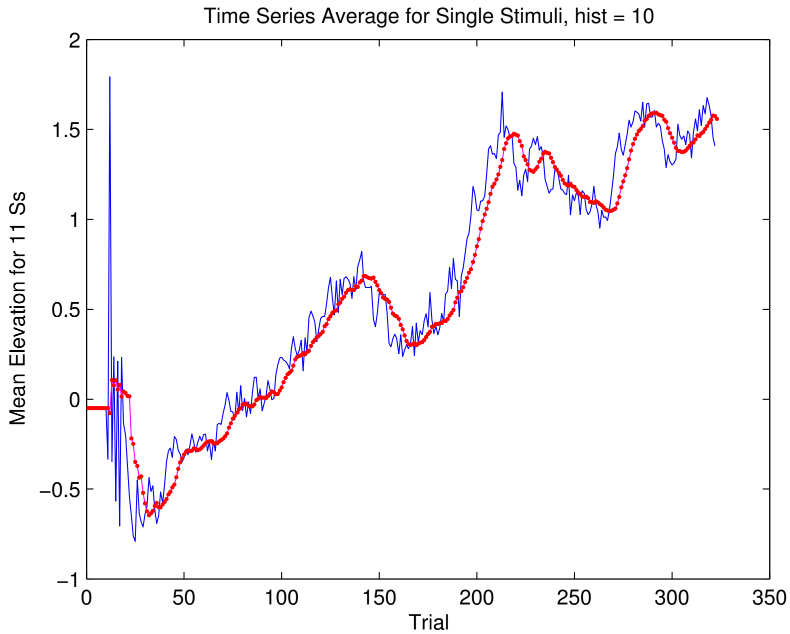

Figure 38: Time Series Averaged (hist = 10) elevation scores over all single resolution trials

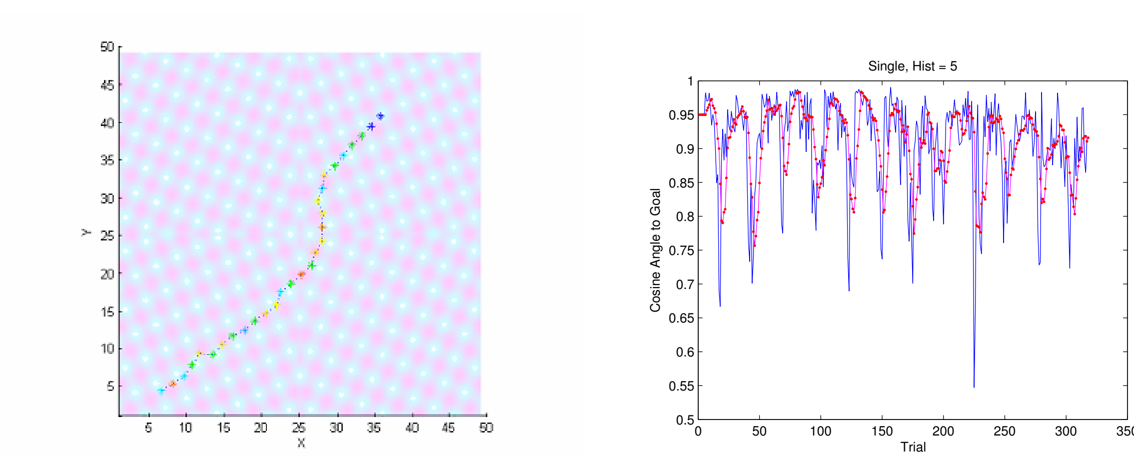

(a) (b)

Figure 39: Time Series Average for Angle-to-Goal Single Resolution. *(a)* Path and levels of resolution taken by a subject superimposed on the terrain, *(b)* Time Series Averaged (hist = 5) angle-to-goal scores over all single resolution trials

3.4.5 As-the-Crow-Flies (ACF) Paths to Goal

What elevation scores result from different start positions? Figure 40 shows as-the-crow-flies (ACF) paths to the goal located at (6,4) from 5 different start positions located at: (34,44), (39,40), (41,38), (35,43) and (37,42) .

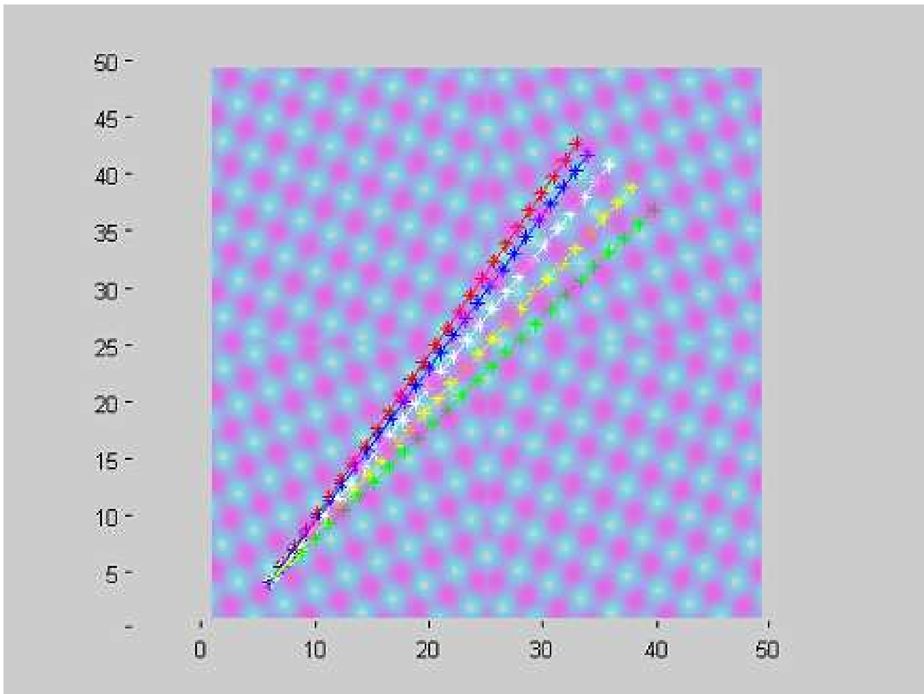

Figure 40: As-the-crow-flies (ACF) paths to the goal located at (6,4) from 5 different start positions.

The nature of the sinusoidal terrain yields elevation scores that vary from step to step in a somewhat oscillatory manner for an ACF path with a step size of 1.8, see Figure 41. For an ACF path, the start position does not largely affect the mean elevation score.

The mean elevation scores range from -0.118 to 0.034 with an overall mean score of -0.03 across all 5 paths, see Table 15. If a participant were to decide not to click

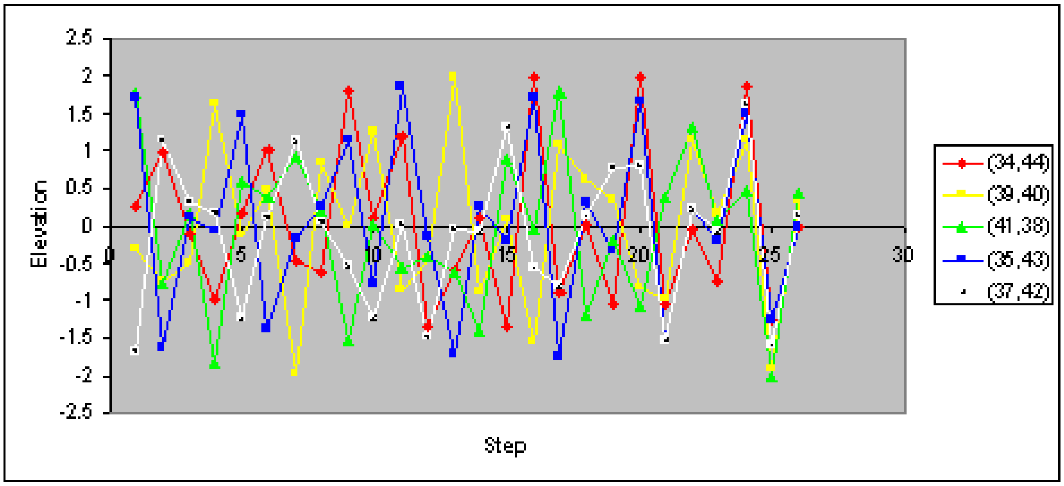

Figure 41: Elevation scores for 5 ACF paths

anywhere, then the elevation component to the overall score would be a small negative value. Therefore the start position did not affect scoring.

	Red	Yellow	Green	Blue	White
Mean	0.032	-0.009	-0.093	0.034	-0.118
Std Dev	1.073498	1.052087	1.021723	1.157015	0.945781
Median	-0.0267	0.031828	0.036136	-0.05401	0.031447

Table 15: ACF Elevation Data

3.4.6 Drone to goal using Best First Search (BFS) Algorithm

The elevation scores of the drone on best first search paths were examined. The drone began at mirror-image equivalent to the ACF simulation paths start positions now located at: (34,6), (39,10), (41,12), (35,7) and (37,8) . The start positions shown here were in the quadrant of the terrain where the drone was situated in the game played by participants , see Figure 42.

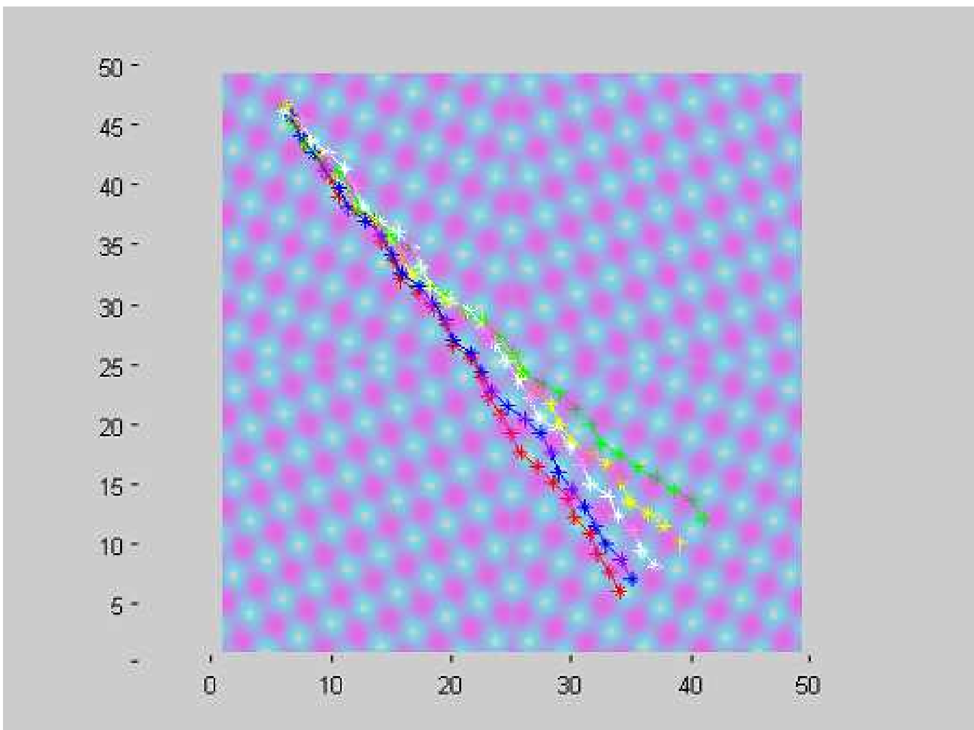

Figure 42: 5 BFS paths of drone to goal (6,46) from different start positions.

The overall mean score for the 5 paths is 0.03. Since the overall mean is positive, BFS on average outperforms ACF, see Figure 43. The shape of the curves retain some oscillation again due to the sinusoidal terrain.

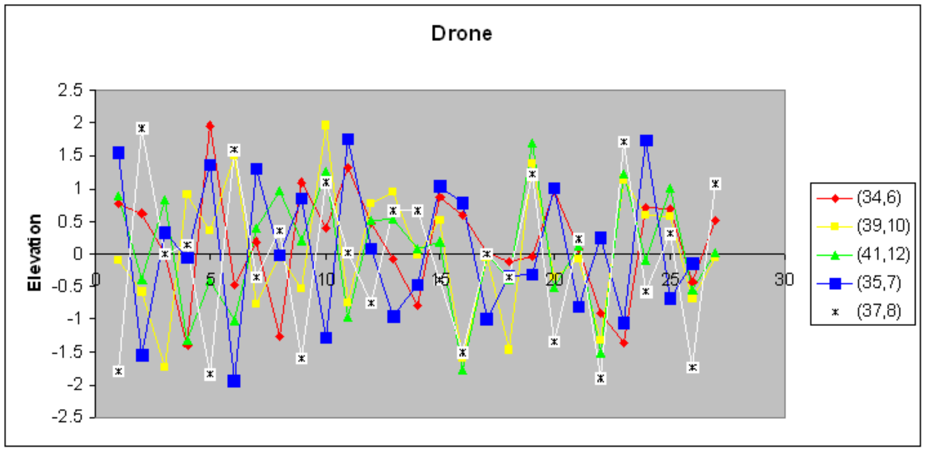

Figure 43: Elevation scores for drone to goal using best-first-search (BFS) algorithm.

3.4.7 Learning Curves

When a person repeats a task, learning occurs in a sigmoidally, with a slow begining, followed by accelerated performance, and then reaching a plateau [95]. Here, subjects scored more points with single stimuli than converging resolution stimuli, Figure 44. In the single resolution mode, subjects began by scoring reasonably well, then as they continue to play more trials, they explore different strategies that sometimes decrease their score. By the end of the trials, they learned how to increase their scores by clicking magenta and heading to the goal.

3.4.8 Converging Stimuli *vs* Single Resolution Navigation Results

Subjects score more points when viewing single than converging resolution stimuli, Figure 45. The mean score for subjects in the converging mode was 71.05 and the mean score for single was 74.65, Table 16.

	Converging	Single
Mean	71.05	74.65
Std Dev	2.48	2.95
p(two-tail)	0.00963	

Table 16: Converging *vs* Single stimuli scores

3.5 Discussion

In the navigation studies, humans learned to make better path estimates using elevation and direction to goal with limited information over a series of trials with: *(a)*

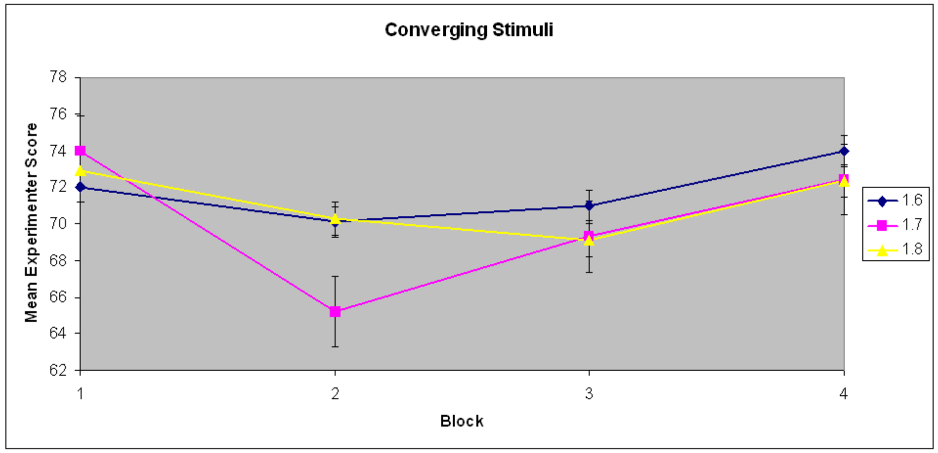

(a)

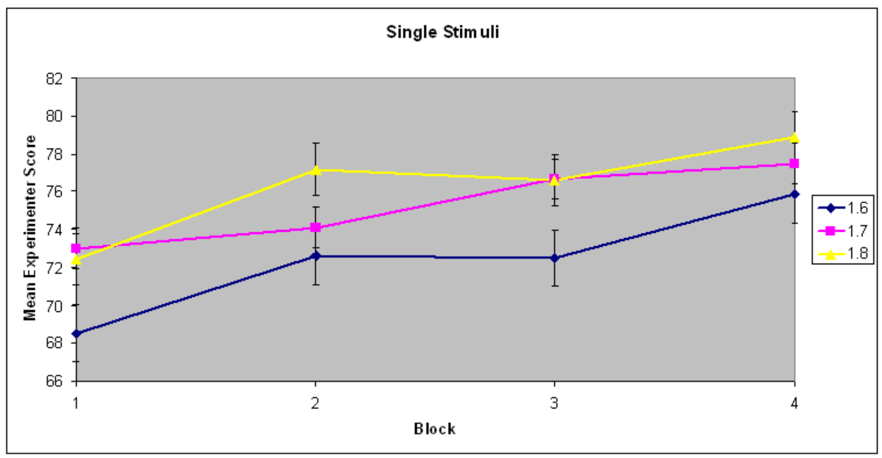

(b)

Figure 44: Learning curves for converging and single resolution stimuli. *(a)* Converging results, *(b)* Single resolution. Colors indicate participants competing against drone step-sizes of 1.6 (blue), 1.7 (pink), and 1.8 (yellow). Participants had a constant step-size of 1.8.

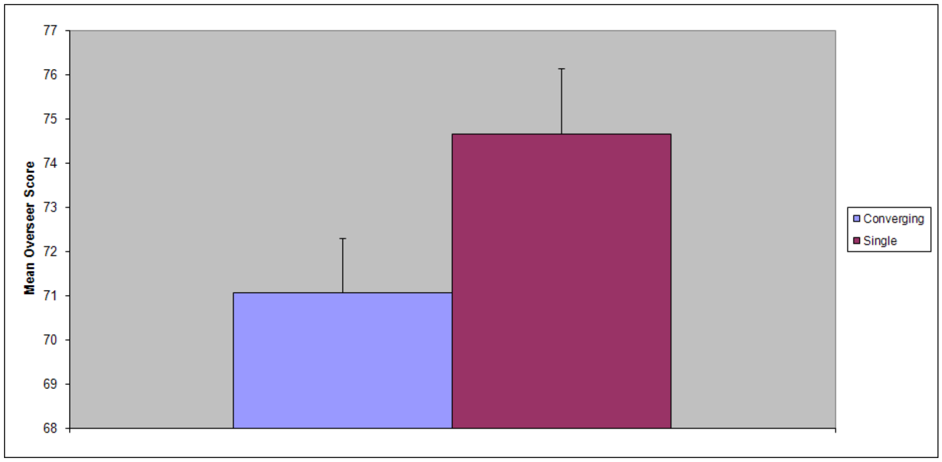

Figure 45: Subjects score more points when viewing single than converging stimuli resolution stimuli. Range of scores (68-77) was a reasonable order of magnitude for subjects to comprehend.

limited view of the terrain and *(b)* less than perfect resolution of the terrain. Also, participants scored more points in the single resolution trials than with converging stimuli. The data suggest that subjects learned to click magenta areas of the terrain especially as shown in the single resolution trials while heading toward the goal. The additional, changing resolution, views during the converging stimuli condition may have led participants to form more hypotheses (many of which may not have been accurate) of how to score points and yielded lower scores than with single resolution stimuli.

It is somewhat surprising that humans learn the scoring parameters of elevation and angle-to-goal better in the single resolution mode than in the converging resolution mode. One might think that in the converging mode the additional views, albeit lower resolution view than the single mode, would assist participants in learning the scoring parameters.

Since participants learned the scoring parameters in the single resolution mode, the result suggests that participants learned the strategy to click magenta colors while heading towards the goal. Also, the result indicates that subjects learn without needing the full resolution of the terrain.

Jacobs *et al* [42] found increased activity in entorhinal cortex while subjects navigated through a virtual world. Future work could involve participants playing the navigation game developed here to test whether the activity in entorhinal cortex increases during navigation with visually degraded stimuli plus a restricted view of the terrain. In addition, since participants learn to estimate an optimal route from a start position to the goal, activity in intraparietal cortex (known for increased activity during estimation [65]) would be expected to increase.

4 Path Optimization Methods and Results

4.1 Introduction

In human studies (see Chapter 3) with the drone using best-first-search, the optimal path was not known. This chapter examines algorithms for finding optimal paths. Fixed-step paths from a start location to a goal are compared to paths restricted to grids over different terrains.

4.2 Examples of Terrains

Terrains with irregular patterns were created for this study to compare the performance of algorithms. In addition to the sinusoidal terrain which has quad symmetry and a regular pattern (see Chapters 2 and 3), a plasma fractal terrain and a terrain based on the Complex Ginzburg-Landau Equation (CGLE), Eqn 10 were produced.

Terrains include:

(1) sinusoidal, Eqn 9, Figure 46(a)

$$z = \cos\frac{2\pi}{3}x + \sin\frac{2\pi}{3}y \tag{9}$$

(2) plasma fractal, Figure 46(b)

(3) 2D chaos (based on the Complex Ginzburg-Landau Equation, Equation 10) Figure 46(c)

$$\partial_T A = A + (1 + i\alpha)\nabla^2 A - (1 + i\beta)|A|^2 A \tag{10}$$

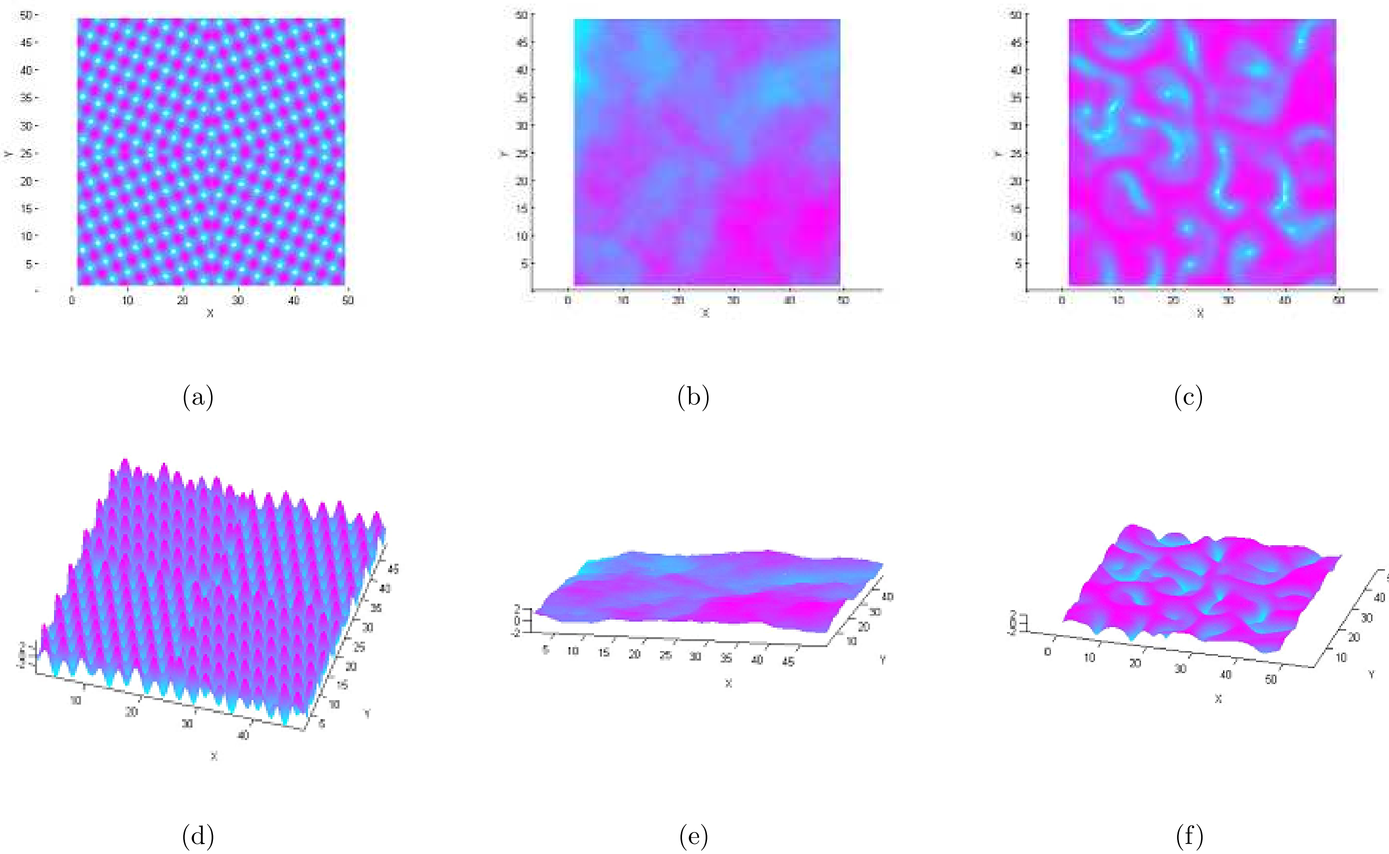

Figure 46: Examples of the terrains: *(a)* sinusoidal, *(b)* plasma fractal, *(c)* Complex Ginzburg-Landau, *(d)* rotated sinusoidal, *(e)* rotated plasma fractal, *(f)* rotated Complex Ginzburg-Landau.

Figure 47 shows different rotated views of the sinusoidal terrain to illustrate the peaks and valleys of the terrain.

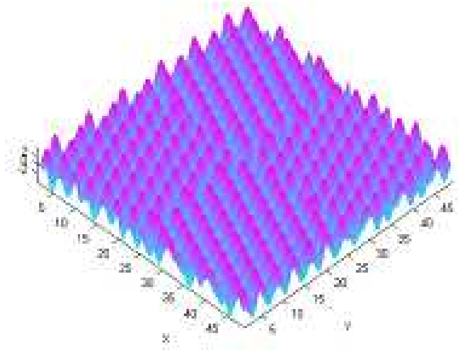

(a)

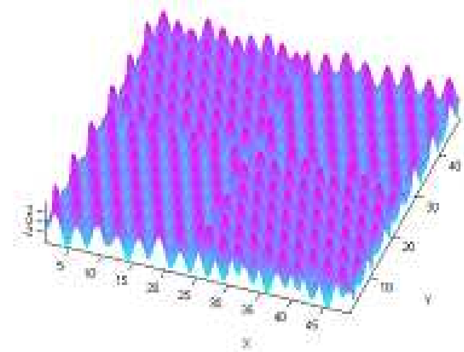

(b)

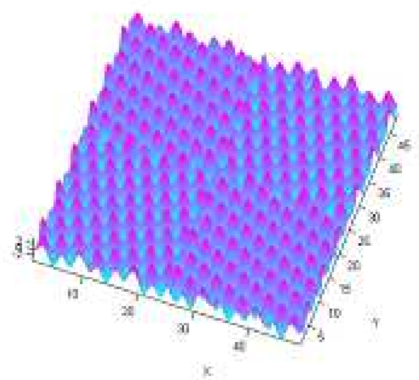

(c)

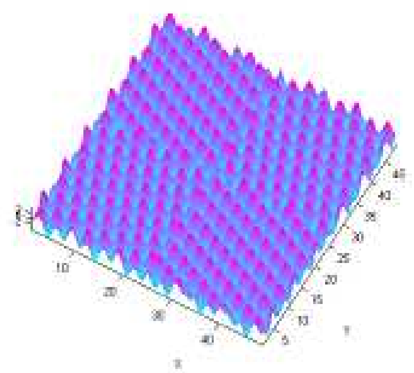

(d)

Figure 47: Rotated sinusoidal terrains: *(a)* view(45,45), *(b)* view(20,40), *(c)* view(20,60), *(d)* view(30,60).

Plasma fractals are cloud-like patterns [22]. The terrain was generated by code that was extensively modified from Arjun Viswanathan 1999 Plasma.m code found in the Matlab repository, where $n = 7$ and aa was the input matrix. To assess the terrain, sequential numbers were used as input for a 4x4 matrix shown in Table 17 producing the terrain, Figure 48 with no randomness.

```
for i=1:n;
    r = size(aa,1);c=size(aa,2);
    xi = [1:(r-1)/(2*r-1):r];
    yi = [1:(c-1)/(2*c-1):c];
    aa = interp2(aa,xi,yi','cubic');
end
```

1	1	1	1
2	2	2	2
3	3	3	3
4	4	4	4

Table 17: 4x4 input matrix

Randomness was inserted into the code shown below, while using the same input matrix, to produce an irregular pattern, Figure 49.

```
for i=1:n;
    r = size(aa,1);c=size(aa,2);
    xi = [1:(r-1)/(2*r-1):r];
```

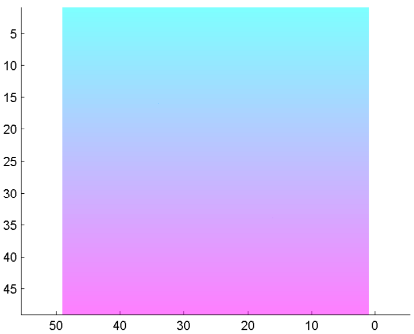

Figure 48: Terrain generated by plasma fractal code with no randomness.

```
    yi = [1:(c-1)/(2*c-1):c];

    aa = interp2(aa,xi,yi','cubic');

    step=2^(-i);

    dev=rands(size(aa, 1), size(aa, 2) ) * (step);

    aa=aa+dev;

end
```

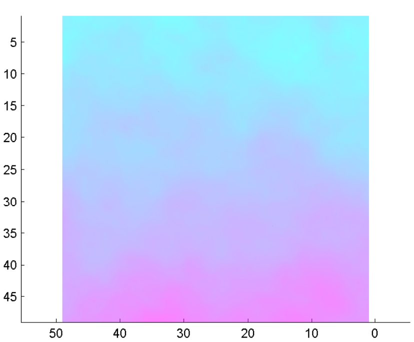

Figure 49: Terrain generated by plasma fractal code with randomness.

Furthermore, by randomizing the center 4 indices to the input matrix (Table 18), with no additional randomness inserted produces a terrain (Figure 50) that is regular with a more negative (cyan) region in the center.

1	1	1	1
2	-0.60169	0.32278	2
3	-0.1609	-0.44488	3
4	4	4	4

Table 18: 4x4 input matrix with inner 4 elements randomized.

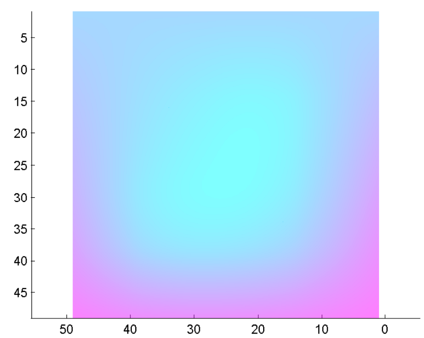

Figure 50: Terrain generated by plasma fractal code with randomness and 4 random elements in the input array.

By adding randomness through the algorithm, the terrain shown in Figure 51 was generated.

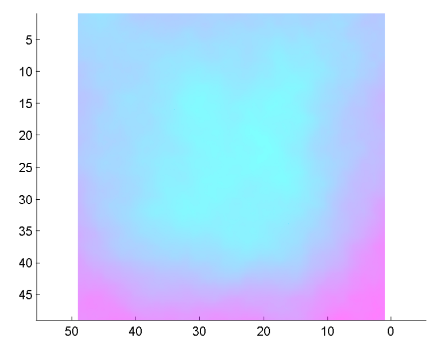

Figure 51: Terrain generated by plasma fractal code with randomness and 4 random elements in the input array plus randomness added through the algorithm.

When all elements of the array are randomized (Table 19), the terrain shown in Figure 52.

-0.63913	0.050738	0.26178	0.10343
0.12194	-0.9024	0.38752	0.61798
0.21567	0.79349	0.64479	0.34337
0.2535	-0.92687	-0.10881	0.23738

Table 19: 4x4 input matrix. All elements randomized.

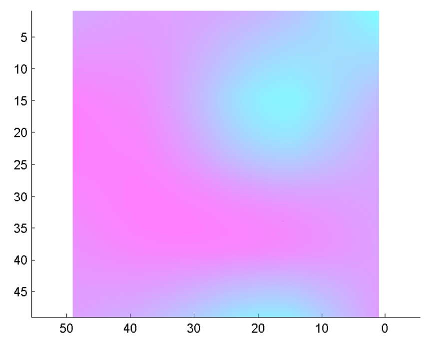

Figure 52: Terrain generated by plasma fractal code with a random input array.

The random array (values shown in Table 19) when used as input to the algorithm with randomness produced a cloud-like irregular terrain, Figure 53.

Fast fourier transform (FFT) analyses of the sinusoidal, plasma fractal and CGLE terrains are shown in Figures 54, 55, 56. The FFT reveals a larger amplitude in the sinusoidal terrain than the plasma fractal and CGLE terrains. The frequencies in the plasma fractal and CGLE terrains are less than the sinusoidal terrain, suggesting that the sinusoidal terrain is a more regular pattern terrain.

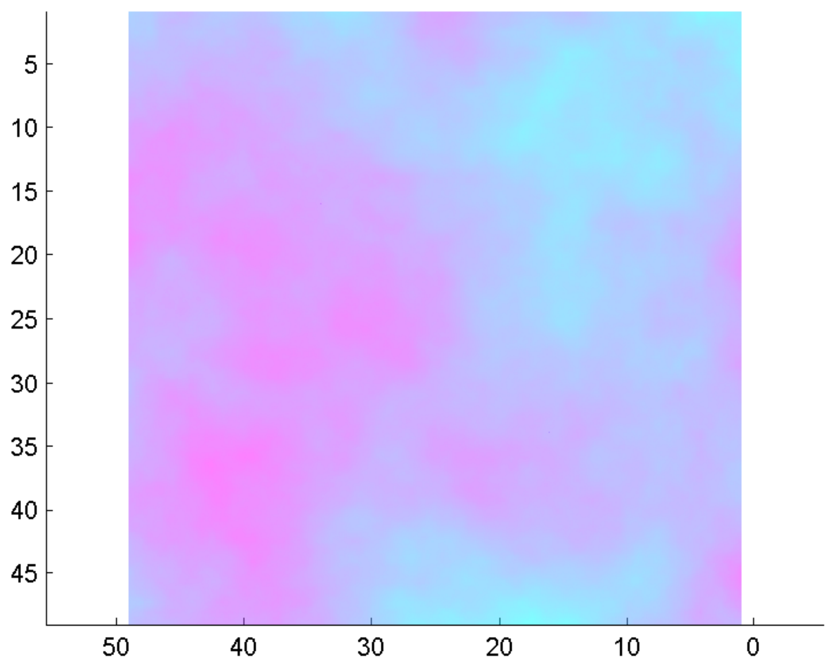

Figure 53: Terrain generated by plasma fractal code with a random input array and randomness from algorithm.

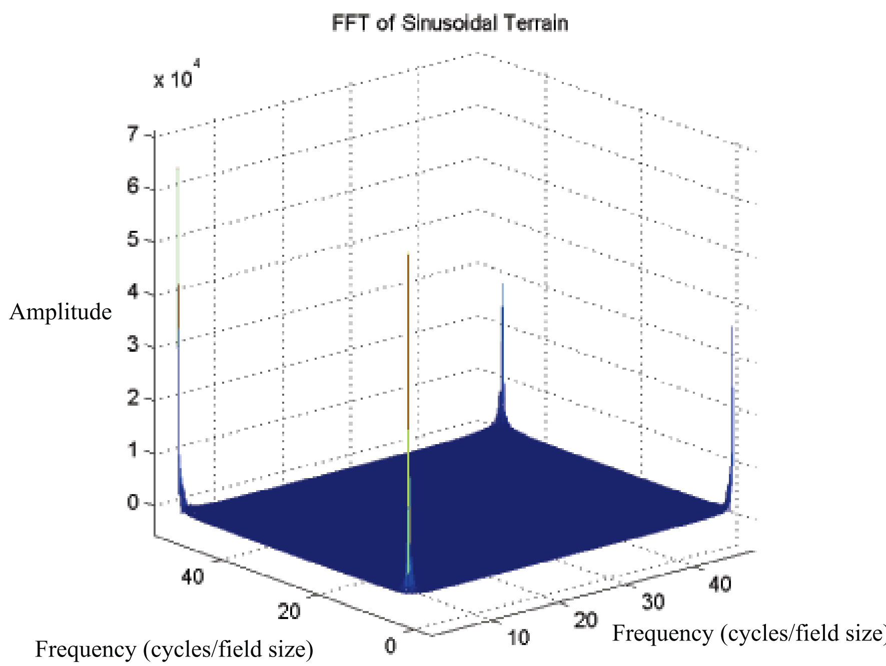

Figure 54: FFT of the sinusoidal terrain.

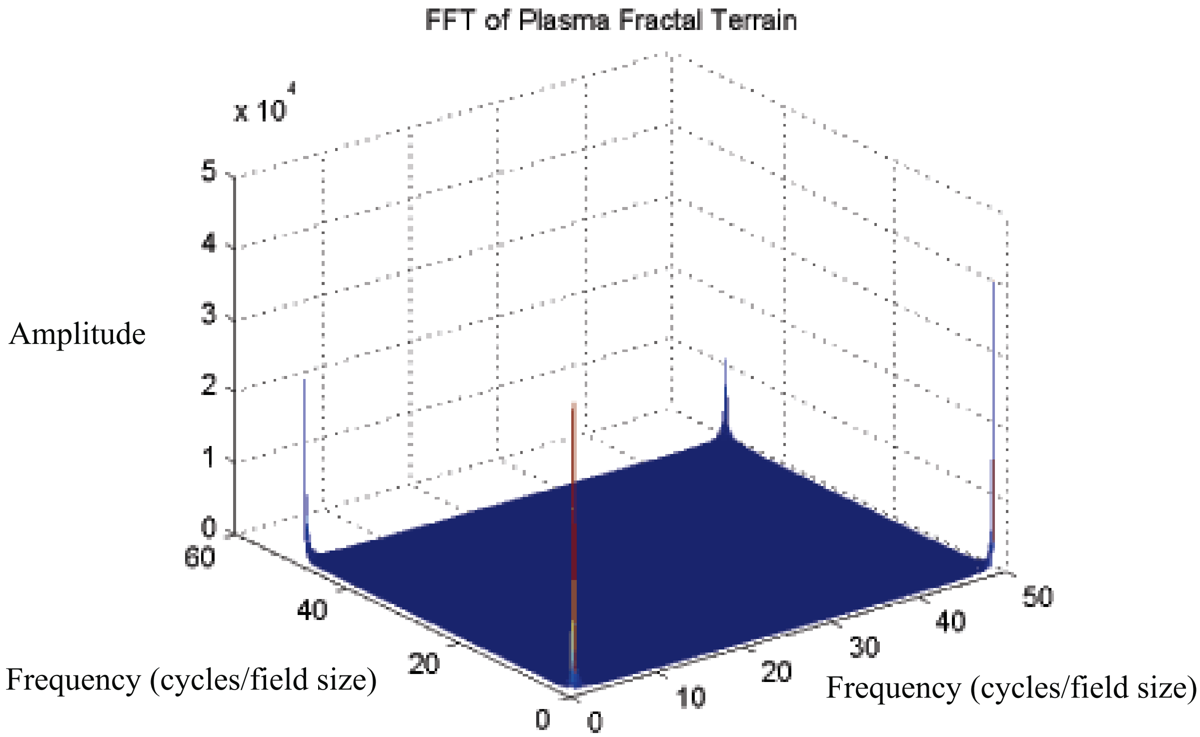

Figure 55: FFT of the plasma fractal terrain.

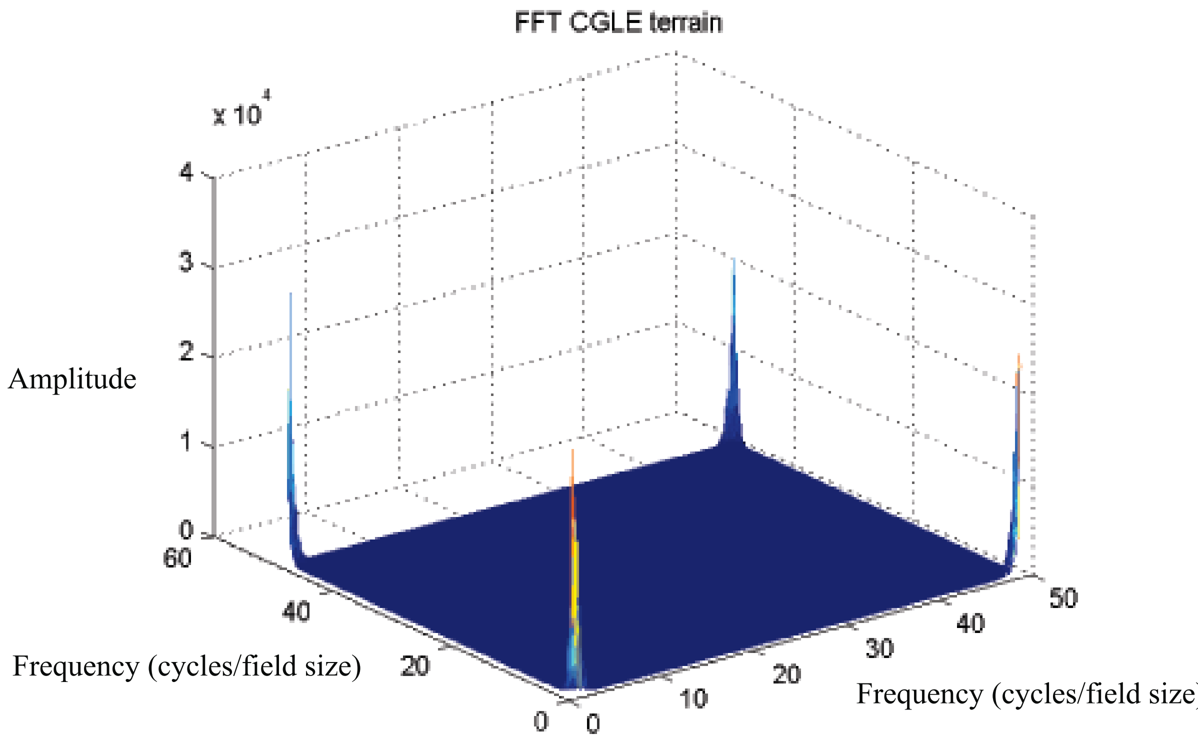

Figure 56: FFT of the CGLE terrain.

The Complex Ginzburg-Landau Equation (CGLE) [4], Equation 10, is a nonlinear equation used to model superconductivity. Equation 11 is a scaled complex field. The parameters, α and β are the linear and nonlinear terms respectively.

$$A = R * e^{i\phi} \tag{11}$$

In the CGLE terrain used in the following experiments, $\alpha = -0.5$ and $\beta = 2.999$. Small changes in α and β can produce different terrains, Figures 57, 58.

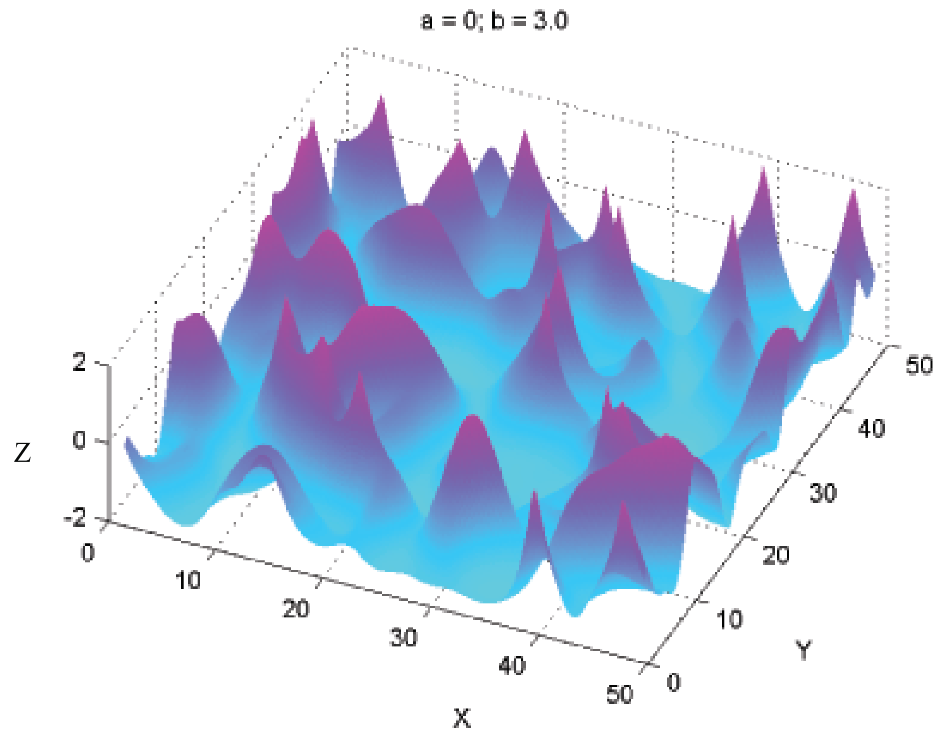

Figure 57: CGLE irregular terrain with $\alpha = 0$ and $\beta = 3$.

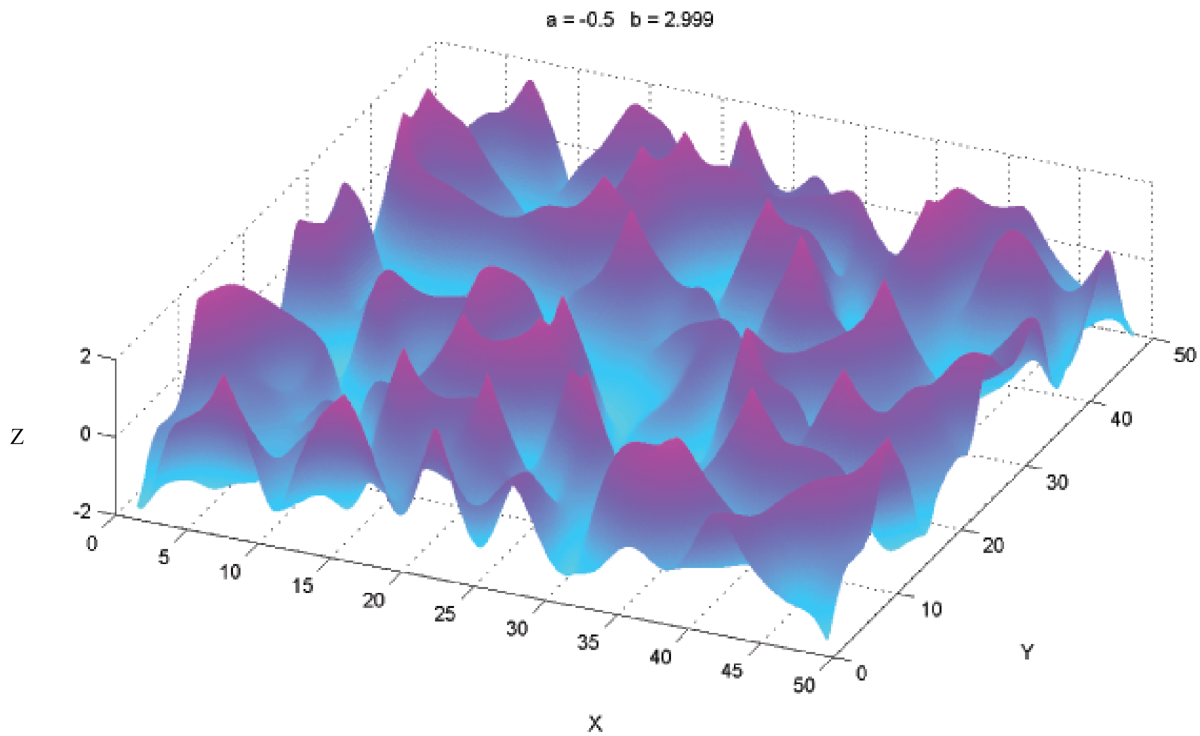

Figure 58: CGLE irregular terrain with $\alpha = -0.5$ and $\beta = 2.999$.

4.3 Methods of Optimization

Path optimization used the following methods:

(1) Best First Search

(2) A* algorithm

(3) Dijkstra's Algorithm (Grid)

(4) Breeding Algorithm

In setting up the optimization scenario, optimal paths were sought determined by the score achieved from a start location to a goal. For us, step sizes were always equal. Performance of different search algorithms was examined over multiple terrains.

4.4 Best First Search (BFS)

Best First Search (BFS), Figure 59 accumulates a path to goal by adding the best jump from its current location.

The algorithm is represented here in pseudo-code: 1. Define a list of points one step-size ahead of current position

2. Compute scores of each point (Equations 12, 13)

3. Select point with highest score and move to that point

4. Repeat steps 2-3 until reach goal location

In the context of the navigation game, BFS examines 21 possible headings in an arc centered around the direct angle-to-goal point one step ahead and computes elevation plus angle-to-goal data, see Equations 12, 13. From this set of next-step choices, BFS selects the one with the highest score.

$$BFSchoice(ii) = cos(AngleToGoal(ii)) + elev(ii) \tag{12}$$

$$Winner = max(BFSchoice) \tag{13}$$

4.5 A* Algorithm Grid-based

A* improves on BFS by including an estimated-distance-to-goal term in the cost equation (Equation 3)to find optimal paths, Equation 14, where $g(n)$ is the cost and $h'(n)$ is the estimated distance to the goal. A* keeps nodes at earlier levels in the search space open. If a node at a earlier level in the search cue has a lower cost than the current node, then A* returns to the earlier level and expands the search through

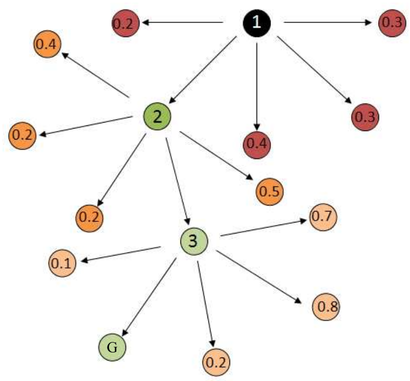

Figure 59: Best first search schematic. Start location indicated by black circle "1". Point with highest score and which the algorithm selects as the winner at each iteration is shown in green. ("G" = goal).

that node, see Figure 60.

$$f(n) = g(n) + h'(n) \tag{14}$$

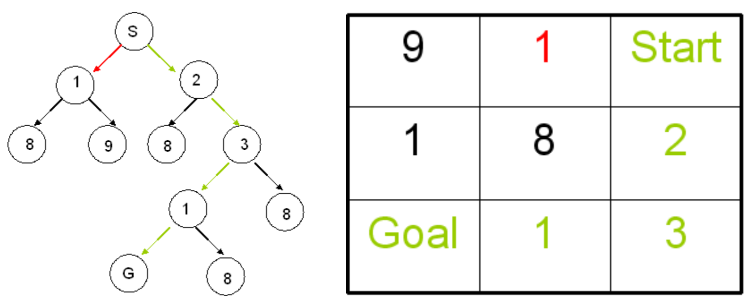

(a) (b)

Figure 60: (a) Node tree diagram using A* , (b) Example of A* finding the lowest cost path (2+3+1)

4.6 Dijkstra's Algorithm Grid-based

Dijkstra's Algorithm [16] is a special case of A* also using a grid-based approach in the search for the optimal path, see pseudocode below. Dijkstra's algorithm differs from A* because Dijkstra's algorithm examines every node in the grid.

Pseudocode:

1. Assign distance of infinity to each point

2. Define a list Q containing all the points in the grid

3. while Q not empty

```
        u = point with smallest cost
        for each neighbor v of u compute cost (Equation 3)
           cost_new = cost_current + cost_u_to_v
           if cost_new < cost_current
              cost_current = cost_new
           end
        end
end
```

Grids can come in different sizes. However, there is a computation cost associated with increasingly larger grids. A comparison of grid size and computation time is shown in Table 20. As the size of the grid increases, so does the computational time.

The total number of unique paths can be computed using a grid-based search. Figure 61 shows the number of unique paths for grids ranging in size from 2x2 to 14x14. For square grids, as the size of the grid increases, the number of paths increases exponentially, Figure 62.

Grid size (units)	Time (sec)
6 x 6	4.29
8 x 8	4.31
10 x 10	4.48
12 x 12	4.81
14 x 14	5.24
16 x 16	6.23
18 x 18	6.89
20 x 20	7.82

Table 20: Grid size *vs* computation time

Grid size (x)

Grid size (y)	1	2	3	4	5	6	7	8	9	10	11	12	13	14
1		1	1	1	1	1	1	1	1	1	1	1	1	1
2		2	3	4	5	6	7	8	9	10	11	12	13	14
3			6	10	15	21	28	36	45	55	66	78	91	105
4				20	35	56	84	120	165	220	286	364	455	560
5					70	126	210	330	495	715	1001	1365	1820	2380
6						252	462	792	1287	2002	3003	4368	6188	8568
7							924	1716	3003	5005	8008	12376	18564	27132
8								3432	6435	11440	19448	31824	50388	77520
9									12870	24310	43758	75582	125970	203490
10										48620	92378	167960	293930	497420
11											184756	352716	646646	1144066
12												705432	1352078	2496144
13													2704156	5200300
14														10400600

Figure 61: Number of unique paths in grid sizes 2x2 to 14x14.

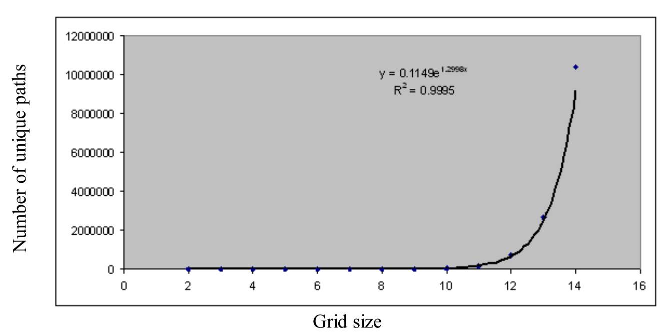

Figure 62: The number of unique paths (*y-axis*) increases exponentially with increasing square grid size (*x-axis*).

Dijkstra's algorithm can be used in the terrains. A comparison of the results of Dijkstra's algorithm using an 8x8 grid over different terrains is shown in Figures 63, 64, 65. Dijkstra's algorithm scores the most points in the sinusoidal terrain, followed by the CGLE, and then the plasma fractal terrain.

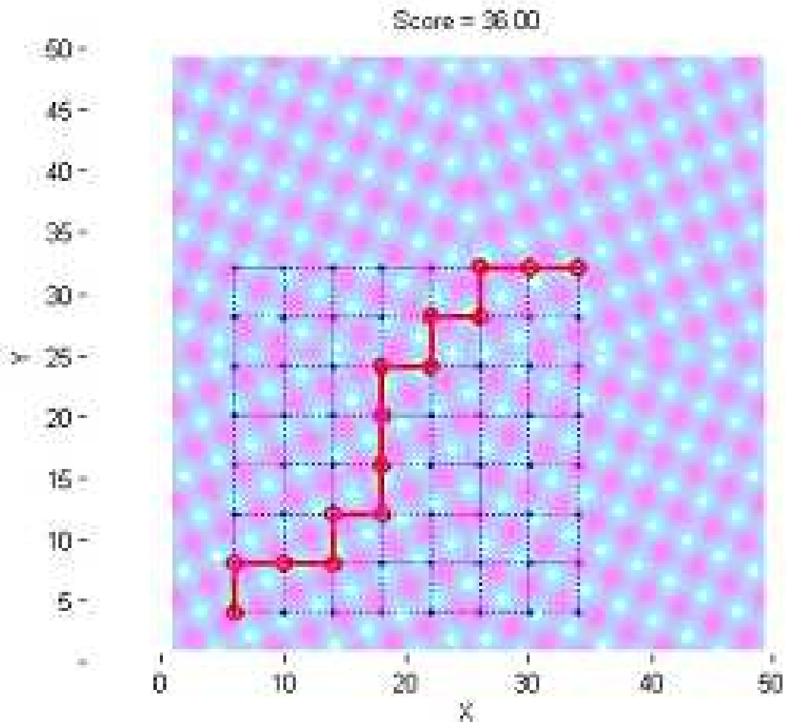

Figure 63: Dijkstra's algorithm using an 8x8 grid on the sinusoidal terrain scoring 36 points.

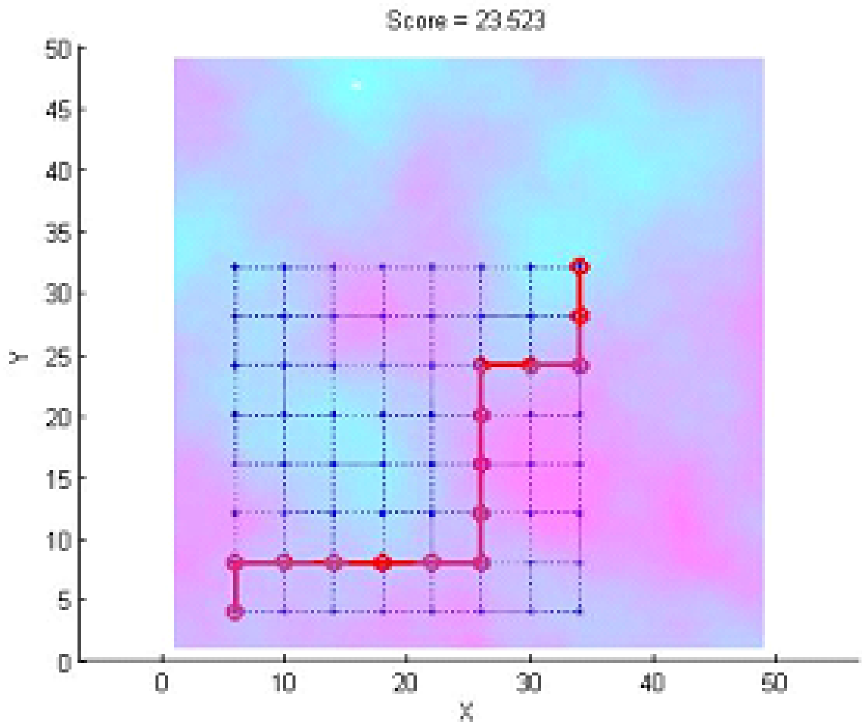

Figure 64: Dijkstra's algorithm using an 8x8 grid on the plasma fractal terrain scoring 23.523 points.

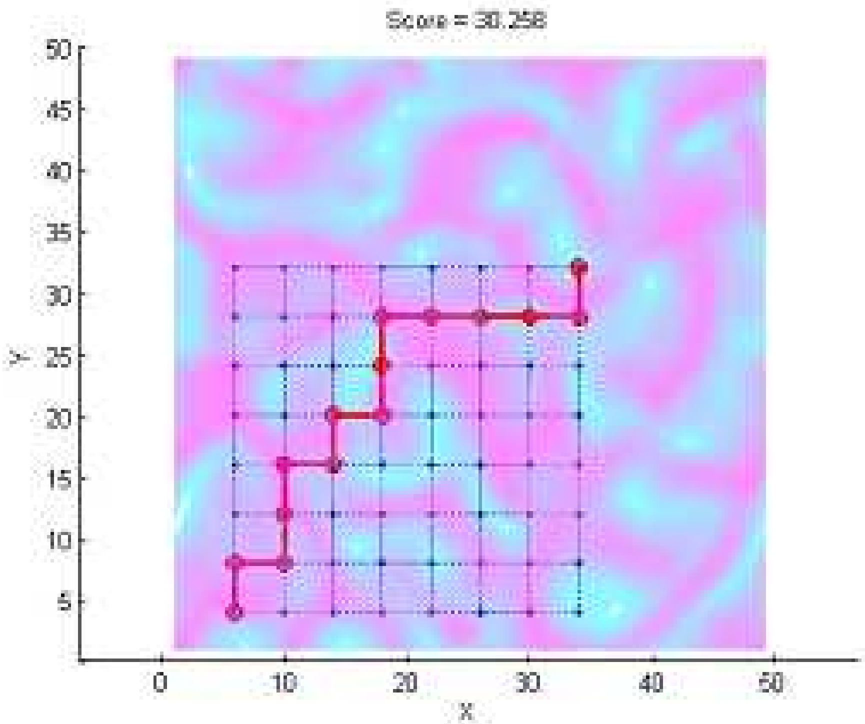

Figure 65: Dijkstra's algorithm using an 8x8 grid on the CGLE terrain scoring 30.528 points.

Dijkstra's grid algorithm results using a 21x21 grid *vs* BFS over different terrains is shown in Figure 66. The start position is located in the upper-right quadrant (46,44) of the terrain with the goal situated in the lower-left quadrant (6,4). In order to get to the goal, paths traverse a variety of sections of the terrain. The path with the highest number of points using a grid occurs with the sinusoidal terrain scoring 47 points. BFS scores more points in each terrain than the grid algorithm. The highest BFS path scores 65 points with the CGLE terrain. The results indicate that when starting from the same point and allowing the search algorithm to access to an open terrain (as opposed to a fixed grid), BFS algorithm outperforms the grid algorithm.

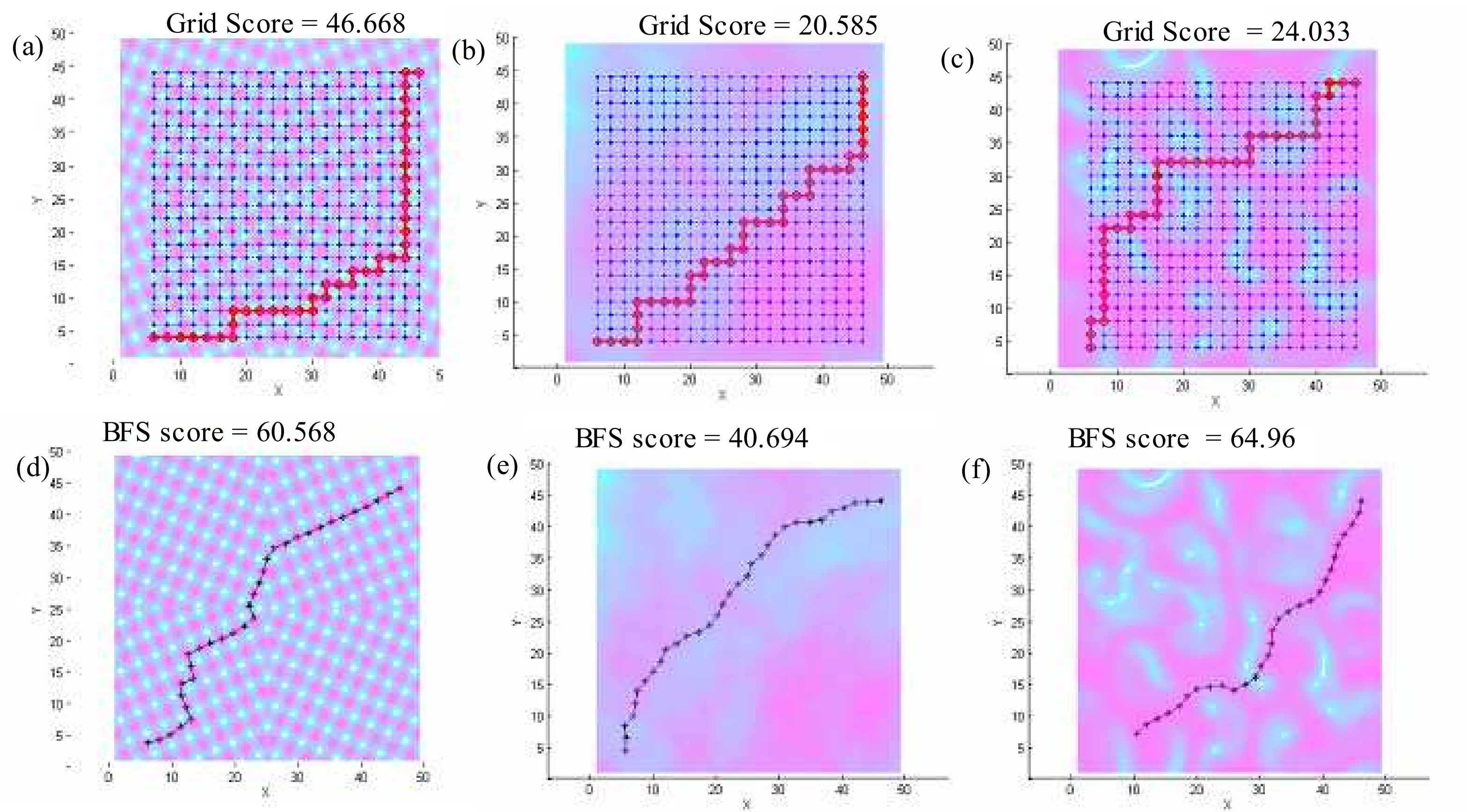

Start = (46,44)
Goal = (6,4)
Stp_sze = 2

Algorithm	Sine Cosine	Plasma Fractal	CGLE
Grid Score =	47	21	24
BFS Score =	61	41	65

Figure 66: Dijkstra's grid (21x21) algorithm across 3 terrains: (a) sinusoidal, (b) plasma fractal, and (c) CGLE, compared to BFS across 3 terrains: (d) sinusoidal, (e) plasma fractal, and (f) CGLE. BFS scored more points than Dijkstra's grid based algorithm in each of the 3 terrains.

4.7 Breeding Algorithm

In the 1960s John Holland [35] (University of Michigan) created breeding algorithms (also known as genetic algorithms). A breeding algorithm can be defined as a computational method of search using first generation population (parents), selection based on certain criteria, and mutation to produce the next generation offspring. Recombination of "chromosomes" allows the breeding algorithm to go from the current generation to the next.

In biology, chromosomes are coiled strings of DNA; a chromosome is composed of a string of 4 nucleic acids (cytosine, thymine, adenine, and guanine). In computer science chromosomes are represented by data structures, such as a binary string: 0110001110. Fitness of individuals (data structures) is used as a metric in the selection process. Populations of individuals are called generations. Breeding algorithms begin by randomly producing a parent generation. In the case of the present work, the parent paths are randomly generated with the condition that to be a "valid" path, a path must end near the goal. After the first generation of individuals (parents), the breeding algorithm applies selection and mutates the path to produce a new generation. Each iteration produces a new generation and the process is repeated for a user defined number of generations or until performance asymptotes.

Breeding algorithms distinguish themselves from other search methods by their effectiveness in finding near optimal solutions in a large search space. To achieve such performance, breeding algorithms do not need to find all solutions, but instead use only a small fraction of candidates to find near optimal solutions.

The algorithm is shown below:

1. Generate random paths from start to goal locations.

2. Evaluate score of each path.

3. Rank order paths.

4. Select top-ranking paths.

5. Create next generation by mutating a random point in each path to generate new paths.

6. Store the parent generation

7. Repeat steps 2-6 until number of generations has been reached or error criteria has been reached.

Simulated evolution continues to produce new generations from the fittest members of the previous generation. Over many generations, a near optimal family of solutions arises.

Breeding algorithms are not restricted by grids; the search space has no bias. The advantage of an unrestricted search space is the opportunity to discover one or more paths that would not necessarily be possible on a grid.

4.7.1 Mutations

Different types of mutations can be used to generate new paths. 3 varieties of mutations are used in the following experiments include: Addition, Deletion, and Slider. One mutation occurs per path.

4.7.2 Addition

Addition mutation adds a point to a random location in the path and continues to add points until the new section joins the original path while maintaining equal step sizes, Figures 67, 68.

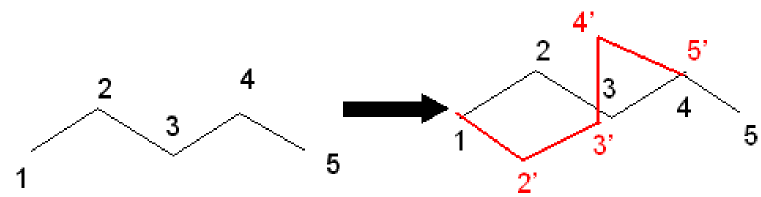

Figure 67: Addition Mutation

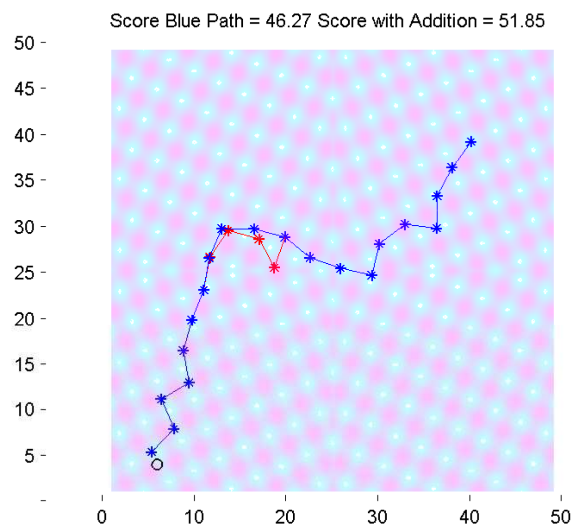

Figure 68: Addition Mutation. *Left:* Example of a section of original path. *Right:* Addition mutated path (red).

4.7.3 Deletion

Deletion mutation searches for a section in the path for which the condition, Expression 15, is true. Figure 69 shows an example of a deletion mutation. One or more points can be removed from the original path and a new path is formed.

$$StepsAway * step > AsCrowFliesDist + step \tag{15}$$

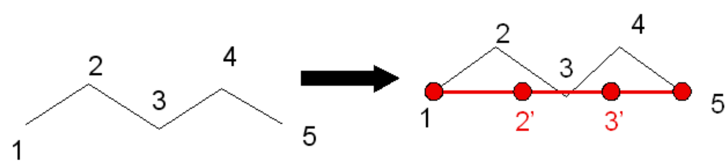

Figure 69: Deletion Mutation. *Left:* Example of a section of original path. *Right:* Deletion mutated path (red); point 2 of the original path was deleted and the new mutated path was formed (red).

4.7.4 Slider

Slider mutation shifts the position of one or more nodes in the path while maintaining an equal step size, Figure 73. Examples of 1 point, 2 point, and 3 point slider mutations are shown in Figures 70, 71, 72. In the 3 point mutation (Figure 72), points 1 and 5 are fixed. Point 3 slides along the line perpendicular to the line intersecting points 2 and 4. New points P: 2', 3', 4' are computed using Equations 16, 17 and replace points P: 2, 3, 4 to create a new path.

$$(P_2'x - P_1x)^2 + (P_2'y - P_1y)^2 = 3.5^2 \tag{16}$$

Figure 70: Slider Mutation. *Left:* Example of a section of original path. *Right:* Slider mutated path (red).

Figure 71: Slider Mutation. *Left:* Example of a section of original path. *Right:* Slider mutated path (red).

$$(P_2'x - P_3'x)^2 + (P_2'y - P_3'y)^2 = 3.5^2 \tag{17}$$

4.7.5 Breeding Algorithm Results and Discussion

The top 16 of 1000 random paths in the sinusoidal terrain are shown in Figure 74. Paths are scattered along the diagonal (as-the-crow-flies) path towards the goal located at (6,4). The BFS path and the near optimal breeding path are shown in Figure 75. The mutated path differs from the BFS in 14 out of 24 BFS path points. The breeding algorithm scores 6% more points than BFS after 20 generations, Figures 76. The larger number of points scored by the breeding algorithm can be attributed to the ability of the breeding algorithm to mutate and find higher scoring points.

The breeding algorithm scored 57.7 after 5 generations while the BFS algorithm scored 25.3 with the plasma terrain, Figure 77. The more than twofold increase in number of points with the breeding algorithm could again be due to the flexibility of

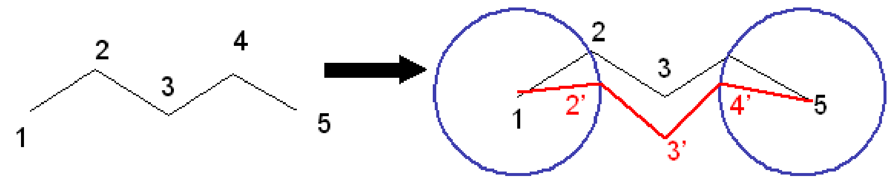

Figure 72: Slider Mutation. *Left:* Example of a section of original path. *Right:* Slider mutated path (red).

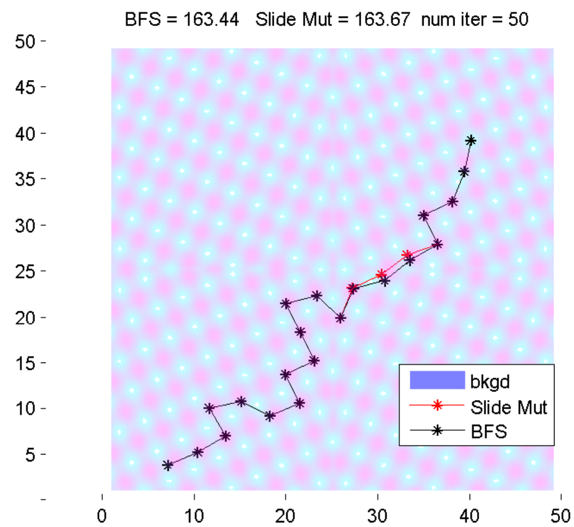

Figure 73: Slider Mutation outperforms BFS

the breeding algorithm to mutate and find near optimal paths.

In the CGLE terrain, the BFS algorithm scored 128.7 points while the breeding algorithm scored 231.3 points, Figure 78. The breeding algorithm immediately finds a path that exceeds the BFS score indicating that a higher scoring path can easily be found.

Table 21 presents a summary of the performance of BFS vs the breeding algorithm. The scores in the plasma fractal terrain are lower than the sinusoidal and CGLE terrains due to the cyan region producing negative elevation scores.

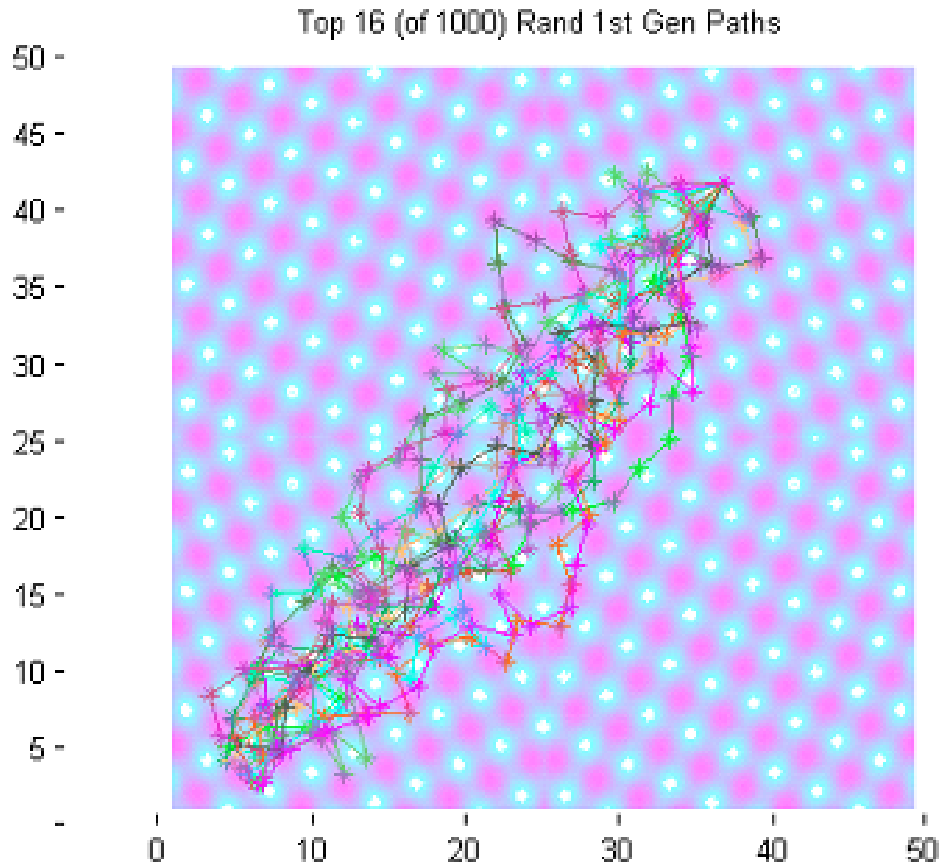

Figure 74: Top 16 (of 1000) Random 1st generation (parents) paths on sinusoidal terrain.

Algorithm	Sinusoidal	Plasma Fractal	CGLE
BFS	194.38	25.3	128.7
BA	206.02	57.7	231.3

Table 21: Summary of BFS vs breeding algorithm (BA) performance in the sinusoidal, plasma fractal and CGLE terrains.

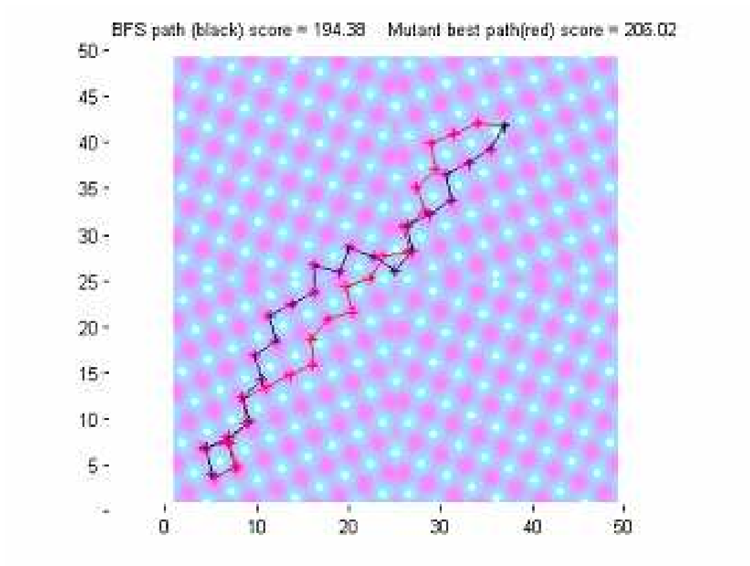

Figure 75: Best First Search (black) scores 194.38 points and best mutated path (red) scores 206.02 points.

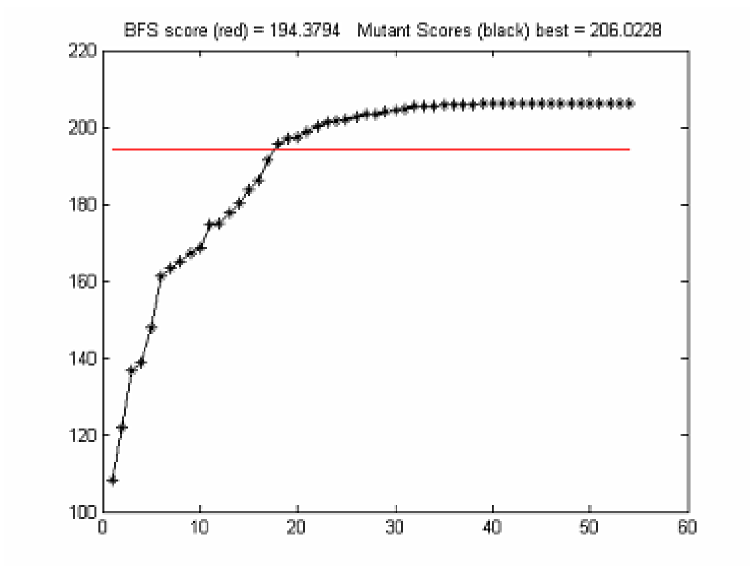

Figure 76: Breeding algorithm performance over 55 generations. Score (y-axis) vs Generation (x-axis)

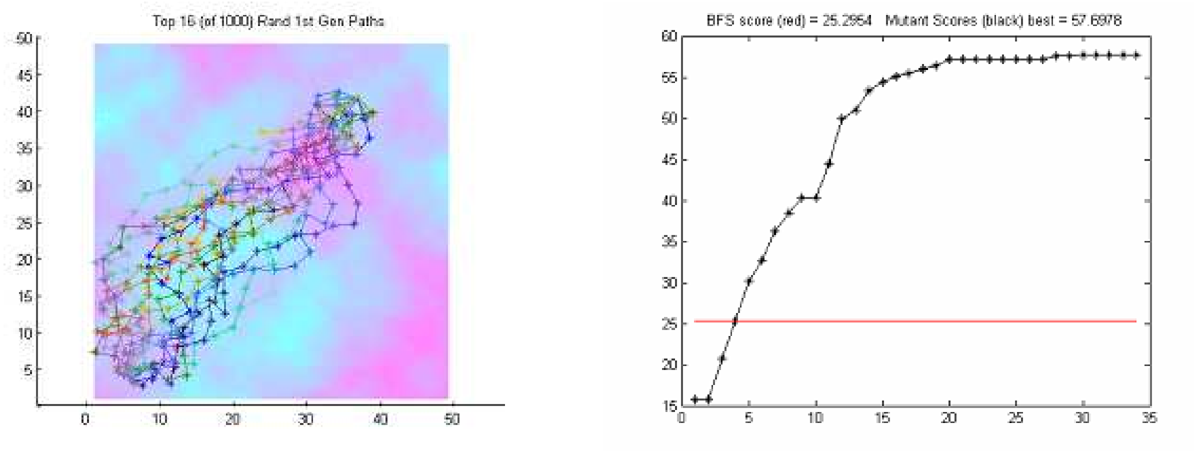

(a) (b)

Figure 77: (a) Top 16 (of 1000) Random 1st generation (parents) paths in Plasma Fractal terrain , (b) Score (y-axis) vs Generation (x-axis)

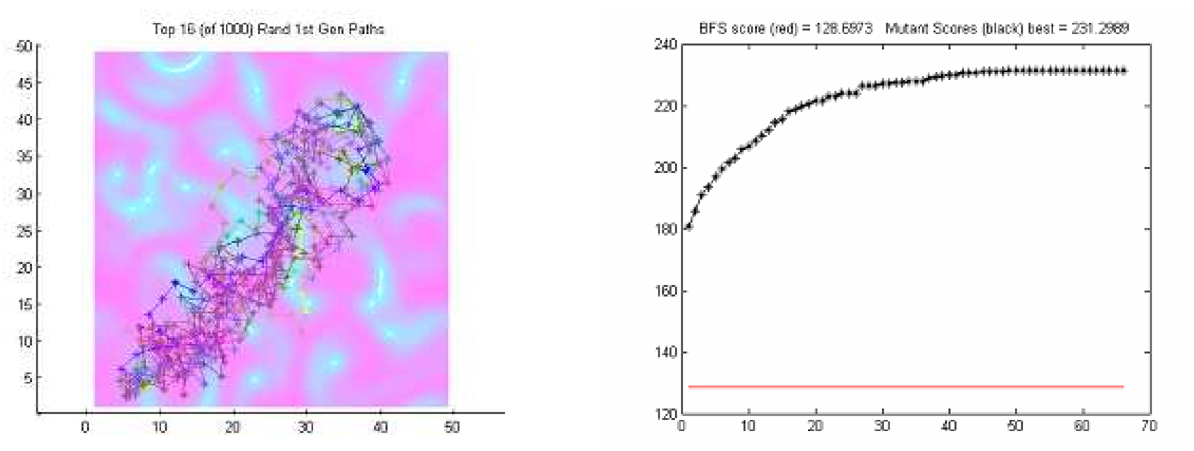

(a) (b)

Figure 78: (a) Top 16 (of 1000) Random 1st generation (parents) paths in CGLE terrain , (b) Score vs Generation

4.8 Neural Network for Learning Local Terrain

A neural network [3] is a computational representation of the elements of the nervous system. The fundamental unit of the nervous system is the neuron. The brain is composed of about 100 billion neurons. Neurons communicate via electrochemical signals. Neurons can receive input through their dendrites. As a neuron receives input, the voltage inside the neuron increases, and if the voltage crosses a threshold then an action potential occurs and the neuron sends a signal down its axon causing its synapse to release neurotransmitters.

In computer science, neural networks are models of neurons that can be used for learning. Weights are numbers representing synapses. Weights are associated and multiplied with each input to a neuron, Figure 79. Weights can be positive or negative representing excitatory or inhibitory responses respectively. Inputs are multiplied by their weights, summed together and then modified by a nonlinearity function, such as a $tanh$ compression function.

Neural networks involve 3 types of units: *(1)* input, *(2)* hidden, and *(3)* output, Figure 80. All inputs are connected to all neurons in the hidden layer. Both the input to and output from hidden units are within the neural network. The number of hidden units is chosen by the designer of the neural network. Output units export data from the neural network.

Neural networks learn by training. Training is achieved by adjusting weights based on a learning rule. For example, Hebb [33] proposed a learning rule that $\Delta w_j k = \mu y_j y_k$ where μ is the learning rate and j and k are two units.

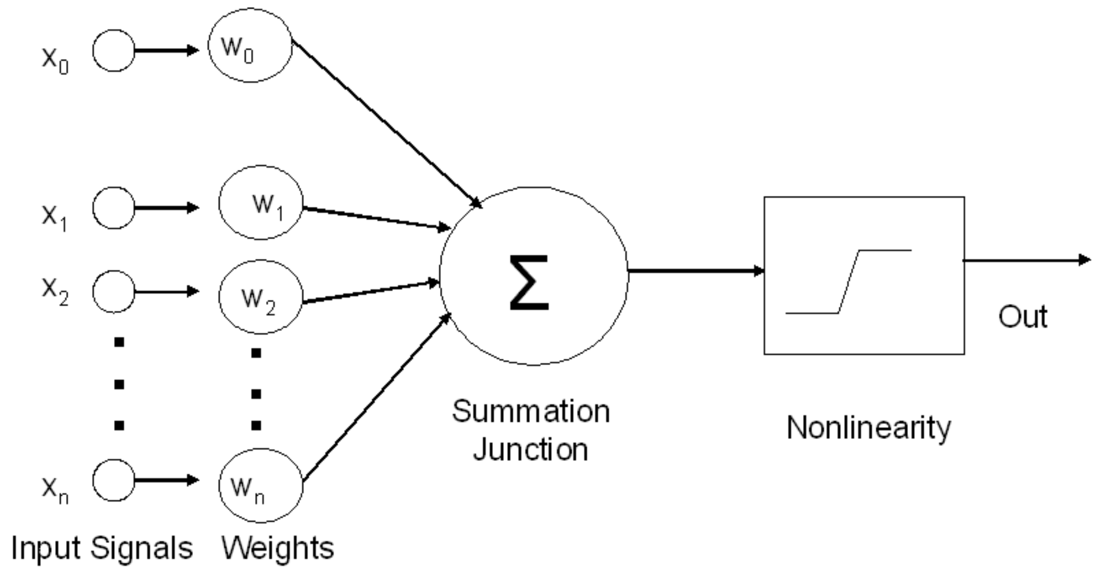

Figure 79: Example of a neural network. Inputs $(x_1...x_n)$ are multiplied by weights $(w_1...w_n)$

A neural network was implemented for learning the local terrain. The network is shown in Figure 81. 16 random training set points and validation set points were generated. From these points, x' and y' inputs were formed. For least mean squared error (LMS, Table 22) the 16 x 16 matrix (**MM**) was multiplied by the elevations (**z**) (column vector) to compute the weights, Equation 18. Weights are then updated using Hebb's Rule.

$$\vec{\mathbf{W}} = \mathbf{MM^{-1}} * \vec{\mathbf{z}} \tag{18}$$

5 hidden units and a learning rate of 0.1 were used in the neural network. Training set and validation set results for learning the terrain are shown in Table 23 and Figure 82. Mean error was 4.5566, much lower than using LMS with an error of 33.262.

One-pattern-at-a-time learning was used for more accurate results than batch

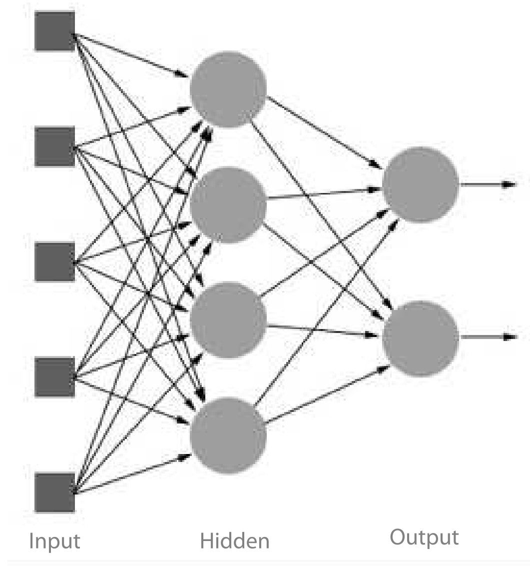

Figure 80: 3 layers used in neural networks: input, hidden, and output

learning (faster). The neural network learns the terrain and by looking 2 steps ahead can find a better path than the best-first-search algorithm , Table 24

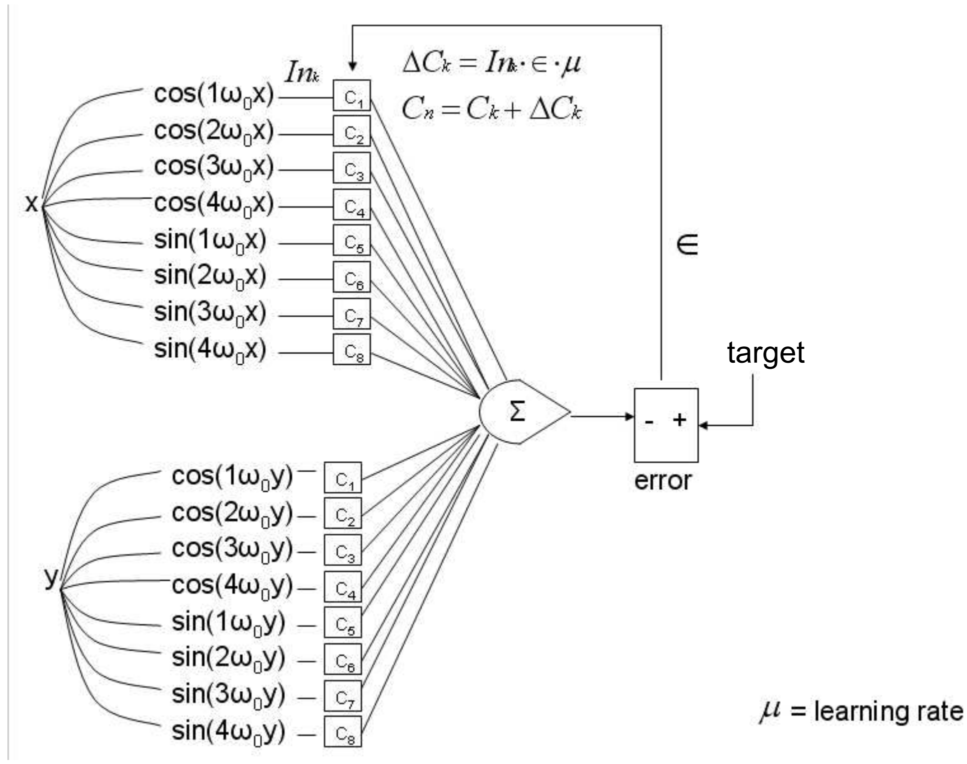

Figure 81: Neural network used in learning the local terrain, where μ is the learning rate and ϵ is the feedback error.

-0.35011	-0.35011	-0.35011	-0.56401	-0.29287	0.27114
-0.49684	-0.49684	-0.49684	3.0067	0.091215	2.9155
-1.3379	-1.3379	-1.3379	-0.13112	-0.58732	0.4562
0.11576	0.11576	0.11576	-2.4482	-0.15913	2.2891
-0.019441	-0.019441	-0.019441	-0.21607	0.024718	0.24079
0.55409	0.55409	0.55409	0.80399	-0.028697	0.83269
-0.44946	-0.44946	-0.44946	-0.60046	0.047152	0.64761
-1.5902	-1.5902	-1.5902	-2.3491	-1.1763	1.1728
-1.2794	-1.2794	-1.2794	-2.1416	-0.60917	1.5324
-0.72585	-0.72585	-0.72585	4.0404	0.1273	3.9131
0.3726	0.3726	0.3726	-0.4393	-0.12364	0.31567
0.9181	0.9181	0.9181	3.3014	0.74822	2.5532
1.9064	1.9064	1.9064	4.8679	1.981	2.8869
-0.096435	-0.096435	-0.096435	-0.41826	0.0067262	0.42499
-1.2988	-1.2988	-1.2988	-13.647	-1.485	12.162
-0.012702	-0.012702	-0.012702	-0.60665	0.041242	0.64789

Table 22: Least Mean Square error for 16 points with total error of 33.26

Training	Validation
-0.35011	-0.2809
-0.49684	-0.2697
-1.3379	-1.2954
0.11576	0.26242
-0.019441	-0.02691
0.55409	0.60022
-0.44946	-0.30523
-1.5902	-1.6992
-1.2794	-1.5336
-0.72585	-0.84195
0.3726	0.42045
0.9181	0.91832
1.9064	1.5377
-0.096435	-0.015664
-1.2988	-1.3054
-0.012702	-0.18199

Table 23: Neural network learning terrain. *Left*: Training, *Right*: Validation

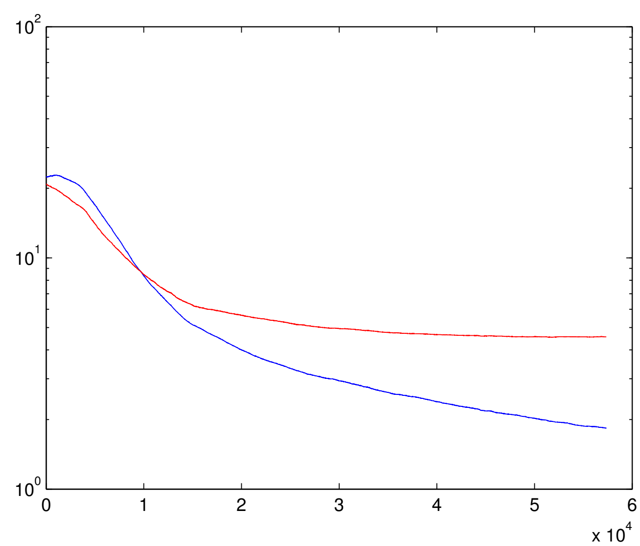

Figure 82: Neural network training (*red* = validation set, *blue* = training set).

BFS	NN 2 step ahead
3	4
2	3
1	2
1	2
9	8
7	7
9	7
9	7
9	7
9	8

Table 24: *Left*: Best first search (BFS), *Right*: Neural network (NN) having access to 2 steps ahead. NN prediction with 2 steps ahead beats BFS 90% of cases.

4.9 Summary

Computational search algorithms were implemented to find optimal paths across a variety of terrains (including the sinusoidal field used in the navigation game, Chapter 3). The breeding algorithm (BA) outperformed best-first-search (BFS). The BA mutated paths by sliding points, adding points, and deleting points to find optimal paths. In the sinusoidal terrain, a somewhat regular terrain, the BA outperformed BFS by 6%. In the more chaotic terrains, plasma fractal and CGLE, the BA outperformed BFS by 1.3 fold and 80% respectively.

The neural network learned sinusoidal terrain. The use of Hebbs rule learning in the neural network produced less error than a least-mean-square approach. The neural network also showed the ability to beat BFS 90% of the time by extrapolating beyond one-step-ahead and by looking two-steps-ahead.

5 Numerosity Estimation of Physical Objects By Vision and Touch

5.1 Introduction

A numerosity estimation used task combining vision and touch, and compared those results to estimation with vision or touch alone. Each participant was asked to estimate after 2 min the number of real-world objects (candies) in a sealed transparent bag. The experiment had five conditions:

(1) vision plus touch

(2) binocular

(3) monocular

(4) video

(5) touch (blindfolded)

The data indicate significantly better estimation in the vision plus touch condition versus all the unimodal conditions. Estimation with binocular vision was significantly better than estimation while watching a video of the bagged objects. Estimates made by participants watching the video were not significantly different than estimates from blindfolded participants.

5.2 Previous work on estimating quantities

For decades researchers have been interested in how perception affects quantitative estimation. Researchers have examined estimation of: lines (Muller-Lyer 1889) and number of dots [8, 71, 8, 11, 12, 6, 27, 28, 32].

Studies of estimating dot count have shown that there are two processes for handling numbers of items: (1) subitizing and (2) estimating. Kaufman et al [46] proposed the term subitizing to indicate dot count less than six. The properties of subitizing include: fast response time, accuracy, and pre-attentiveness. Whereas the properties of estimating include: six or more items, slow response times (about twice as long as subitizing), incorrect counts [13] of the correct number, and controlled attention.

Kaufman et al's [46] subjects viewing 210 random dot display, projected onto a screen for 200 msec, underestimated the total number by 23.8%, Figure 83. Since area goes as the square of perimeter, Kaufman et als subjects may have attended too much to dots around the edge of the arrangement.

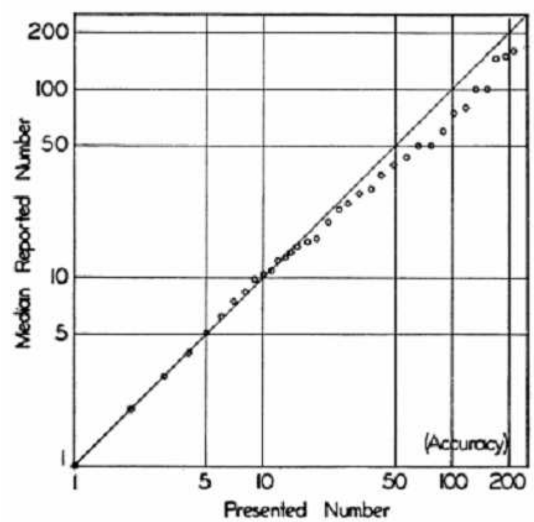

Figure 83: Median estimates of number of dots shown on a screen. Kaufman *et al* [46]

Ginsberg [27] arranged dots in concentric rings in two arrangements: (1) regular and (2) random and participants viewed the dots for 2.24 sec. His subjects overestimated by 12.6%, 91 dots in a regular arrangement and significantly underestimated by 22.2%, 91 dots in a random arrangement, Table 25.

Dots	7	19	37	61	91
Regular	6.93	26.43	41.00	85.00	102.52
Random	6.98	21.19	36.04	51.05	70.50
p	ns	<.01	<.05	<.001	<.001

Table 25: Mean estimates of different numbers of dots and arrangements. Adapted from Ginsberg [27].

Researchers have used two methods for studying estimation: direct [2, 36, 37, 78, 55, 44] and pairwise [81, 1]. The direct method asks participants to make a quantitative assessment, such reporting the number of dots on a screen.

The pairwise method has a participant compare two (or more) samples presented simultaneously. Pairwise comparisons have focused on area estimates [2, 78, 55, 1, 44]. However, the pairwise method does not provide as much information as the direct method because subjects responses are generally limited to binary (base 2) responses. Adamic et al [1] used both direct and pairwise methods for estimating the area of irregular shapes. In the pairwise condition, Adamic et al had subjects compare 2 shapes simultaneously for 15 sec and decide which was larger in area and by what factor the perceived larger shape was bigger than the perceived smaller shape. In comparing the results from direct and pairwise estimation of area, Adamic et al found the standard deviation decreased but not the mean in the pairwise condition.

Burr and Ross [11, 72] discovered a compelling illusion that supports the idea of numerosity as being a fundamental perception. In one version (2008 supplemental materials) they had a subject adapt for several seconds to a 6° field of many dots

(400) just lateral to a fixation point. The adapting field then disappears and the subject is shown two separate fields of dots (test and probe) and asked to choose which field had more. The test field is shown where the adapting field had been. When the test and probe fields have the same number of dots (say 30), the test field appears to have dramatically fewer dots than the probe. Gaze must be maintained on a central fixation point for the illusion to hold. Their results present a caution to experiments where a subject may have a chance to stare for a while at a dot pattern while trying to estimate the number of dots seen.

A review of the literature does not produce many examples of estimation while watching video. Shim et al [76] had subjects watch video of a person lifting weights and then estimate the weight lifted. They found that participants overestimated weights under 15 kg and underestimated weights over 15 kg (up to 100 kg).

Domini and Caudek [17] used a rotating 3-D cluster of dots on a screen and asked participants to estimate when a probe dot appeared aligned in depth with two nearby target dots having both the same velocity and disparity. They found participants were able to perceive structure from motion. Domini and Caudek proposed a probabilistic model based on analysis of optic flow to reconstruct 3-D shape.

Researchers have studied numerosity estimates by tactile perception [23]. Humans can perceive tactile sensation either actively or passively. Active touch involves a participant's fingers moving over a surface. In passive touch a participant's arm or leg is immobilized while applying tactile stimulation to the participants skin. Researchers studying numerosity have focused on passive tactile perception. Gallace et al [24] studied numerical estimation by using 5 vibrotactile stimuli placed on different parts of the body (above the elbow, wrist, below knee, waistline, and calf). Gallace [24] examined subitizing in tactile stimuli. Riggs et al [69] also used passive tactile perception, restricted to only the subjects fingertips. Vega-Bermudez et al [91] showed there was no difference in performance between active and passive tactile perception. For numerosity estimations involving touch, either active or passive tactile perception can be utilized.

Plaisier et al [66] examined tactile numerosity judgments (direct method) of 1 to 16 spheres using blindfolded subjects. Spheres were 1.86 cm in diameter, weighed 29 g each (suspended from wires). They found that for stimulus size of 1 to 3 spheres, subjects made no errors. However, as the stimulus set size increased past 3, participants made more errors. Plaisier et al found subitizing for haptic perception of tangible stimuli, but since the largest element of their stimulus array was 16 the effect of large number of stimuli on haptic judgments is unknown.

The ability of blind subjects to estimate has been studied. Castronovo and Seron [14] studied the ability of blind subjects to estimate using the auditory modality for the presentation of the stimulus and then haptic control of the response. Castronovo and Seron had blind subjects listen to a voice stating a number between 5 to 64 and instructed a subject to reproduce the number by clicking a button that many times. Castronovo and Seron showed that with stimulus magnitudes greater than 14 sighted participants increasingly overestimated while blind subjects showed accuracy.

Researchers have extended the study of numerosity estimation by changing the stimuli from dots to shapes, have sought to understand the way we process and compare shapes, and have found that shape affects estimation of area [2, 55]. However, the literature reveals a lack of agreement on stimulus characteristics that account for objects with the same area but different shape being perceived as being different in area. On the one hand, Anastasi [2] used a variety of outlines of shapes (rhombus, square, star, diamond, equilateral triangle, cross, and circle) and found a positive correlation between estimated area and perimeter. On the other hand, Smith [78] created irregular randomly shaped objects and showed a negative correlation between area estimation and perimeter.

Held et al [34] examined bimodal perception using vision and touch for subjects who were congenitally blind but whose vision had been partially restored. Within 48 hours of the restoration surgery, subjects were asked to make two comparison tasks using LEGO-style shapes: within-modality and cross-modality. In the within-modality condition a subject touched a sample shape and then touched two shapes, one of which was the same sample and the other was a distractor shape. In the cross-modality condition a subject touched the sample and then viewed two shapes and decided which shape matched the sample. Held et al found that at 48 hours, subjects demonstrated excellent performance in the within-modality task but only performance near chance for the cross-modality condition. After 4 more days of experience, subjects demonstrated significant improvement in the cross-modality condition.

Most visual numerosity estimation tasks have asked subjects to look at dots on a screen. The effects of vision and touch on estimation performance under the same conditions were investigated. Tangible real-world shapes were used for direct numerosity estimation by both senses.

5.3 Arrangement

Items can be arranged in either regular or irregular arrays, Figure 84. In the regular arrangement a subject could count the number of candies in two rows (7 and 8) and multiply (7x4 + 8x4 = 60) to get the correct answer in 10 sec. Whereas, counting the number of items in the irregular arrangement is hard to do in 10 sec but possible in 2 mins. The bag used in the experiment contains 305 items which is large enough to prevent subjects from counting the total number of items in either 10 sec or 2 min.

Figure 84: *Left*: Regular arrangement of 60 M&M's. *Right*: Irregular arrangement of 100 M&M's.

5.4 Methods

Participants were 88 men and 77 women from Brown University, Table 26. Participants were tested one at a time. Each subject was given a consent form from the approved Brown University Institutional Review Board protocol. A subject participated in only one condition; no participant ran more than one condition.

After signing the consent form the subject heard a script about what he or she was to do:

"I will hand you a clear plastic bag of candy. The bag contains peanut M&Ms, jelly beans, and gummy worms. Your task is to estimate the total number of objects in

Modality	Male	Female
Vision plus Touch	25	27
Vision Only	17	13
Monocular	12	9
Video	16	14
Touch Only	18	14
Totals	88	77

Table 26: Number of subjects in each condition. Each subject was randomly selected to participate in only one of the five conditions.

the bag. I will ask you to write on a piece of paper your estimate after 2 minutes. I will keep track of time."

The bag contained 305 candies (138 peanut M&M's, 152 jelly beans, 15 gummy worms). There were six colors of M&Ms(red, orange, yellow, green, blue, and brown) and assorted colors of gummy worms and jelly beans, Figure 85.

A preliminary study was conducted and asked subjects (8M, 5F) to count by hand all the peanut M&Ms they were given in a sealed transparent plastic bag. When the number of items was larger than 150, it was not possible to count all the items within the alloted time. For the main experiment the bag contained 305 candies of 3 different sizes.

Five conditions were arranged: (1) vision plus touch (2) vision (3) monocular (4) video and (5) touch (blindfolded). The same bag of candy was used in all conditions.

In the vision plus touch condition (25 men and 27 women), participants were told that they could handle and look at the bag, but not open it.

In the vision condition (17 men and 13 women) a participant was seated in front

Figure 85: Example of quart size candy bag containing 305 candies (138 peanut M&Ms, 152 jelly beans, 15 gummy worms) used in all conditions

of a turntable (32.5 cm in diameter). The bag of candy was placed on the turntable about 40 cm from the participants eyes. Participants were told that they could rotate the turntable by the edge but were not allowed to touch the bag.

The monocular condition (12 men and 9 women) was the same as the vision condition except that the participant was asked to wear an eye patch on their non-dominant eye (determined by testing prior to experiment by viewing an object in the distance, closing one eye, and observing whether the object moved).

During the video condition (16 men and 14 women), a participant watched a video of the candy bag on top of the turntable rotating 2 cycles/min for 2 min. on a ViewSonic 1926 monitor with the participant seated 40 cm from the screen. The image appeared the same size in visual angle (20 deg) as the vision condition.

For the touch condition (18 men and 14 women), each participant put on a blindfold, was handed the candy bag and then told to estimate by touch the number of items in the bag within 2 min.

5.5 Results

Participants estimated most accurately in the vision plus touch condition, followed by the vision, monocular, video, and touch (least accurate estimation) conditions, Table 27.

	Vision+Touch	Vision	Monocular	Video	Touch
Mean	316.6	253.9	235.1	207.5	202.7
Median	275	250	216	205	175
SD	185.7	91.6	70.6	82.7	103.7
N	52	30	21	30	32

Table 27: Mean, Median, Standard Deviation, and Number of Participants Across Different Sensory Modalities in Estimating the Number of Candies in the Bag Containing 305 Items.

The mean estimate of 316.6 in the vision plus touch condition was not significantly different (using the t-value and t-test) from the correct answer of 305 ($t_{51} = 0.449$, $p = 0.655$). The vision plus touch condition was significantly different from all other conditions using two-tailed t-tests, Table 28.

Binocular visual information yielded estimates closer to the correct answer than the video ($p = 0.0443$) or blindfold ($p = 0.0435$) conditions. Participants who viewed the video of the candy bag did not perform significantly different from the blindfolded subjects ($p = 0.839$). Subjects wearing an eye patch (monocular condition) estimated

	vs Correct Ans (305)	Vision	Monocular	Video	Touch
Vision+Touch	0.655	0.0445*	0.0083*	0.0005*	0.0005*
Vision	0.005*		0.4119	0.0443*	0.0435*
Monocular	0.0002*			0.2085	0.1827
Video	$4.62\text{x}10^{-}7*$				0.8391
Touch	$4.09\text{x}10^{-}6*$				

Table 28: Two-tailed p-values comparing each sensory modality condition to each other and to the correct answer of 305. Asterisk (*) indicates significant difference.

significantly worse than vision plus touch participants, but monocular subjects were not significantly different from binocular vision subjects nor blindfolded.

After 2 minutes of blindfold inspection, 13 of the subjects were asked to remove the blindfold and given 10 secs to make another estimate, Table 29. The estimates made after blindfold removal were not significantly different from their 2 min estimates (p = 0.804; a demonstration of anchoring [88] to a prior thought, and away from the vision plus touch answer of 316.

	2 min Blindfold Estimate	10 sec estimate after removing blindfold
Mean	183	174.46
Median	150	170
SD	99.09	72.19
N	13	13

Table 29: Mean, median, standard deviation, and number of subjects who estimated the number of objects in a bag in the blindfolded condition and then removed blindfold after 2 min and made another estimate 10 sec later.

To extend the parameter space, subjects were first handed a bag with 222 items, then a bag with 444 items, and asked for estimates at 10 sec and 2 min in each case.

It was hypothesized that a subject would have access to the signals of Golgi tendon organs and be able to sense weight for a comparison [56]. In Table 30 are the summary results.

	222 (10 sec)	222 (2 min)	444 (10 sec)	444 (2 min)
Mean (n = 19)	172	192	384	429
Male (n = 10)	197	202	379	465
Female (n = 9)	147	182	390	393

Table 30: Means and number of participants who estimated the number of objects in a bag containing 222 objects and 444 objects after 10 sec and 2 mins

When the ratios of the 444_est / 222_est were compared for the three categories in Table 5 the differences from the correct ratio of 2.0 were insignificant (0.36 >> 0.05). Table 31 shows calculations:

	444/222 (10 sec)	444/222 (2 min)
All subjects significance	0.36	0.35
Male	0.53	0.37
Female	0.29	0.30

Table 31: Ratio of 444 to 222

5.6 Discussion

A task was developed in which subjects are asked to estimate the number of centimeter-size candies in a clear plastic bag containing hundreds of items. The following was found:

1. The sensory combination of vision plus touch produces more accurate estimates than either of the senses alone.

2. Subjects who saw a real bag of candy (binocular condition) rotating on a turntable estimated better than participants who saw a video of the same action, at the same visual angle.

3. Somewhat surprisingly, video viewing was not significantly different from blindfolded exploration results in estimation accuracy.

The neural locations for estimation have been explored using fMRI. Piazza et al [65] showed that numerosity estimation of visual stimuli occurs in the right intraparietal cortex. Kitada et al [47] found activation in right prefrontal cortex for subjects performing a touch estimation task. For bimodal stimulation using vision and touch [54, 53], Macaluso and Driver (2001) showed increased activity in the intraparietal sulcus. Possibly the vision plus touch condition selectively activated intraparietal sulcus neurons to achieve its better performance.

Participants making estimates closer to the correct answer in the binocular vision condition, compared to the video condition, are utilizing stereo depth information. In a future study subjects could estimate after viewing with liquid crystal goggles, a 3D video of the candy bag rotating on the turntable; such estimates could improve to be better than monocular viewing.

Regarding binocular vision the primate visual system consists of two pathways: (1) ventral "what" stream through the temporal lobe and (2) dorsal "where" pathway to the parietal lobe. Studies suggest that perception of 3D shape involves both the dorsal and ventral pathways [62, 63]. Since the results show participants estimating closer to the correct answer in the vision condition than in the video condition, subjects could be using both dorsal and ventral streams while viewing the real-world candy bag (vision task) but only using the dorsal pathway when watching the video. The combination of dorsal and ventral stream activity likely improves estimation.

6 Direct and Pairwise Area Estimation of Rigid Physical Shapes

A perceptual task was used in which a participant is asked to estimate the area of three-dimensional real world shapes. Participants were allowed to view and touch the shapes. Two estimation methods were used (1) direct and (2) pairwise. Participants were 21 students from Brown University. The average error estimated by participants in the direct method was 14.43%. The error decreased to 0.34% in the pairwise method where participants were simultaneously handed two different shapes. Both direct and pairwise methods when used with three-dimensional stimuli showed considerable decreases in error rates over previous two-dimensional results. The author is the first to demonstrate that pairwise comparisons improve area estimation accuracy with real world shapes.

6.1 Introduction

Mehler and Bever [58] examined discrimination of relative numbers of objects by children. They were interested in determining the development of quantity conservation: the ability to discern that are more items in one array even though the perceptual information is different. Mehler and Bever studied over 200 children ranging in age from 2 years 4 months to 4 years 7 months. They used two types of stimuli: (1) clay pellets and (2) M & M's (edible). They asked children to decide which array contained more items, Figure 86. In Figure 86(a) the number of objects is equal in both rows and the perceptual length of each row is equal, whereas in Figure 86(b) the top row is perceptually longer than the bottom row while the bottom row (shorter length) contains more items. Figure 86(c) depicts the last permutation: top row has fewer items and shorter length than the bottom row.

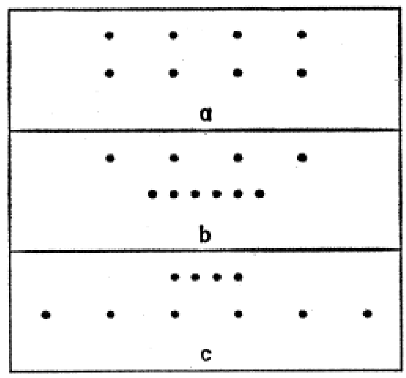

Figure 86: *(a)* equal spacing and number of M&M's; *(b)* top row longer line, fewer M&M's than bottom row; *(c)* top row shorter line and fewer M&M's than bottom row. (From Mehler & Bever [58])

Mehler and Bever found that the children fall into three groups. The first group were the 2 year to 3 year old children who were able to correctly discriminate the relative number of objects. Whereas, the 3 year to 4 year olds seemingly fell prey to perceptual influences and picked the longer row with fewer items. However, children over 4 years regain the quantity conservation ability and correctly pick the row with more objects.

Interestingly, Mehler and Bever found quantity conservation across all age groups when they used M & M's instead of clay pellets. Mehler and Bever speculate that by instructing the children to "take the row you want to eat and eat all the M & M's in that row", they sufficiently motivated the children and found quantity conservation.

Piaget [64] critiqued Mehler and Bever's study and extended their work to the perception of volume. Part of Piaget's criticism involved the lack of a condition involving: an equal number of objects in both rows but having either the top or bottom row longer than the other row (same number of objects but spaced farther apart), Figure 87. Piaget found that children reported the longer row as containing more objects thereby indicating no conservation. Piaget studied how 29 children perceive the volume of a liquid in different size cylinders. He poured a liquid from a low wide cylinder into a tall skinny cylinder and asked children which cylinder contained more liquid. Piaget found that children thought the tall narrow cylinder contained more liquid. He concluded that the one-dimension of height was used for volume estimation.

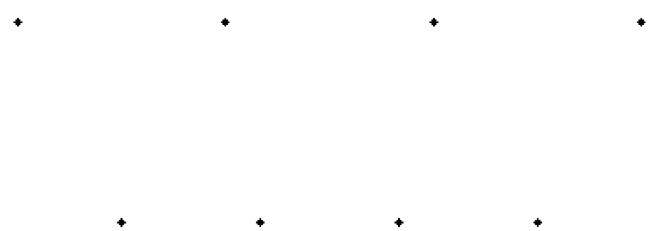

Figure 87: Evenly spaced dots with top row forming a longer line than the bottom row. Both rows have the same number of dots.

Shapes are a fundamental component of the perception of the world [59]. Shapes come in a myriad of sizes and forms. Researchers have sought to understand the way we process and compare shapes and have found that shape affects estimation of area [2, 55]. However, the literature reveals a lack of agreement on stimulus characteristics that account for objects with the same area but different shape being perceived as being different in area. On the one hand, Anastasi [2] used a variety of outlines of shapes (rhombus, square, star, diamond, equilateral triangle, cross, and circle) and found a positive correlation between estimated area and perimeter. On the other hand, Smith [78] created irregular randomly shaped objects and showed a negative correlation between area estimation and perimeter.

Holmberg and Holmberg [36] used rectangles and demonstrated an effect of elongation; as the height-to-width ratio increased so did the estimated area. However, Holmberg and Wahlin [37] did not find an elongation effect. Warren and Pinneau [92] also studied the effect of form on apparent area. Warren and Pinneau used pairwise comparisons of circles, squares, triangles and crosses. They found two groupings for apparent area: *(1)* circle with square and *(2)* triangle with cross. Warren and Pinneau concluded that participants equated the shapes in what they call: "the maximum vertical dimension".

Martinez and Dawson [55] investigated the discrepancy between positive correlation for geometric shapes and negative correlations for random shapes between area and perimeter. Martinez and Dawson used stimuli from six form classes: triangles, quadrilaterals, polygons, ellipses, stars, and irregular figures made from white paper, Figure 88. For each participant, six figures were randomly placed in a row and subjects were asked to rank order the shapes. In the first part of their experiment the shapes in each row came from the same class of shape; in the second part of the experiment, the shapes in each row came from different classes of shapes. Martinez and Dawson found negative correlations of area with perimeter for non-geometric shapes as well as geometric shapes, seemingly in agreement with Smith [78] but in contradiction to Anastasi [2] and Holmberg and Holmberg [36].

Researchers have used two methods for estimation: direct [2, 37, 78, 55, 44] and pairwise [81, 93, 5, 38, 1]. The direct method involves asking participants to make an

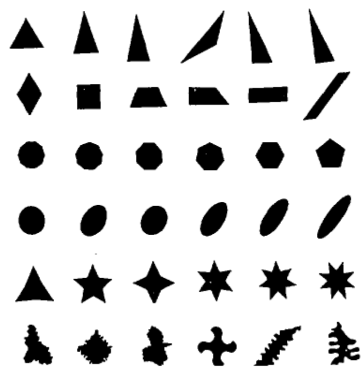

Figure 88: Catalog of six classes of shapes from top to bottom: triangles, quadrilaterals, polygons, ellipses, stars, and irregular. Adapted from Martinez and Dawson [55]

assessment of a stimulus. The pairwise method entails having a participant compare two shapes.

The pairwise method has been used in bimodal perception (vision and touch) studies of hand held weights [93, 5, 38]. In the classic study, Weber placed a weight in each hand of a participant. He found that participants were able to discriminate between 21 g and 20 g weights, 42 g and 40 g weights and so on. He showed that the just noticeable difference in all weight comparisons was 5% of the lighter weight.

The hypothesis was that there would be an increase in gain of accuracy for three-dimensional real-world shapes than two-dimensional shapes, and that the pairwise method would produce smaller area estimation error than the direct method.

6.2 Methods

Sample

Participants were 21 undergraduate and graduate students from Brown University (13 men and 8 women), ranging from 19 to 33 years (M = 23 yr., SD = 4).

Measures

In the first part of the experiment (direct estimation method), each participant was instructed to estimate by vision-plus-touch the area of a shape using the unit square area as a reference, Figure 89. The area of each shape was 10 units. A participant was handed each of the five shapes (one at a time), in a random order, plus the reference unit square and was given 15 seconds per shape to make an estimate. After 15 sec, shapes were taken away from participant and returned to an opaque storage box.

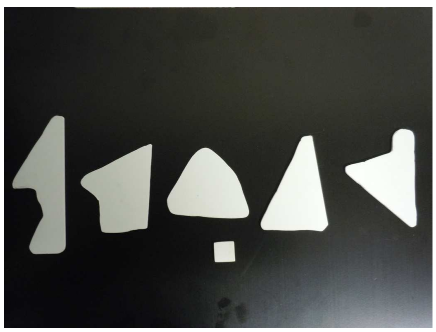

(a)

(b)

Figure 89: *(a)*: Shapes 1 - 5 (left to right) and unit reference square. *(b)*: Hand holding one of the five shapes

In the second part of the experiment (pairwise estimation method), a participant was handed two shapes at a time in a random order and given 15 seconds to make a judgment. Participants were instructed to decide which of the two shapes was larger in area (and if larger by what percent) or if both shapes were equal in area. Ten comparisons were made by each subject to complete all possible combinations of pairs of shapes.

Stimuli

5 three-dimensional shapes all equal in area were used for both parts of the experiment. The contours of the shapes were the same as those created by Adamic et al [1]. Each shape weighed 14.2 g and the unit reference square weighed 1.42 g. The shapes were cut from a sheet of 1/8 inch white styrene.

6.3 Results

The direct method for area estimation produced an overall error of 14.43%, Table 32. The percent error for each shape in the direct method ranged from 11.00 to 17.41%. The overall mean area estimate was 9.39 with standard deviations ranging from 1.11 to 2.28 across the five shapes.

Estimation Method	Shape 1	Shape 2	Shape 3	Shape 4	Shape 5	All
Direct						
Error (%)	16.67	13.96	11.00	13.10	17.41	14.43
M	9.00	9.84	9.76	8.88	9.45	9.39
Mdn	9.00	10.00	10.00	9.00	9.00	9.00
SD	1.77	1.84	1.45	1.11	2.28	1.74
Pairwise						
Error (%)	0.36	0.57	0.27	0.20	0.29	0.34
M	10.04	10.06	10.03	10.02	10.03	10.04
Mdn	10.00	10.00	10.00	10.00	10.00	10.00
SD	0.12	0.15	0.09	0.09	0.10	0.11

Table 32: Statistical results for direct method and pairwise methods of area estimation

The pairwise method for area estimation produced an overall error of 0.34%. The percent error for each shape ranged from 0.09 to 0.15. The overall mean estimate was

10.04 with a standard deviation of 0.11.

The author examined whether participants improve their estimates across the five runs using the direct method (with the order of the five shapes randomly picked for each subject). The average error which participants made on their fifth run was no better than the average error on their first run. Figure 90 shows the mean percent error for participants across the five presentations of shapes in the first part of the experiment (direct method). Since participants do not receive any feedback on their estimates, the result of no significant difference between the average errors across trials can be expected.

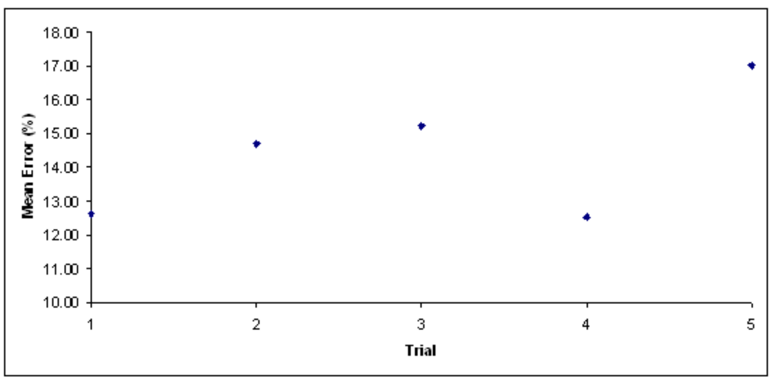

Figure 90: Mean Percent Error for each trial using the direct area estimation method. Subjects were given shapes in a random order, so each trial contains estimates from different shapes.

Figure 91 shows the mean estimates for each trial of the direct method part of the experiment. Trials 1,2,4 and 5 are not significantly different from the correct answer of 10 at the 5% two-tailed p value level (Trial 3 is significantly different from the correct area estimate of 10).

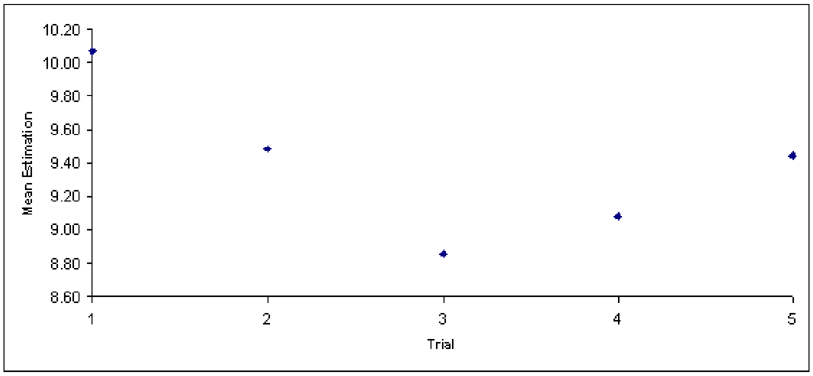

Figure 91: Mean estimates for each trial using the direct area estimation method. Subjects were given shapes in a random order, so each trial contains estimates from different shapes. Each shape had an area of 10 units.

6.4 Discussion

Adamic et al [1] found that participants make more accurate area estimates in the pairwise condition than in the direct method for two-dimensional stimuli and that the gain in accuracy for two-dimensional stimuli was 20.24%, almost double the 11.78% gain for one-dimensional stimuli [48]. The participants made more accurate area estimates with the pairwise method than with the direct method. The 0.34% overall error in the pairwise method was less than the 14.43% error in the direct method.

In order to compare the participants' error to the error obtained in Adamic et al's [1], Adamic et al's data set was recreated based on their means and standard deviations. The data was significantly different from Adamic et al [1] ($p < 0.002$).

When the tangible shape results were compared with two-dimensional [1] results, the error for the participants using physical objects was 11.32% less than the two-dimensional error in the direct method.

In the pairwise method, the participants assessing physical stimuli had less error than the two-dimensional error; the 0.34% error in the three-dimensional pairwise method was less than the 5.51% two-dimensional pairwise error [1]. One reason for the improvement in both methods of the three-dimensional task could be because participants could handle the shapes. By using a bimodal approach, participants seem to utilize the combination of visual and tactile sensory information and make better area estimations.

The mean estimates for the participants were approximately the same as the two-dimensional mean estimates in Adamic et al. However, the standard deviation for the participants is 55% less than the two-dimensional results in the direct method and 11% less than the two-dimensional pairwise method. The data suggest that even though participants estimate, on average, close to the correct answer in both two-dimensional and the real-world objects, the smaller standard deviations with the real-world shapes suggests that participants are consistently closer to the correct answer when using tangible shapes.

Future studies are needed to address the issue of stimuli projected onto a screen versus real-world shapes. The author plans to film a stereoscopic video of the real-world shapes for both direct and pairwise area estimation. Subjects would be asked to wear 3-D goggles to view the 3-D video on a 3-D computer screen (NVIDIA Vision system). The author suspects that participants watching the 3-D video would make more accurate estimates in both the direct and pairwise methods than in previous one-dimensional and two-dimensional results, but less accurate than the three-dimensional real world shape results.

Piazza et al. [65] showed in an fMRI study that relative numerosity estimation of static images occurs in the right intraparietal cortex. Future fMRI studies need to investigate the neural activity of participants performing area estimations of tangible shapes to determine if the same cortical areas are active during area estimations of tangible shapes.

Another future study would be to blindfold subjects and have them estimate the area of the three-dimensional shapes via both the direct and pairwise methods. The author speculates that blindfolded participants would have higher error in both methods than non-blindfolded participants.

7 Conclusions and Future Directions

In this thesis the author has examined the topics of navigation and estimation. In path integration studies, humans learned to make better path estimates using elevation and direction to goal with limited information: *(a)* limited view of the terrain and *(b)* less than perfect resolution of the terrain.

Furthermore, the path optimization studies showed how breeding algorithms can find optimal paths through the terrain. The neural network demonstrated simulated learning of a limited view of the terrain and then extrapolation to nearby locations to compute paths for which a best-second-search finds a better path than the best-first-search algorithm.

Future work could involve a three-dimensional version of the game in which subjects would wear 3-D goggles while completing the same task. The purpose of the experiment would be to examine the effect of depth perception of the terrain on human performance in path exploration.

The theme of estimation from location in an open terrain in a virtual (computer generated) setting was continued to estimating by watching a video of number of items in an enclosed space, and then compared to estimation performance of real tangible items. In the numerosity estimation experiment, estimates improved when sensory modalities of vision and touch were combined. Subjects who viewed a real bag containing a variety of shapes and sizes of candy rotating on a turntable made more accurate estimates that subjects who saw a video of the same action, at the same visual angle of size. Future work in this area could pursue mental rotation of 3-

D images by having participants view a 3-D video of the bag of candy and estimating the number of items.

From estimation of number of items in a bag, dimensionality was extended to area estimation of irregular rigid physical shapes. The error for the participants using physical objects was 11.32% less than the two-dimensional error in the direct method of Adamic *et al.* [1] suggesting that area estimation performance is enhanced with real world tangible items.

In the pairwise method, the participants assessing physical stimuli had less error than the two-dimensional error; the 0.34% error in the three-dimensional pairwise method was less than the 5.51% two-dimensional pairwise error [1]. One reason for the improvement in both methods of the three-dimensional task could be because participants could handle the shapes. By using a bimodal approach, participants seem to utilize the combination of visual and tactile sensory information and make better area estimations.

Future studies are needed to address the issue of stimuli projected on a screen versus real-world shapes. One study could involve filming a stereoscopic video of the real-world shapes for both direct and pairwise area estimation. Subjects would be asked to wear 3-D goggles to view the 3-D video on a 3-D computer screen (NVIDIA Vision system). The author suspects that participants watching the 3-D video would make more accurate estimates in both the direct and pairwise methods than in previous one-dimensional and two-dimensional results, but less accurate than the three-dimensional real world shape results.

8 Appendix A: Definitions and Discussion

8.1 Definition of Performance

Performance: a measure of success or failure in a task.

In 1908 Yerkes and Dodson [97] showed that arousal affects performance. Yerkes and Dodson found that performance in rats in a discrimination task varied by the stimulus strength (electrical shock). As the stimulus strength increased, rats were able to perfectly complete the discrimination task in fewer number of trials.

After the stimulus strength reached a certain point (different for each set, where each set differed in the amount of brightness making the task easy, medium, or hard), rats needed an increased number of attempts to until they achieved 100% accuracy in the discrimination task. Rats performed at an optimal level (requiring the least number of trials) when the stimulus strength was at an optimal strength for the rats.

Yerkes and Dodson graphically represented the trend of a decrease in number of trials followed by an increase in number of trials by a "U-shaped" curve, Figure 92

8.2 Definition of Quality

Quality: description of a characteristic or attribute of an object or image. For example, a blurry photograph could be referred to as a **poor quality** image.

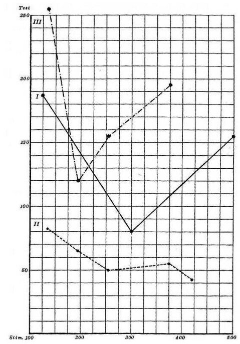

Figure 92: U-shaped curve showing number of tests for a rat to complete discrimination task vs stimulus strength (units). Minima of the plots represent the best (optimal) performance, from Yerkes & Dodson [97]

8.3 Definition of Numerosity

Numerosity: number of items in an array

9 Appendix B: IRB Approved Protocols and Consent Forms

9.1 IRB Approved Protocol and Consent Form for Navigation Experiment

LAY-PERSON SUMMARY We are interested in navigation with uncertainty. In particular, we are finding out what happens when the quality of environmental feedback is inversely linked to navigation speed: How is navigation of a fast-moving rover affected when its view of the world begins to blur? While some of our work is mathematical modeling of navigation as a feedback problem, and other aspects have to do with robotics, a major effort of our investigation is a desire to consider how humans deal such uncertainty.

To that end we have developed a "computer game" which presents the player(s) with a "mogul field" of hills and valleys. The player is aware only of his nearby surroundings, but an "overseer" keeps a more comprehensive score that accounts for distance from goal and time duration of the trial. By linking the score of a pathway from start to goal with how well the player stays on higher elevations, then blurring the view of the field at higher speed, we can study how humans learn to increase their scores in repeated trials. An analogy: Imagine night skiing guided only by a head-mounted lamp.

In a more complex version of the game, the subject will experience the uncertainty of a drone appearing on a "collision" course; the player and the drone can bounce off each other like billiard balls, with, from the players point of view, an unpredictable effect on his or her final score.

After studying the subjects navigational improvements we should be able to formulate a hypothesis which explains the learning process. We should be able to cast the hypothesis into the form of an algorithm that we can code into the drone rover. We will be interested to measure human performance against such a "smart drone."

Another aspect of our work: program a computer to search for the optimal path to goal, given the scoring components of the overseer function.

FUNDING: At one point (2002-2005) some the Navigating with Uncertainty research was supported by a grant from the McCune Foundation, but now it is self-funded.

SPECIFIC AIMS OF THE HUMAN SUBJECTS COMPONENT: PURPOSE: To score the navigation from start to goal of repeated trials by human subjects. The results will allow us to formulate a hypothesis about how human learning of a navigation path takes place. PROCEDURES: A player will be given a questionnaire, about handedness, visual acuity, and video game experience. The player will then receive instructions about what to expect, after which the game will be turned on. If during the first trial, the player seems to use the mouse improperly then the game will be paused for brief coaching. At the end of a trial, if the subject has met some scoring threshold, he or she may be offered the reward of a piece of candy. We will ask the subject to play the game about a dozen times, keeping in computer memory the exact (X, Y) path of each trial. PATICIPANT POPULATION: We intend to recruit males and females 18 years of age of older. To begin with, we would like to have a range of ages. RECRUITMENT OF SUBJECTS: We will seek out students in the engineering building, Barus & Holley, by posting signs. I may ask some of my same-aged (50+) neighbors in Rumford, and in the Rhode Island Rose Society, if they would like to try the game. CONFIDENTIALITY: A coded identification will designate each subject in any paper or seminar. No publicly available computer will store information about subjects.

SAMPLE RECRUITING POSTER: Daniels Lab seeking subjects to play a video game which challenges players in a navigation task. Subjects will play the game several times over the course of an hour or so. Reward of Lindt truffle for defeating a drone navigating a mirror-image path on the same "mogul field" 3-D navigation surface. Subject results will enter a database supporting our research on "Navigating with Uncertainty." Contact Jerry_Daniels@brown.edu for details.

POSSIBLE RISKS: It is difficult to imagine any physiological or mental risks to playing a computer game (using a mouse) a dozen or so times. Each start-to-goal trial will last a few minutes. Using a mouse has less mechanical danger than improper use of a keyboard for carpal tunnel syndrome. While there may be mild stress for someone trying to think which direction to step next in a game trial, it doesnt seem to rise to the level of warning subjects about. The main "danger" of video games would seem to be becoming addicted to play; our game should be nowhere near enough appealing that players will want to "take it home" and play all night.

CONSENT: Each subject will be asked to read and sign the Consent Form reproduced below.

CONSENT FORM for playing Navigation Video Game

You are invited to participate in a study of how humans navigate in a “mogul field” to a target in a computer simulated environment. We ask you to read this form. After reading it, you should feel free to ask any questions you like before agreeing to participate in the study.

The study is being conducted by researchers in the Division of Engineering at Brown University. In the experiment, you will spend about an hour at a computer, using a mouse to click on where you want to move next in a simulated field.

The experiment is designed to help us understand how quality of visual feedback affects navigation performance. Youll be given details about how to “play the game” at the start of your session. Before you start, you will fill out a questionnaire about your visual acuity, possible color blindness and previous video game playing experience. If, while playing, your score surpasses some threshold, you’ll be given your choice of reward, such as Lindt truffle.

After your session is over we may ask you a few questions about what strategies you came up with during the course of play.

The risks involved are minimal: the same as playing a video game. This study is not a treatment for any disorder. There are no direct benefits from participating. No cost is involved for you.

We will identify you as a subject in our database with a random number. The records of this study will be kept confidential to the extent of the law. In any report we might publish or speak about publically, we will not divulge information that would allow someone to identify you as a participant. Research records will be kept in files accessible only to researchers and scholars in this field of study.

Your participation is voluntary; refusal to participate (or continue once started) will not affect your current or future relations with Brown University. You are free to withdraw from the study at any time.

The research described here is led by Prof. J.D. Daniels. Please ask him or graduate student John Raiti any questions you have related to this document. Prof. Daniels phone: 401 863 1347.

If you have any questions regarding your rights as a research participant, you my may contact Susan Toppin or Dorinda Williams, Brown University Research Protections Office, 401-863-2777.

You will be given a copy of this form for your records.

"I agree to participate in the study. By signing below you testify that you are at least 18 years of age and have read, understand, and agree with the statements above. "

Signature Date

QUESTIONNAIRE: (for Navigation Game Player)

Are you right or left handed? What hand do you control a computer mouse with?

Is your vision acuity normal, or corrected to Dept of Motor Vehicles normal?

Are you colorblind ?

Age: (You must be 18 or older)

Gender:

What is your videogame experience?

Are you on any medication that may affect your motor coordination?

GAME INSTRUCTIONS Make your way from a start position to a goal (shown briefly at start of game) by double clicking the mouse in the direction you want to go. Game will be over when you are within a step of the goal. You may appreciate the color of the place where you step correlated with your score for that step. The square patch around your position will become more detailed the longer you wait. If you wait too long your position will be automatically advanced in the direction of the goal. Your score may be lower the longer you wait. Two scores are always displayed after you advance: o TOP of screen shows cumulative score o BOTTOM of screen shows score for current jump

9.2 IRB Approved Protocol and Consent Form for Estimation Experiments

LAY-PERSON SUMMARY We have an IRB allowing us to test subjects viewing patterns presented on a computer screen; the subjects respond by moving and clicking a mouse. We have some results suggesting that it matters how quickly a subject responds. We see in a Feb 17, 2006 publication in Science researchers who support the idea that a rapid ("blink") response can be better than a more delayed "cognitive" response when the problem has many features that are difficult to optimize by thought processes.

We want to try a more direct test of the blink hypothesis. We will present a subject with 3 sealed clear plastic bags, one containing 111 jelly beans, peanut M&Ms and gummy worms, and the other two bags with 222 and 444 items respectively. Each subject will be asked to make immediate (less than 15 seconds) estimates of the number of items in each bag, write down the estimates, then take another 2 minutes to do whatever the subject wants (short of opening the bags) to refine his or her estimates, then write down the revised estimates.

The problem given is “complex” because the bag has no definite shape and there are three different items inside.

Our inclination is to think the blink hypothesis is not true, that subjects will do better after thinking for two minutes. If so, the result will help us set aside our concerns that our computer screen testing is influenced by first impression guessing.

We do know from the work of Kaufman, from 1949, that given a large number of items to guess the count of, subjects tend to guess below the correct answer. We have preliminary evidence among myself, my graduate student and an undergraduate in the lab that that might be the case also for our plastic bag problem.

Citations: Kaufman et al., “Discrimination of visual number,” Am. J. Psychology 62: 498 (1949). Dijksterhuis et al., “On making the right choice,” Science 311: 1005 (2006). Malcolm Gladwell, Blink: The Power of Thinking Without Thinking, (2005).

FUNDING: The proposed project will be self-funded.

SPECIFIC AIMS OF THE HUMAN SUBJECTS COMPONENT: PURPOSE: To compare how well a person estimates based on first impression versus thinking about a problem for a few more minutes. PROCEDURE: A subject will be handed 3 clear plastic bags with various numbers of different items in them, and asked to make instant estimates of how many are in each bag, then allowed a few minutes to revise the first impression. PATICIPANT POPULATION: We intend to recruit males and females 18 years of age of older. We estimate we may need as many as

100 participants, based on the worked cited above by Dijksterhuis et al. and our own checks of variability in estimating. RECRUITMENT OF SUBJECTS: We will seek out students in the Brown engineering building, Barus & Holley, by posting signs. CONFIDENTIALITY: A coded identification will designate each subject in any paper or seminar. No publicly available computer will store information about subjects.

SAMPLE RECRUITING POSTER: Daniels Lab seeking subjects to participate in an estimation experiment. The experiment will take less than 5 minutes. Contact Jerry_Daniels@brown.edu for details.

POSSIBLE RISKS: It is difficult to imagine any physiological or mental risks to looking at and lifting up 3 bags of assorted snacks. The heaviest of the 3 bags will weigh only 2kg. Stretching our imagination, we have said that one of the items would be peanut M&Ms. so Could there be a problem if a person has a peanut allergy? No. Subjects are not allowed to open the bag, or eat the snacks. And the peanut is normally encased in a thick chocolate coating.

CONSENT: Each subject will be asked to read and sign the Consent Form reproduced below.

CONSENT FORM for Item Count Estimation Experiment

You are invited to participate in a study of how humans estimate the number of items in an enclosed space. After reading this form, you should feel free to ask any questions you like before agreeing to participate in the study.

The study is being conducted by researchers in the Division of Engineering at Brown University. In the experiment, you will spend less than 5 minutes estimating the number of items in each of 3 clear plastic bags.

The risks involved are minimal.

We will identify you as a subject in our database with a random number. The records of this study will be kept confidential to the extent of the law. In any report we might publish or speak about publicly, we will not divulge information that would allow someone to identify you as a participant. Research records will be kept in files accessible only to researchers and scholars in this field of study.

Your participation is voluntary; refusal to participate (or continue once started) will not affect your current or future relations with Brown University. You are free to withdraw from the study at any time.

The research described here is led by Prof. J.D. Daniels. Please ask him or graduate student John Raiti any questions you have related to this document. Prof. Daniels phone: 401 863 1347.

If you have any questions regarding your rights as a research participant, you my may contact Susan Toppin or Dorinda Williams, Brown University Research Protections Office, 401-863-2777.

You will be given a copy of this form for your records.

"I agree to participate in the study. By signing below you testify that you are at least 18 years of age and have read, understand, and agree with the statements above."

Signature Date

QUESTIONNAIRE: (for Item Count Estimation Experiment)

Is your vision acuity normal, or correctable to Dept of Motor Vehicles standards?

Are you colorblind?

Age: (You must be 18 or older)

Gender:

INSTRUCTIONS We will show you three clear plastic bags. Each bag contains jelly beans, peanut M&Ms, and gummy worms. You should make a rapid estimate (less than 15 seconds) of how many you think are in each bag. Write down your 3 estimates. You then have another two minutes to revise your estimates. Write down your revised estimates and youre finished.

References

[1] P. Adamic, V. Babiy, R. Janicki, W. Kakiashvili, W. Koczkodaj, and R. Tadeusiewicz. Pairwise comparisons and visual perceptions of equal area polygons. *Perceptual and Motor Skills*, 108:37–42, 2009.

[2] A. Anastasi. The estimation of area. *Journal of General Psychology*, 14:201–225, 1936.

[3] J Anderson. *An introduction to Neural Networks*. MIT, 1995.

[4] I.S. Aranson and L Kramer. The world of the complex ginzburg-landau equation. *Reviews of Modern Physics*, 74:99–143, 2002.

[5] L. Arons and F.W. Irwin. Equal weights and psycholphysical judgments. *Journal of Experimental Psychology*, 15(6):733–751, 1932.

[6] J. Atkinson, M.R. Francis, and F.W. Campbell. The dependence of the visual numerosity limit on orientation, colour, and grouping in the stimulus. *Perception*, 5(3):335–342, 1976.

[7] M. Bar. A cortical mechanism for triggering top-down facilitation in visual object recognition. *Journal of Cognitive Neuroscience*, 15(4):600–9, 2003.

[8] H Barth, N. Kanwisher, and E. Spelke. The construction of large number representations in adults. *Cognition*, 86:201–221, 2003.

[9] R.E. Bedford and G. Wyszecki. Wavelength discrimination for point sources. *J. Opt. Soc. Am.*, 48:129–35, 1958.

[10] J.S. Bruner and M.C. Potter. Interference in visual recognition. *Science*, 144:424–5, 1964.

[11] D. Burr and J. Ross. A visual sense of number. *Current Biology*, 18:425–428, 2008.

[12] B. Butterworth. Numerosity perception: How many speckles on the hen? *Current Biology*, 18:R388–R389, 2008.

[13] D. Cassenti, T. Kelley, and T. Ghirardelli. Underestimating numerosity of items in visual search tasks. *Journal of Experimental Psychology: Human Perception and Performance*, 33(5):1089–1106, 2010.

[14] J. Castronovo and X. Serono. Numerical estimation in blind subjects: evidence of the impact of blindness and its following experience. *Journal of Experimental Psychology: Human Perception and Performance*, 33:1089–1106, 2007.

[15] P. Cavanaugh. *Vision and Visual Dysfunction: Limits of Vision*, pages 234–50. MacMillan, 1991.

[16] E.W. Dijkstra. A note on two problems in connexion with graphs. *Numerische Mathematik*, 1:269–271, 1959.

[17] F. Domini and C. Caudek. 3-d structure perceived from dynamic information: a new theory. *Trends in Cognitive Science*, 7(10):444–449, 2003.

[18] J.T. Enns and V. DiLollo. What's new in visual masking. *Trends in Cognitive Sciences*, 4(9):345–52, 2000.

[19] B. Fischhoff. Hindsight $\neq$ foresight: The effect of outcome knowledge on judgment under uncertainty. *Journal of Experimental Psychology: Human Perception and Performance*, 1:288–99, 1975.

[20] P. Foo, W.H. Warren, A. Duchon, and M.J. Tarr. Do humans integrate routes into a cognitive map? map- versus landmark-based navigation of novel shortcuts. *Journal of Exp Psych: Learning, Memory, and Cognition*, 31(2):195–215, 2005.

[21] A.P. Fornos, J. Sommerhalder, B. Rappaz, A.B. Safran, and M. Pelizzone. Simulation of artificial vision, III: do the spatial or temporal characteristics of stimulus pixelization really matter? *Investigative Ophthalmology and Visual Science*, 46(10):3906–12, 2005.

[22] A. Fournier, D. Fussell, and L. Carpenter. Computer rendering of stochastic models. *Communications of the ACM*, 25:371–384, 1982.

[23] A. Gallace, H.Z. Tan, and C. Spence. Numerosity judgments for tactile stimuli distributed over the body surface. *Perception*, 35(2):247–266, 2006.

[24] A. Gallace, H.Z. Tan, and C. Spence. Can tactile stimuli be subitised? an unresolved controversy within the literature on numerosity judgments. *Perception*, 37(5):782–800, 2008.

[25] I. Gauthier. Visual priming: The ups and downs of familiarity. *Current Biology*, 10:R753–R756, 2000.

[26] S. Gepshtein and M.S. Banks. Viewing geometry determines how vision and haptics combine in size perception. *Current Biology*, 13:483–8, 2003.

[27] N. Ginsberg. Perceived numerosity, item arrangement, and expectancy. *The American Journal of Psychology*, 91:267–273, 1978.

[28] N Ginsberg. Numerosity estimation as a function of stimulus organization. *Perception*, 20(5):681–686, 1991.

[29] K. Grill-Spector, T. Kushnir, T. Hendler, and R. Malach. The dynamics of object-selective activation correlate with recognition performance in humans. *Nature Neuroscience*, 3(8):837–43, 2000.

[30] E.M. Harley, K.A. Carlsen, and G.R. Loftus. The "saw-it-all-along" effect: demonstrations of visual hindsight bias. *Journal of Experimental Psychology: Learning, Memory, and Cognition*, 30(5):960–8, 2004.

[31] L.D. Harmon and B. Julesz. Masking in visual recognition: Effects of two-dimensional filtered noise. *Science*, 180:1194–7, 1973.

[32] L He, J Zhang, T Zhou, and L Chen. Connectedness affects dot numerosity judgment: Implications for configural processing. *Psychonomic Bulletin and Review*, 16:509–517, 2009.

[33] D Hebb. *The organization of behavior*. Wiley, 1949.

[34] R Held, Y Ostrovsky, B deGelder, T Gandhi, S Ganesh, U Mathur, and P Sinha. The newly sighted fail to match seen with felt. *Nature Neuroscience*, 14:551–553, 2010.

[35] J. Holland. *Adaptation in natural and artificial systems : an introductory analysis with applications to biology, control, and artificial intelligence*. University of Michigan Press, 1975.

[36] L. Holmberg and L. Holmberg. The perception of the area of rectangles as a function of the ratio between height and width. *Psychological Research Bulletin*, 9(3):1–6, 1969.

[37] L. Holmberg and E. Wahlin. The influence of elongation on the judgment of the area of certain geometrical figures. *Psychological Research Bulletin*, 9(1):1–11, 1965.

[38] A.H. Holway, J.E. Smith, and M.J. Zigler. On the discrimination of minimal differences in weight: Ii. number of available elements as variant. *Journal of Experimental Psychology*, 20(4):371–380, 1937.

[39] Y. Hou. Visual cryptography for color images. *Pattern Recognition*, 36:1619–29, 2003.

[40] http://www.williams.edu/Biology/Faculty_Staff/hwilliams/Orienteering/course.html.

[41] L.M. Hurvich and D. Jameson. An opponent-process theory of color vision. *Psychological Review*, 64:384–404, 1957.

[42] J Jacobs, M.J. Kahana, A.D. Ekstrom, M.V. Millison, and I Fried. A sense of direction in human entorhinal cortex. *PNAS*, 107(14):6487–6492, 2010.

[43] T.W. James, G.K. Humphrey, J.S. Gati, R.S. Menon, and M.A. Goodale. The effects of visual object priming on brain activation before and after recognition. *Current Biology*, 10:1017–24, 2000.

[44] M. Kahrimanovic, W.M. Tiest, and M.L. Kappers. Haptic perception of volume and surface area of 3-d objects. *Attention, Perception and Psychophysics*, 72(2):517–527, 2010.

[45] M. Katkov, M. Tsodyks, and D. Sagi. Singularities in the inverse modeling of 2AFC contrast discrimination data. *Vision Research*, 46:259–66, 2006.

[46] E.L. Kaufman, M.W. Lord, T.W. Reese, and J. Volkmann. The discrimination of visual number. *The American Journal of Psychology*, 62:498–525, 1949.

[47] R Kitada, T Hashimoto, T Kochiyama, T Kito, T Okada, M Matsumura, S Lederman, and N Sadato. Tactile estimation of the roughness of gratings yields a graded response in the human brain: an fmri study. *NeuroImage*, 25:90–100, 2005.

[48] W.W. Koczkodaj. Statistically accurate evidence of improved error rate by pairwise comparisons. *Perceptual and Motor Skills*, 82:43–48, 1996.

[49] Á. Kristjánsson, D. Wang, and K. Nakayama. The role of priming in conjunctive visual search. *Cognition*, 85:37–52, 2002.

[50] M.S. Livingstone and D.H. Hubel. Psychophysical evidence for separate channels for perception of form, color, movement, and depth. *Journal of Neuroscience*, 7:3416–68, 1987.

[51] G.R. Loftus and E.M. Harley. Why is it easier to identify someone close than far away? *Psychonomic Bulletin & Review*, 12:43–65, 2005.

[52] F.L. Long, Z. Yang, and D. Purves. Spectral statistics in natural scenes predict hue, saturation, and brightness. *PNAS*, 103(15):6013–18, 2006.

[53] E Macaluso. Multisensory processing in sensory-specific cortical areas. *The Neuroscientist*, 12:327–338, 2006.

[54] E Macaluso and J Driver. Spatial attention and crossmodal interactions between vision and touch. *Neuropsychologia*, 39:1304–1316, 2001.

[55] N. Martinez and W.E. Dawson. Ranking of apparent area for different shapes of equal area. *Perceptual and Motor Skills*, 37:763–770, 1973.

[56] P. Matthews. *Mammalian muscle receptors and their central actions.* Edward Arnold Press, 1972.

[57] C. McCollough. Color adaptation of edge-detectors in the human visual system. *Science*, 149:1115–1116, 1965.

[58] J. Mehler and T.G. Bever. Cognitive capacity of very young children. *Science*, 158(3797):141–142, 1967.

[59] K.M. Michels and L. Zusne. Metrics of visual form. *Psychological Bulletin*, 63:74–86, 1965.

[60] A.L. Nagy and R.R. Sanchez. Critical color differences determined with a visual search task. *Journal of the Optical Society of America A*, 7(7):1209–17, 1990.

[61] K.N. Ochsner, C.P. Chiu, and D.L. Schacter. Varieties of priming. *Current Opinion in Neurobiology*, 4:189–94, 1994.

[62] G Orban, S Sunaert, J Todd, P Van Hecke, and G Marchal. Human cortical regions involved in extracting depth from motion. *Neuron*, 24:929–940, 1999.

[63] A Paradis, V Cornilleau-Peres, J Droulez, P Van de Moortele, E Lobel, A Berthoz, D Le Bihan, and J Poline. Visual perception of motion and 3-d structure from motion: an fmri study. *Cerebral Cortex*, 10:772–783, 2000.

[64] J. Piaget. Quantification, conservation, and nativism. *Science*, 162(3857):976–979, 1968.

[65] M. Piazza, A. Mechelli, C.J. Price, and B. Butterworth. Exact and approximate judgements of visual and auditory numerosity: An fmri study. *Brain Research*, 1106:177–188, 2006.

[66] M Plaisier, W Bergman, and A Kappers. One, two, three, many - subitizing in active touch. *Acta Psychologica*, 131:163–170, 2009.

[67] Quinlan P.T. and G.W. Humphreys. Visual search for targets defined by combinations of color, shape, and size: An examination of the task constraints on feature and conjunction searches. *Perception & Psychophysics*, 41(5):455–72, 1987.

[68] G. Rainer and E.K. Miller. Effects of visual experience on the representation of objects in the prefrontal cortex. *Neuron*, 27:179–89, 2000.

[69] K.J. Riggs, L. Ferrand, D. Lancelin, L. Fryziel, G. Dumur, and A. Simpson. Subitizing in tactile perception. *Psychological Science*, 17:271–275, 2006.

[70] E.T. Rolls. Face processing in different brain areas, and critical band masking. *Journal of Neuropsychology*, 2:325–60, 2008.

[71] J. Ross. Discrimination of number without counting. *Perception*, 32:867–870, 2003.

[72] J Ross and D Burr. Vision senses number directly. *Journal of Vision*, 10:1–8, 2010.

[73] M.F.S. Rushworth and T.E.J. Behrens. Choice, uncertainty and value in prefrontal and cingulate cortex. *Nature Neuroscience*, 11(4):389–97, 2008.

[74] J.M. Rybash. Implicit memory and aging: a cognitive neuropschological perspective. *Developmental Neuropsychology*, 12:127–79, 1996.

[75] J. Sadr and P. Sinha. Object recognition and random image structure evolution. *Cognitive Science*, 28(2):259–87, 2004.

[76] J. Shim, L.G. Carlton, and J. Kim. Estimation of lifted weight and produced effort through perception of point-light display. *Perception*, 33(3):277–291, 2004.

[77] S. Shimojo, Y. Kamitani, and S. Nishida. Afterimage of perceptually filled-in surface. *Science*, 293(5535):1677–1680, 2001.

[78] J.P. Smith. The effects of figural shape on the perception of area. *Perception and Psychophysics*, 5:49–52, 1969.

[79] K. Srinivas. Representation of rotated objects in explicit and implicit memory. *Journal of experimental psychology: learning, memory, and cognition*, 21(4):1019–36, 1995.

[80] J.R. Stroop. Studies of interference in serial verbal reactions. *Journal of experimental psychology*, 18:643–662, 1935.

[81] L.L. Thurstone. A law of comparative judgment. *Psychological Review*, 34:278–286, 1927.

[82] S.P. Tipper. The negative priming effect: inhibitory effects of ignored primes. *Quarterly Journal of experimental psychology*, 37A:571–90, 1985.

[83] A.M. Treisman. Perceptual grouping and attention in visual search for features and for objects. *Journal of Eaperimental Psychology. Human Perception & Performance*, 8:194–214, 1982.

[84] A.M. Treisman and G. Gelade. A feature-integration theory of attention. *Cognitive Psychology*, 12:97–136, 1980.

[85] A.M. Treisman, M. Sykes, and G. Gelade. Selective attention and stimulus integration. In S. Dornic, editor, *Attention and performance VI*. Erlbaum, 1977.

[86] E. Tulving and D.L. Schachter. Priming and human memory systems. *Science*, 247(4940):301–306, 1990.

[87] M.T. Turvey. Inferences from an information-processing analysis of masking with patterned stimuli. *Psychological Review*, 80(1):1–52, 1973.

[88] A. Tversky and D. Kahneman. Judgment under uncertainty: heuristics and biases. *Science*, 185:1124–1131, 1974.

[89] W.R. Uttal, T. Baruch, and L. Allen. The effect of combinations of image degradations in a discrimination task. *Perception & Psychophysics*, 57(5):668–81, 1995.

[90] J.A. van Esch, E.E. Koldenhof, A.J. van Doorn, and J.J. Koenderink. Spectral sensitivity and wavelength discrimination of the human peripheral visual field. *Journal of the Optical Society of America. A*, 1(5):443–50, 1984.

[91] F. Vega-Bermudez, K.O. Johnson, and S. Hsiao. Human tactile pattern recognition: active versus passive touch, velocity effects, and patterns of confusion. *Journal of Neurophysiology*, 65(3):531–546, 1991.

[92] J.M. Warren and S.R. Pinneau. Influence of form on judgment of apparent area. *Perceptual and Motor Skills*, 5:7–10, 1955.

[93] E.H. Weber. De subtilitate tactus [on the sensitivity of the touch sense]. In *De pulsu, resorptione, auditu et tactu: Annotationes anatomicae et physiologicae*. Leipzip: Koehler, 1934.

[94] C.L. Wiggs and A. Martin. Properties and mechanisms of perceptual priming. *Current Opinion in Neurobiology*, 8:227–33, 1998.

[95] R. Woodworth. *Experimental Psychology*, chapter 14, pages 609–612. Holt, Rinehart, and Winston, third edition, 1971.

[96] W.D. Wright and F.G Pitt. Hue-discrimination in normal colour-vision. *Proceedings of the Physical Society*, 46(3):459–73, 1934.

[97] R.M. Yerkes and J.D. Dodson. The relation of strength of stimulus to rapidity of habitformation. *Journal of Comparative Neurology and Psychology*, 18:459–82, 1908.

This dissertation by John G. Raiti is accepted in its present form by the Department of Biomedical Engineering as satisfying the dissertation requirement for the degree of Doctor of Philosophy.

Date_______________ ___________________________________

Jerry Daniels, Advisor

Recommended to the Graduate Council

Date_______________ ___________________________________

James Anderson, Reader

Date_______________ ___________________________________

Gustav Engbretson, Reader

Date_______________ ___________________________________

John Stein, Reader

Date_______________ ___________________________________

Rashid Zia, Reader

Approved by the Graduate Council

Date_______________ ___________________________________

Peter Weber, Dean of the Graduate School